SANDIA REPORT
SAND2010-5844
Unlimited Release
Printed September 2010

Performance Limits for Exo-Clutter Ground Moving Target Indicator (GMTI) Radar

Armin W. Doerry

Prepared by
Sandia National Laboratories
Albuquerque, New Mexico 87185 and Livermore, California 94550

Sandia National Laboratories is a multi-program laboratory managed and operated by Sandia Corporation, a wholly owned subsidiary of Lockheed Martin Corporation, for the U.S. Department of Energy's National Nuclear Security Administration under contract DE-AC04-94AL85000.

Issued by Sandia National Laboratories, operated for the United States Department of Energy by Sandia Corporation.

Available to DOE and DOE contractors from
U.S. Department of Energy
Office of Scientific and Technical Information
P.O. Box 62
Oak Ridge, TN 37831

Telephone: (865) 576-8401
Facsimile: (865) 576-5728
E-Mail: reports@adonis.osti.gov
Online ordering: http://www.osti.gov/bridge

Available to the public from
U.S. Department of Commerce
National Technical Information Service
5285 Port Royal Rd.
Springfield, VA 22161

Telephone: (800) 553-6847
Facsimile: (703) 605-6900
E-Mail: orders@ntis.fedworld.gov
Online order: http://www.ntis.gov/help/ordermethods.asp?loc=7-4-0#online

SAND2010-5844
Unlimited Release
Printed September 2010

Performance Limits for Exo-Clutter Ground Moving Target Indicator (GMTI) Radar

Armin W. Doerry
Reconnaissance and Surveillance Systems Department

Sandia National Laboratories
PO Box 5800
Albuquerque, NM 87185-0519

ABSTRACT

The performance of a Ground Moving Target Indicator (GMTI) radar system depends on a variety of factors, many which are interdependent in some manner. It is often difficult to 'get your arms around' the problem of ascertaining achievable performance limits, and yet those limits exist and are dictated by physics. This report identifies and explores those limits, and how they depend on hardware system parameters and environmental conditions. Ultimately, this leads to a characterization of parameters that offer optimum performance for the overall GMTI radar system.

While the information herein is not new to the literature, its collection into a single report hopes to offer some value in reducing the 'seek time'.

ACKNOWLEDGEMENTS

The author is grateful to Ann Raynal and Jeff Hollowell for their review of early drafts of this report, and their helpful suggestions.

This report was funded by General Atomics Aeronautical Systems, Inc. (ASI) Reconnaissance Systems Group (RSG).

Sandia National Laboratories is a multi-program laboratory managed and operated by Sandia Corporation, a wholly owned subsidiary of Lockheed Martin Corporation, for the U.S. Department of Energy's National Nuclear Security Administration under contract DE-AC04-94AL85000.

CONTENTS

FOREWORD

Fundamental to the quality of a GMTI radar system performance is its Signal to Noise Ratio (SNR). Noise is in fact error in the rendering of the data from which decisions of target detection are made, and is due to a variety of phenomena from a variety of sources. The equation that evaluates SNR with respect to additive thermal noise is commonly called the Radar Equation. It is discussed in a multitude of texts and other references, but seldom with enough detail and background to fully appreciate the many nuances and parameter trades available to a system designer. Indeed, the various texts often make different simplifying assumptions along the way such that apparent inconsistencies exist between them.

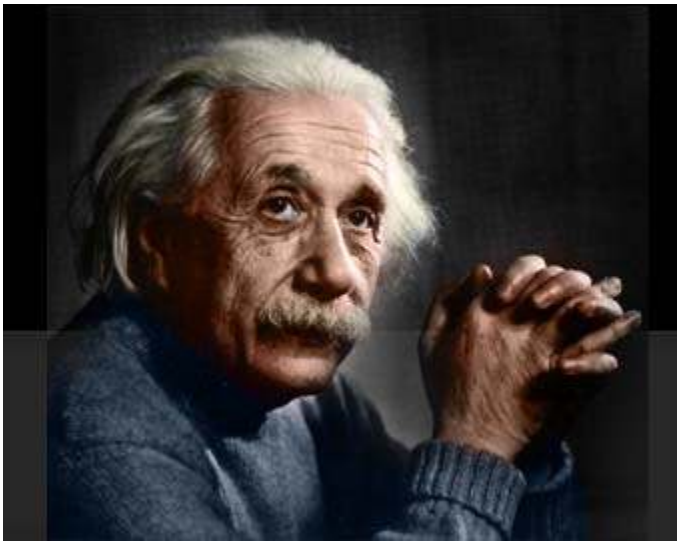

"Nothing happens until something moves" – Albert Einstein

1 Introduction

Ground Moving Target Indicator (GMTI) radar performance is dependent on a multitude of parameters, many of which are interrelated in non-linear fashions. Seemingly simple questions such as "What range can we operate at?", "What resolution can we get?", "How fast can we fly?", and "What frequency should we operate at?", are often (and rightly so) hesitantly answered with a slew of qualifiers (ifs, buts, givens, etc.).

These invariably result in performance studies that trade various parameters against each other. Nevertheless, general trends can be observed, and general statements can be made. Furthermore, performance bounds can be generated to offer first order estimates on the achievability of various performance goals. This report attempts to do just this.

The ultimate aim of a GMTI radar is to first detect, and then characterize, moving objects with a high Probability of Detection (P_D), while maintaining a low Probability of False Alarm (P_{FA}). A principal radar metric to achieve this is the Signal-to-Noise (energy) Ratio (SNR) in the GMTI range-Doppler map.

An earlier report performed a similar analysis for Synthetic Aperture Radar (SAR) performance.[1] Much of the analysis in this report builds on this earlier work. We will refer to the earlier report several times hereafter.

Endo-Clutter GMTI

While this report concerns itself with Exo-clutter GMTI, one might naturally wonder about any inferences to Endo-clutter GMTI. To this question we offer the following comments.

1. If the clutter is low enough, and in particular if the clutter level is below the noise level, then the SNR analysis in this report remains applicable.

2. If the clutter levels are indeed significant, then the presence of clutter will certainly not *improve* GMTI detectability. Consequently, the detectability limits presented herein continue to provide legitimate bounds. That is, an exo-clutter range limit due to SNR will not be exceeded with endo-clutter processing.

Target Trackers

A particularly powerful marriage is the output of a GMTI radar (its detection reports with mensuration) with a target tracker. A tracker's job is to ascertain a target's trajectory, both in a forensic and in a predictive sense. Much literature can be found on various tracking algorithms. Nevertheless, trackers are beyond the scope of this report.

We do note without further elaboration, however, that moving targets can sometimes be 'tracked' into the endo-clutter region.

Figure 1. GMTI display for detected target, and cross-cued EO image using General Atomics Lynx SAR, and CLAW operator display. (Courtesy of General Atomics Aeronautical Systems, Inc. All Rights Reserved.)

2 The Radar Equation

We address here the SNR in the GMTI Range-Doppler (RD) map, or image. A brief recap on the development of this equation is as follows.

For a single pulse, the Received (RX) power at the antenna port is related to the Transmitted (TX) power by

$$P_r = P_t G_A \left(\frac{1}{4\pi R^2} \right) \sigma \left(\frac{1}{4\pi R^2} \right) A_e \left(\frac{1}{L_{radar} L_{atmos}} \right) = \frac{P_t G_A A_e \sigma}{(4\pi)^2 R^4 L_{radar} L_{atmos}}, \quad (1)$$

where

P_r = received signal power (W),
P_t = transmitter signal power (W),
G_A = transmitter antenna gain factor,
A_e = receiver antenna effective area (m^2),
σ = target Radar Cross Section (m^2),
R = range vector from target to antenna (m),
L_{atmos} = atmospheric loss factor due to the propagating wave,
L_{radar} = microwave transmission loss factor due to miscellaneous sources. (2)

The effective noise power that the signal must compete with at the antenna is given approximately by

$$N_r = kTF_N B_N, \quad (3)$$

where

N_r = received noise power (W),
k = Boltzmann's constant = 1.38 x 10-23 J/K,
T = nominal scene noise temperature ≈ 290 K,
F_N = system noise factor for the receiver, and
B_N = noise bandwidth at the antenna port. (4)

Consequently, the Signal-to-Noise (power) ratio at the RX antenna port is effectively

$$SNR_{antenna} = \frac{P_r}{N_r} = \frac{P_t G_A A_e \sigma}{(4\pi)^2 R^4 L_{radar} L_{atmos} (kTF_N) B_N}. \quad (5)$$

A finite data collection time limits the total energy collected, and signal processing in the radar increases the SNR in the RD map by two major gain factors. The first is due to

pulse compression, and the second is due to coherently combining echoes from multiple pulses, that is, pulse integration. This results in

$$SNR_{image} = SNR_{antenna} G_r G_a = \frac{P_t G_A A_e \sigma \, G_r G_a}{(4\pi)^2 R^4 L_{radar} L_{atmos} (kTF_N) B_N}, \tag{6}$$

where

G_r = SNR gain due to range processing (pulse compression),
G_a = SNR gain due to azimuth processing (coherent pulse integration). (7)

The product $G_r G_a$ comprises the signal processing gain.

This relationship is called "The Radar Equation".

At this point we examine the image SNR terms and factors individually to relate them to physical GMTI system parameters and performance criteria.

2.1 Antenna

This report will consider only the monostatic case, where the same antenna is used for TX and RX operation. Consequently, we relate

$$G_A = \frac{4\pi A_e}{\lambda^2}, \tag{8}$$

where λ is the nominal wavelength of the radar. Furthermore, the effective area is related to the actual aperture area by

$$A_e = \eta_{ap} A_A, \tag{9}$$

where

$$\begin{aligned} \eta_{ap} &= \text{the aperture efficiency of the antenna, and} \\ A_A &= \text{the physical area of the antenna aperture.} \end{aligned} \tag{10}$$

Typically, a radar design must live with a finite volume allocated to the antenna structure, so that the achievable antenna physical aperture area is limited. The aperture efficiency takes into account a number of individual efficiency factors, including the radiation efficiency of the antenna, the aperture illumination efficiency of say a feedhorn to a reflector assembly, spillover losses of a feedhorn to a finite reflector area, etc. A typical number for aperture efficiency might be $\eta_{ap} \approx 0.5$.

Putting these into the radar equation yields the expression

$$SNR_{image} = \frac{P_t \left(\eta_{ap}^2 A_A^2\right) \sigma \, G_r G_a}{(4\pi) R^4 \lambda^2 L_{radar} L_{atmos} (kTF_N) B_N}. \tag{11}$$

2.2 Processing Gains

A detailed discussion of processing gain is given in Appendix A of Reference 1.

The range processing gain is due to noise bandwidth reduction during the course of pulse compression. It is straightforward to show that

$$G_r = \frac{T_{eff} B_N}{L_r}, \tag{12}$$

where

T_{eff} = the effective pulse width of the radar, and

L_r = reduction in SNR gain due to non-ideal range filtering. (13)

Sidelobe reduction for GMTI is somewhat more important than for SAR. This is because we are often trying to detect even individual pixels in the presence of sidelobes from bright clutter. Consequently, in the absence of more refined information, typically sidelobe filtering loss $L_r \approx a_{wr} \approx 1.5$ or so, where a_{wr} is the range impulse response broadening factor due to data weighting or windowing.

The effective pulse width differs from the actual TX pulse width in that the effective pulse width is equal to that portion of the real pulse that makes it into the data set. For digital matched-filter processing they are the same, but for stretch-processing the effective pulse width is typically slightly less than the real transmitted pulse width, but still pretty close. We note that it is quite possible to operate a GMTI radar in a manner to make this difference quite large. For the remainder of this report we will optimally presume that the transmitted pulse width is equal to the effective pulse width.

The azimuth processing gain is due to the coherent integration of multiple pulses, otherwise known as Doppler processing. Of course, the total number of pulses that can be collected depends on the radar Pulse Repetition Frequency (PRF) and the Coherent Processing Interval (CPI). Putting all this together yields

$$G_a = \frac{N}{L_a} = \frac{f_p T_{CPI}}{L_a}, \tag{14}$$

where

N = the total number of pulses integrated,

f_p = radar PRF (Hz),

T_{CPI} = Coherent Processing Interval (CPI) time, and

L_a = reduction in SNR gain due to non-ideal Doppler filtering. (15)

Note that in the absence of more refined information, typically $L_a \approx a_{wa} \approx 1.5$ or so, where a_{wa} is the Doppler impulse response broadening factor due to data weighting or windowing.

In addition, Doppler resolution is inversely proportional to T_{CPI}, although it also depends on the non-ideal azimuth filtering to control sidelobes. There is a tacit presumption in this equation that the target itself remains coherent over the desired T_{CPI}. (More on this later.)

Putting these into the radar equation yields

$$SNR_{image} = \frac{P_t T_{eff} f_p T_{CPI} \left(\eta_{ap}^2 A_A^2\right) \sigma}{(4\pi) R^4 \lambda^2 (kTF_N) L_{radar} L_{atmos} L_r L_a} . \tag{16}$$

2.3 The Transmitter

The transmitter is generally specified to first order by 3 main criteria:

1) The frequency range of operation,

2) The peak power output (averaged during the pulse on-time), and

3) The maximum duty factor allowed.

We identify the duty factor as

$$d = T_{eff} f_p = \frac{P_{avg}}{P_t}, \tag{17}$$

where P_{avg} is the average power transmitted during the synthetic aperture data collection period. Consequently, we identify

$$P_t T_{eff} f_p = P_t d = P_{avg}. \tag{18}$$

Transmitter power capabilities and bandwidths are very dependent on transmitter technology. In general, for tube-type power amplifiers, higher power generally implies lesser capable bandwidth, and hence lesser range resolution. The signal bandwidth required for a particular range resolution for a single pulse is given by

$$B_T = \frac{a_{wr} c}{2\rho_r}, \tag{19}$$

where

ρ_r = slant-range resolution required,
a_{wr} = range impulse response broadening factor,
c = velocity of propagation. (20)

There is no typical duty factor that characterizes all, or even most, power amplifiers. Duty factors may range from on the order of 1% to 100% across the variety of power amplifiers available. Typically, a maximum duty factor needed by a pulse-Doppler radar is less than 50%, and usually less than about 35% or so. Consequently, a reasonable duty

factor limit of 35% might be imposed on power amplifiers that could otherwise be capable of more. †

In practice, the duty factor limit for a particular power amplifier may not always be achieved due to timing constraints for the geometry within which the radar is operating, but we can often get pretty close.

We take this opportunity to also note that

$$\lambda = \frac{c}{f}, \tag{21}$$

where f is the radar nominal frequency.

A discussion of representative power amplifier tube capabilities can be found in Reference 1.

In any case, we refine the radar equation to be

$$SNR_{image} = \frac{P_{avg} T_{CPI} \left(\eta_{ap}^2 A_A^2 \right) f^2 \sigma}{(4\pi) c^2 R^4 (kTF_N) L_{radar} L_{atmos} L_r L_a}, \tag{22}$$

noting that the average power is based on the power amplifier's duty factor limit. For wideband radar systems this might be limited to perhaps 35%, but can often be far less.

---

† We are omitting discussion of FMCW radars beyond noting that their duty factor is typically 100%, with *effective* duty factor sometimes somewhat less. This does come at a price of reduced antenna aperture size limits, owing to separate transmit and receive apertures required to maintain isolation, a fact often ignored by FMCW proponents.

2.4 The Target Radar Cross Section (RCS)

The RCS of a target denotes its ability to reflect energy back to the radar. GMTI targets (especially vehicles) tend to be specular in nature, or at least collections of specular reflectors, as opposed to distributed like a vegetation field, albeit with very complex RCS characteristics.

We note that for specular (non-distributed) targets, a variety of frequency dependencies exists, and are characterized in the following table.

Table 1. RCS frequency dependence.

target characteristic	examples	frequency dependence
2 radii of curvature	spheroids	None
1 radius of curvature	cylinders, top hats	F
0 radii of curvature	flat plates, dihedrals, trihedrals	f^2

Distributed targets tend to exhibit a frequency dependence approximately proportional to frequency f.

To meaningfully compare a radar's performance at other frequencies for the same target, the target's frequency dependency must be accounted for. We do this by equating

$$\sigma = \sigma_{ref} \left(\frac{f}{f_{ref}} \right)^n , \tag{23}$$

where

$$n = \text{some power, not necessarily an integer.} \tag{24}$$

A typical GMTI radar specification requires a SNR of perhaps 20 dB for a target RCS of 0 dBsm at Ku-band (nominally 16.7 GHz). This corresponds to $\sigma_{ref} = 0$ dB, with $f_{ref} = 16.7$ GHz. The implication is that the same target reflector might often be dimmer at lower frequencies, and brighter at higher frequencies. However, we need to remember that complicated targets may have complicated frequency dependence.

Additionally, σ_{ref} will exhibit some dependency itself on aspect angles, including grazing angle ψ_g. This is due to the interaction of typically multiple scattering points on a target, and perhaps interaction with the ground.

Nevertheless, folding the RCS dependencies into the radar equation, and rearranging a bit, yields

$$SNR_{image} = \frac{P_{avg} T_{CPI} \left(\eta_{ap}^2 A_A^2\right) \sigma_{ref} \left(\frac{f}{f_{ref}}\right)^n f^2}{(4\pi) c^2 R^4 (kTF_N) L_{radar} L_{atmos} L_r L_a}. \quad (25)$$

2.4.1 RCS Distributions

The complex nature of RCS characteristics of GMTI targets is generally accounted for in a statistical manner. Several statistical scattering models were developed by Peter Swerling[2], and are known as Swerling models. Swerling model characteristics are detailed in Appendix A.

Target RCS characteristics for complex targets are ascertained typically in one of the following three ways.

1. Direct measurements of real targets. This may be from actual flight test data or ISAR turn-table measurements.

2. Measurements of scaled models of targets. This is often from ISAR turn-table measurements.

3. Computer simulation using computer models. Electromagnetic modeling and simulation tools such as Xpatch are often used for this. The various tools available offer varying degrees of fidelity (also requiring varying degrees of computational horsepower).

An examination of the published literature yields some data on target RCS expectations.

2.4.1.1 Vehicle RCS Distribution

Palubinskas and Runge[3] measured the RCS of a VW Golf V passenger car at X-band with VV polarization. At cardinal angles the RCS measurements were usually above 0 dBsm, with values as high as +19 dBsm. At oblique angles, the measured RCS was considerably less, with a mean below 0 dBsm and values as low as −18 dBsm. Over all angles, the mean RCS was +0.5 dBsm with a standard deviation of 7.1 dBsm. Variations of more than 10 dBsm were observed with as little as 0.35 degree aspect change, indicating high sensitivity to aspect angle.

Anecdotal evidence suggests that vehicles tend to observe a Swerling 1 characteristic, that is, composed of many scattering centers with none being dominant. For some targets, however, such as perhaps a pickup truck with a strong reflection from the interior corner of the bed, a reasonably strong argument can be made for Swerling 3 behavior, that is, composed of a number of scattering centers but with one being dominant.

Nixon, et al.,[4] measured 11 full-size T-72 tanks at Ka-band at 5 degree grazing angle. They report a median value of +11.3 dBsm for VV polarization (slightly higher for HH),

with 12.3 dBsm standard deviation, although plots show no measurements less than +7 dBsm.

Giles, et al.,[5] measured both models and full-size tanks of several models at Ka-band. The various models exhibited median values from 11 to 16 dBsm. Mean values were on the order of 2 dB higher, indicating perhaps larger deviations towards greater RCS than deviations to smaller RCS.

Goyette, et al.,[6] measured scaled models of a T-72 tank to determine X-band RCS characteristics of full-size tanks. They show data that indicates a median value in the neighborhood of +11 dBsm, with no data below +6 dBsm.

Anecdotal evidence from analysis of 4-inch resolution SAR images of M-47 tank signatures at Ku-band by Sandia National Laboratories suggest that the RCS is at times dominated by a single strong scattering center, suggesting Swerling 3 characteristics over significant aspect angles, while at other aspect angles, Swerling 1 characteristics are more evident.

Curiously, taken in total, the data suggests that there does not seem to be a strong frequency dependence in the RCS of tank-like vehicles. This observation was also made by Palubinskas, et al.,[7] for civilian passenger vehicles.

2.4.1.2 Dismount RCS Distribution

Published literature on the RCS of dismounts (human bodies) is somewhat anemic at this time, although enough does exist to get an inkling of what one might expect.

Le and Dogaru[8] report on Xpatch modeling of the human body at several frequencies. While acknowledging the limitations of the Xpatch software for this application, they nevertheless report a number of interesting results. For example, at Ku-band, the median RCS for VV polarization varies from −1.6 dBsm at 0 degree grazing angle to −10.4 dBsm at 60 degrees grazing. For HH polarization, the corresponding RCS are −1.8 dBsm to −6.4 dBsm. At 15 degrees grazing HH polarization already exhibits a 3.9 dB advantage over VV polarization (−5.9 for VV, −2.0 for HH). At 30 degree grazing angle, they report a Ku-band VV median value of −8.2 dBsm and show a chart with values between −13 dBsm and 0 dBsm, with 2.6 dBsm standard deviation. They also conclude that "RCS value does not change much with frequency". Their data also shows the clear trend of higher RCS with front and rear views, as one might expect.

To put some of these RCS numbers in perspective, we note that a 20-inch diameter metal sphere exhibits an RCS of −6.9 dBsm in free space. With favorable geometry over a conducting ground plane, this might be amplified to as much as +5.1 dB.

Measurements by Otero[9] show that the human torso dominates RCS over all appendages combined by a factor of 3 to 4 times. This has some important implications. First, it is the motion of the torso that then dominates the Doppler spectrum, and provides the 'detectability' of a dismount. Second, if the motion of body features (e.g. limbs, etc.) are

desired to be detected and measured, then their reduced RCS requires a corresponding improvement in noise equivalent RCS in order to become detectable. These are often referred to as "micro-Doppler" features.

We also note that a target radar signature will depend to some degree on the characteristics of the ground upon which it sits. This is true of all reflecting targets, whether moving or not.[10] In addition, radar signatures will generally depend somewhat on the polarization of the radar wave. There tends to be somewhat greater RCS evident for HH polarization over VV polarization. It is not clear to what degree the ground plane affected polarization performance in the studies cited.

An 'average' human pedestrian walking speed depends on gender and age, but is typically in the neighborhood of 1.25 m/s to 1.5 m/s.

2.4.2 RCS Coherence Time

By definition, for GMTI we are interested in targets that move. As targets move they often change perspective, and perhaps even change shape. Additionally, the target perspective change may also be due in part to radar motion. These in turn may cause a modulation of the radar echo, often described as glint or scintillation. It may also cause a modulation of the expected Doppler response.

We have assumed in the development above that the SNR is proportional to CPI time T_{CPI}. This in turn assumes that the target echo remains coherent for the entire interval T_{CPI}. In doing so, the target echo collapses into a minimum number of Doppler resolution cells, often just one, effecting a desired maximum SNR. To maintain the minimum spread in Doppler space, a target response must be linear phase, and constant amplitude, with time. Any departure from these represents an undesired modulation of the target response that spreads the Doppler response, thereby diminishing SNR in any one range-Doppler resolution cell. This is described as a loss of coherence.

The time interval for which a target response is reasonably linear phase and reasonably constant amplitude is the RCS coherence time. The RCS coherence time for moving targets is typically finite. Making a Doppler measurement over an interval that exceeds the coherence time will manifest as a smearing of the Doppler response, and reduction of the eventual SNR that is otherwise expected.

We note that Doppler smearing is the first effect noticed. As non-linear target motion, or apparent motion, increases beyond effecting Doppler smearing, the range response can also be degraded.

As a practical matter, there is little or no benefit to SNR improvement for CPI length to exceed coherence time, so we might limit

$$T_{CPI} \leq T_{coherence}, \tag{26}$$

where

$T_{coherence}$ = coherence time of the target. (27)

To first order, the coherence time is the inverse of the Doppler bandwidth or spread of the target, that is

$$T_{coherence} \approx \frac{1}{B_{d,}}, \tag{28}$$

where

B_d = the Doppler bandwidth of the target. (29)

We note that this suggests that we might measure target coherence time from the Doppler spreading in a range-Doppler map.

We examine two classes of targets here now, 1) vehicles, and 2) dismounts.

*2.4.2.1 **Vehicle Coherence Time***

If we believe vehicles to be essentially rigid bodies, then RCS characteristics will be constant for any particular perspective. However, the RCS may change considerably even with small changes in perspective, as previously discussed. This is about 'spatial coherence'. Spatial coherence of radar echoes from a random scattering field (like one might expect from a Swerling 1 target) is described by the Van Cittert-Zernike theorem from optics. Essentially, the size of the random scattering field defines its reflected 'beamwidth'. A perspective change larger than a beamwidth will result in decorrelation of the response. This is well known in the field of Interferometric SAR.

The coherence time then becomes the time it takes to change perspective sufficient to lose spatial coherence.

We choose a vehicle model with Swerling 1 characteristics, with randomly phased reflectors over an azimuth extent of

$D_{v,a}$ = the azimuth extent of the vehicle. (30)

The beamwidth, or angular extent of spatial correlation is then calculated as

$$\theta_{coherence} \approx \frac{\lambda}{2D_{v,a}}. \tag{31}$$

Perspective changes equal to, or larger than this will cause effectively complete decorrelation. Even lesser angles will cause partial decorrelation.

(The astute observer will recognize this as the synthetic aperture angle required to achieve a SAR resolution equal to $D_{v,a}$.)

Example

As an example, we note that a Ku-band radar, and for vehicle dimension of 3 m, the angular extent of spatial correlation is 0.003 radians, or 0.17 degrees.

A vehicle may change its perspective towards the radar by one of two ways, 1) the radar's bearing to/from the vehicle changes, or 2) the vehicle itself 'turns'.

1. Radar Motion

Even though a vehicle may be traveling in a straight line with constant speed, the radar itself may be flying with some velocity tangential to the line of sight towards the target. This will cause a perspective change of the target vehicle.

Example

At a 10 km range, an aircraft flying at 75 m/s in a direction normal to the line of sight to a target exhibiting constant speed and direction, will traverse 0.17 degrees in 0.4 seconds. Processing data over a larger angle will begin to resolve Doppler to angular extents smaller than that corresponding to $D_{v,a} = 3$ m, thereby diminishing SNR in any one Doppler resolution cell.

2. Vehicle Motion

GMTI typically assumes vehicle straight-line motion at constant speed. This is in fact not typical even for vehicles on straight roads. Soliday[11] reports a test where vehicles traveling at highway speeds (25-29 m/s) exhibited a normal distribution with about 13 cm standard deviation with respect to their position in their chosen traffic lane. Soliday reports the time dependence of the 'weaving' in terms of "band crossings" per kilometer. If we interpret the crossing of the center-most band as a 'zero crossing', then his reported 4.6 band crossings per km at 29 m/s results in an average period of 15 seconds, and his reported 6.2 band crossings per km at 25 m/s results in an average period of 13 seconds.

Example

Assume a vehicle traveling at constant speed along a straight road, but although attempting to drive straight, the vehicle weaves somewhat with a path that is sinusoidal with a period of 15 seconds, and a peak-to-peak left-right drift of 26 cm. At the peak left or right deviations, the 0.17 degrees will be traversed in about 0.13 seconds.

Note that if the radar frequency were halved, say from Ku-band to lower X-band, the angular extent of spatial correlation would double, allowing a doubling of the coherence time to 0.26 seconds. The same result would be achieved by halving the azimuth extent of the vehicle (interrogating a smaller vehicle).

We note that a perspective change due to vehicle motion is precisely what ISAR uses to provide cross-range resolution.

These examples are no doubt quite squishy. The point of this analysis and these examples is nevertheless that it is probably not reasonable to expect a vehicle's coherence time to exceed several hundred milliseconds. In fact, if the vehicle is turning, or on a curved path, coherence time may be far less.

2.4.2.2 Dismount Coherence Time

As people walk, they offer constantly changing shape and motion. For example, their arms and legs swing forward and aft, and the head and torso bob up and down, side to side, and fore and aft, in addition to twisting and turning. In fact, people are neither rigid bodies, nor do they offer uniform velocity, even of their components. Empirical data were summarized into detailed models by Boulic, et al.[12]

During their strides, a walking dismount's radar echo characteristics change, too, in both magnitude and phase.

Recall that the dominant scatterer of a dismount is his torso, or body. From Boulic, et al, we can derive the model for the body forward/backward velocity departures about the mean while walking to be sinusoidal, that is

$$\Delta v_{body}(t) = \frac{4\pi A_a}{T_{cycle}} \sin\left(2\pi \frac{2}{T_{cycle}} t \right), \tag{32}$$

where

$$\begin{aligned} A_a &= 0.021 \text{ for walking speeds greater than 0.5 m/s or so.} \\ T_{cycle} &= \text{time between strikes of the left heel.} \end{aligned} \tag{33}$$

Both of these parameters are dependent to some degree on walking speed and person height. Note that the velocity is constantly changing about its mean value. This means that the Doppler frequency of the echo from the body is changing, too, in proportion to the velocity change. The velocity in the neighborhood of its fastest change rate is approximated by using the small angle formula

$$\Delta v_{body}(t) = A_a \left(\frac{4\pi}{T_{cycle}} \right)^2 t \, . \tag{34}$$

The maximum Doppler change over some interval Δt is then calculated to be

$$\Delta f_{Doppler} = \left(\frac{2}{\lambda} \right) A_a \left(\frac{4\pi}{T_{cycle}} \right)^2 \Delta t \, . \tag{35}$$

We define coherence time as that time interval which causes the Doppler offset to change an amount equal to the Doppler resolution over that interval. This sets up the equation

$$\frac{a_{wd}}{T_{coherence}} = \left(\frac{2}{\lambda}\right) A_a \left(\frac{4\pi}{T_{cycle}}\right)^2 T_{coherence}. \tag{36}$$

where

a_{wd} = Doppler impulse response broadening factor. (37)

Solving for coherence time yields

$$T_{coherence} = \left(\frac{T_{cycle}}{4\pi}\right) \sqrt{\frac{a_{wd}}{A_a}\left(\frac{\lambda}{2}\right)}. \tag{38}$$

Note that the coherence time will depend on details of human anatomy, such as height, and also depend on walking speed. We refer the reader back to Boulic, et al., for details.

Example

For a human with height 1.67 m (5 ft. 6 in.) walking at 1 m/s, Boulic, et al., calculate T_{cycle} = 1.27 seconds, and A_a = 0.021 m. At Ku-band, and processing with $a_{wd} = 1.5$, we calculate $T_{coherence}$ = 81 ms.

We also note that a 1.81 m (6 ft.) tall person also walking at 1 m/s would calculate to $T_{coherence}$ = 84 ms. However, the 1.67 m tall person slowing their speed to 0.5 m/s would increase coherence time to $T_{coherence}$ = 114 ms.

As with vehicles, these calculations are no doubt also quite squishy. The principal message here is that a walking human will have a coherence time probably on the order of 100 ms or so. This is not to say that longer observation times aren't useful. Longer observations can be decomposed into time-frequency analysis to establish gaits, and perhaps ambulatory and/or anatomical details. However SNR improvement for CPIs longer than the coherence time will likely be less than otherwise expected due to the spreading in Doppler.

Lewis and Rigling[13] discuss an effort into 'focusing' the dismount energy, mainly from the torso, to collapse the energy into fewer resolution cells. This is essentially an 'autofocus' operation on an individual dismount. Their purpose was more to stabilize the target location rather than to increase SNR, and allow for finer Doppler resolution to facilitate micro-Doppler exploitation. Note also that different dismounts would need to be 'focused' differently.

2.5 Radar Geometry

Typically, the radar is specified to operate at a particular height, and over some range swath. The range is already overtly represented in the equation.

In addition, GMTI radar is often a Wide Area Search (WAS) sensor. This means that the radar is typically employed in a scanning mode. The scanning will limit the amount of time that a particular target is within the field of view of the antenna beam. As a consequence, scanning will place an upper limit on T_{CPI}.

We identify

$$T_{CPI} \leq \frac{\theta_{bwaz}}{\omega_{scan,az}}. \tag{39}$$

where

$$\begin{aligned} &\theta_{bwaz} \text{ = nominal antenna beamwidth, and} \\ &\omega_{scan,az} \text{ = azimuth angular scanning rate.} \end{aligned} \tag{40}$$

In spite of being possible, we will not expand this term in our SNR expression to overtly show the dependency on antenna beamwidth and scan rate.

While a detailed discussion is deferred to later in this report, we do mention here that radar geometry does have a large impact on the Minimum Detectable Velocity (MDV) for the GMTI radar, and how a line-of-sight velocity limit translates into a horizontal vehicle velocity on the ground.

2.6 SNR Losses and Noise Factor

The radar equation as presented notes several broad categories of SNR losses.

2.6.1 Signal Processing Losses

These include the SNR loss (relative to ideal processing gains) due to employing a window function. Recall that the window bandwidth (including its noise bandwidth) is increased somewhat. If window functions are incorporated in both dimensions (range and Doppler processing), then we incur a SNR loss typically slightly larger than the impulse response broadening factor, perhaps on the order of 1.5 dB for each dimension.

In particular, the range processing SNR loss due to using a window function can be mitigated by using a waveform with an autocorrelation function that already exhibits the desired sidelobe characteristics. One such class of waveforms are the Non-Linear FM (NLFM) waveforms.[14,15] This would save the typical 1.5 dB that is otherwise lost.

For specular targets we might also incorporate an additional 'straddling' loss due to a target not being centered in a resolution cell. This depends on the relationship of pixel spacing to resolution, also known as the oversampling factor, but might be as high as 3 dB.

2.6.2 Radar Losses

These include a variety of losses primarily over the microwave signal path, but doesn't include the atmosphere. Included are a power loss from transmitter power amplifier output to the antenna port, and a two-way loss through the radome. These are generally somewhat frequency dependent, being higher at higher frequencies, but major effort is expended to keep them both as low as is reasonably achievable. In the absence of more refined information, typical numbers might be 0.5 dB to 2 dB from TX amplifier to the antenna port, and perhaps an additional 0.5 dB to 1.5 dB two-way through the radome.

2.6.3 System Noise Factor

When this number is expressed in dB, it is often referred to as the system noise figure.

The system noise figure includes primarily the noise figure of the front-end Low-Noise Amplifier (LNA) and the losses between the antenna and the LNA. These both are a function of a variety of factors, including the length and nature of cables required, LNA protection and isolation requirements, and of course frequency. Frequency dependence is generally such that higher frequencies will result in higher system noise figures. For example, typical system noise figures for sub-kilowatt radar systems are 3.0 dB to 3.5 dB at X-band, 3.5 dB to 4.5 dB at Ku-band, and perhaps 6 dB at Ka-band.

2.6.4 Atmospheric Losses

Atmospheric losses depend strongly on frequency, range, and the nature of the atmosphere (particularly the weather conditions) between radar and target. Major atmospheric loss factors are atmospheric density, humidity, cloud water content, and rainfall rate. These conspire to yield a 'loss-rate' often expressed as dB per unit distance, that is very altitude and frequency dependent. The loss-rate generally increases strongly with frequency, but decreases with radar altitude, owing to the signal path traversing a thinner average atmosphere.

A typical radar specification is to yield adequate performance in an atmosphere that includes weather conditions supporting a 4 mm/Hr rainfall rate on the ground.

We identify the overall atmospheric loss as

$$L_{atmos} = 10^{\frac{\alpha R}{10}}, \tag{41}$$

where α = the two-way atmospheric loss rate in dB per unit distance.

Nominal two-way loss rates from various altitudes for some surface rain rates are listed in the following tables. While numbers listed are to several significant digits, these are based on a model and are quite squishy.[16,17]

Incorporating atmospheric loss-rate overtly into the radar equation, and rearranging a bit, yields

$$SNR_{image} = \frac{P_{avg} T_{CPI} \left(\eta_{ap}^2 A_A^2\right) \sigma_{ref} \left(\frac{f}{f_{ref}}\right)^n f^2}{(4\pi) c^2 (kTF_N)(L_{radar} L_r L_a) R^4 10^{\frac{\alpha R}{10}}}. \tag{42}$$

Implicit in the radar equation is that atmospheric loss-rate a depends on *f* in a decidedly nonlinear manner (and not necessarily even monotonic near specific absorption bands – of note are an H_2O absorption band at about 23 GHz, and an O_2 absorption band at about 60 GHz).

Table 2. Two-way loss rates (dB/km) in 50% RH clear air.

Radar Altitude (kft)	L-band 1.5 GHz	S-band 3.0 GHz	C-band 5.0 GHz	X-band 9.6 GHz	Ku-band 16.7 GHz	Ka-band 35 GHz	W-band 94 GHz
5	0.0119	0.0138	0.0169	0.0235	0.0648	0.1350	0.7101
10	0.0110	0.0126	0.0149	0.0197	0.0498	0.1053	0.5357
15	0.0102	0.0115	0.0133	0.0170	0.0400	0.0857	0.4236
20	0.0095	0.0105	0.0120	0.0149	0.0333	0.0721	0.3476
25	0.0087	0.0096	0.0108	0.0132	0.0282	0.0616	0.2907
30	0.0080	0.0088	0.0099	0.0119	0.0246	0.0541	0.2515
35	0.0074	0.0081	0.0090	0.0108	0.0218	0.0481	0.2214
40	0.0069	0.0075	0.0083	0.0099	0.0196	0.0434	0.1977
45	0.0064	0.0069	0.0076	0.0090	0.0176	0.0392	0.1774
50	0.0059	0.0064	0.0071	0.0083	0.0161	0.0360	0.1617

Table 3. Two-way loss rates (dB/km) in 4 mm/Hr (moderate) rainy weather.

Radar Altitude (kft)	L-band 1.5 GHz	S-band 3.0 GHz	C-band 5.0 GHz	X-band 9.6 GHz	Ku-band 16.7 GHz	Ka-band 35 GHz	W-band 94 GHz
5	0.0135	0.0207	0.0502	0.1315	0.5176	2.1818	8.7812
10	0.0126	0.0193	0.0450	0.1107	0.4062	1.7076	7.7623
15	0.0117	0.0175	0.0391	0.0920	0.3212	1.3311	6.4537
20	0.0106	0.0150	0.0314	0.0714	0.2453	1.0082	4.8836
25	0.0096	0.0132	0.0264	0.0584	0.1979	0.8108	3.9218
30	0.0088	0.0118	0.0228	0.0496	0.1662	0.6788	3.2796
35	0.0081	0.0107	0.0201	0.0431	0.1433	0.5838	2.8178
40	0.0074	0.0098	0.0180	0.0382	0.1259	0.5122	2.4701
45	0.0069	0.0089	0.0163	0.0342	0.1121	0.4558	2.1967
50	0.0064	0.0082	0.0149	0.0310	0.1012	0.4109	1.9793

Table 4. Two-way loss rates (dB/km) in 16 mm/Hr (heavy) rainy weather.

Radar Altitude (kft)	L-band 1.5 GHz	S-band 3.0 GHz	C-band 5.0 GHz	X-band 9.6 GHz	Ku-band 16.7 GHz	Ka-band 35 GHz	W-band 94 GHz
5	0.0166	0.0373	0.1531	0.4910	1.8857	7.3767	23.0221
10	0.0159	0.0347	0.1282	0.3829	1.4091	5.6330	21.0363
15	0.0146	0.0307	0.1060	0.3020	1.0738	4.3037	17.7448
20	0.0128	0.0249	0.0816	0.2289	0.8097	3.2377	13.3520
25	0.0113	0.0211	0.0665	0.1844	0.6459	2.5944	10.6964
30	0.0102	0.0184	0.0563	0.1546	0.5425	2.1651	8.9251
35	0.0093	0.0163	0.0488	0.1331	0.4658	1.8578	7.6569
40	0.0085	0.0147	0.0431	0.1169	0.4081	1.6269	6.7043
45	0.0078	0.0133	0.0386	0.1042	0.3630	1.4467	5.9604
50	0.0073	0.0122	0.0349	0.0940	0.3270	1.3027	5.3667

2.7 Other Useful Expressions and Observations

The radar equation comes in a plethora of versions based on different parameters. We begin with the expression

$$SNR_{image} = \frac{P_{avg} T_{CPI} \left(\eta_{ap}^2 A_A^2\right) \sigma_{ref} \left(\frac{f}{f_{ref}}\right)^n f^2}{(4\pi) c^2 (kTF_N)(L_{radar} L_r L_a) R^4 10^{\frac{\alpha R}{10}}}. \tag{43}$$

Another useful variant expression is

$$SNR_{image} = \left(\frac{P_{avg} G_A^2 \lambda^2 T_{CPI} \sigma_{ref}}{(4\pi)^3 (kTF_N) R^4}\right)\left(\frac{1}{L_{radar} 10^{\frac{\alpha R}{10}}}\right)\left[\frac{1}{L_r L_a}\right]\left[\frac{f}{f_{ref}}\right]^n. \tag{44}$$

Some useful observations include

- PRF can be traded for pulse width to keep P_{avg} constant.
- SNR does not depend on range resolution (for a point target).
- SNR does depend on Doppler resolution. Finer Doppler resolution requires larger T_{CPI}, which improves SNR.
- There is no SNR overt dependence on grazing angle, although σ_{ref} itself may exhibit some dependence on grazing angle as previously discussed, and atmospheric loss depends on height and range.
- Input Noise bandwidth B_N has no direct effect on ultimate image SNR. Signal bandwidth does not explicitly impact SNR directly, but rather through a looser dependence on perhaps L_r.

2.8 Grouping Parameters due to Geometry, Hardware, and Processing

Influential parameters can be divided into three principal categories, namely

1. Radar operating geometry,
2. Radar hardware limitations, and
3. Radar signal processing.

We now examine the radar equation with respect to these categories. The Radar Equation in the previous development can easily be manipulated to be

$$SNR_{image} = \frac{P_{avg} G_A^2 \lambda^2 T_{CPI} \sigma}{(4\pi)^3 (kTF_N) R^4 L_{radar} L_{atmos} L_r L_a}. \tag{45}$$

Rather than specifying the image SNR with respect to some target scene RCS, the radar equation for GMTI can be written in a manner that assumes that image SNR is unity for some target RCS. Indeed, the achievable 'Noise Equivalent' RCS can be calculated as

$$\sigma_N = \frac{\sigma}{SNR_{image}} = \frac{(4\pi)^3 (kTF_N) R^4 L_{radar} L_{atmos} L_r L_a}{P_{avg} G_A^2 \lambda^2 T_{CPI}}. \tag{46}$$

This is an analogous measure to Noise Equivalent Reflectivity for SAR systems. It recognizes that building a radar to achieve 20 dB SNR for a 0 dBsm RCS target is the same radar to achieve 15 dB SNR for a −5 dBsm RCS, or a 30 dB SNR for a +10 dBsm RCS. Specific thresholds for SNR or RCS depend on processing choices. What is achievable depends on their ratio as allowed by the underlying data. Generally, this 'Noise Equivalent' RCS number is desired to be as low as possible.

To facilitate the subsequent discussion, we may rewrite this equation with parameters grouped as

$$\sigma_N = 64\pi^3 kT \left(\frac{R^4}{T_{CPI}} \right) \left(\frac{F_N L_{radar} L_{atmos}}{P_{avg} G_A^2 \lambda^2} \right) (L_r L_a). \tag{47}$$

The parameters preceding the parentheses are constants that will not be discussed any further.

Radar operating geometry

The first set of parameters $\left(R^4/T_{CPI}\right)$ deal with the radar platform's physical relationship with respect to the target scene. This is about where the radar is and what it is looking at. These parameter are important to the radar designer as it certainly impacts the needed functionality of the hardware design, in particular timing and control, but otherwise is not controllable by the radar hardware designer.

We have included T_{CPI} here because it is often limited by scanning rates, which is of course a dynamic geometry thing.

Radar hardware limitations

The second set of parameters $\left(F_N L_{radar} L_{atmos}\right)/\left(P_{avg} G_A^2 \lambda^2\right)$ deal with radar hardware limitations. These need to be selected by a hardware designer based on the limitations of radar geometry and environment, but mindful of the needs of the radar signal processing. The purpose of the hardware is to provide usable data to the signal processor, but otherwise cannot control how the signal processor chooses to specifically process the data into an image.

Radar wavelength λ is a fundamental parameter of the hardware. The antenna gain G_A is normally fixed by its construction. The transmitter is limited by its hardware to some maximum P_{avg}, although it may be specified via a maximum peak transmitter power with some maximum duty factor. The radar duty factor, in turn, is proportional to both radar PRF and pulse width. Some radar geometries may affect allowable duty factors and hence P_{avg}, but achievable P_{avg} under these circumstances is still a radar hardware design limitation. The receiver will also exhibit some noise figure F_N that is a function of its construction.

Hardware system losses are embodied in L_{radar}. The atmospheric propagation loss L_{atmos} is a function of geometry, but is also a function of the radar operating wavelength λ. More commonly, a weather model is specified for the radar that is wavelength independent (e.g. clear air, or must accommodate 4 mm/Hr rain, etc.) When a weather model is specified, in addition to the geometry, then the radar designer does have some control over the specific value for L_{atmos} via selecting the radar wavelength.

Radar signal processing

The third set of parameters $(L_r L_a)$ deal with signal processing issues in the image formation processor. Fundamental limits exist within the data on achievable σ_N. These can, of course, always be made worse with signal processing, but not better than the hardware-limited data can support.

The nature of range sidelobe filtering will coarsen range resolution by the factor a_{wr}, and reduce the range processing gain with respect to ideal matched filtering by a factor L_r. Similarly, the nature of Doppler sidelobe filtering will coarsen azimuth resolution by the factor a_{wa}, and reduce the azimuth processing gain with respect to ideal matched filtering by a factor L_a.

3 Performance Issues

What follows is a discussion of several issues impacting performance of a GMTI radar.

3.1 Relating SNR to Probabilities

A comprehensive discussion relating Probability of Detection and Probability of False Alarm to SNR is given in Appendix B. We provide a brief summary here.

Generally, GMTI processing will be coherent processing. Consequently, SNR gain will be coherent processing gain. The minimum SNR after coherent processing, and assuming no non-coherent integration, and before any envelope detection, is then required to be

$$SNR_{\text{coherent}} = \left(\sqrt{-\ln(P_{FA})} - \frac{Q^{-1}(P_D)}{\sqrt{2}} \right)^2 , \tag{48}$$

where the relevant desired probabilities are

$$\begin{aligned} P_D &= \text{Probability of Detection,} \\ P_{FA} &= \text{Probability of False Alarm.} \end{aligned} \tag{49}$$

The Probability of Detection (P_D) is the likelihood of detecting a target that is present. The Probability of False Alarm (P_{FA}) is the likelihood of declaring a detection when no target is present.

We also identify the Inverse Q function as

$$Q^{-1}(w) = z \tag{50}$$

in terms of the Normal Q function, such that $w = Q(z)$, where

$$Q(z) = \int_z^\infty \frac{1}{\sqrt{2\pi}} e^{-\frac{x^2}{2}} dx . \tag{51}$$

The Normal Q function is discussed in some more detail in Appendix C.

The Probability of False Alarm is more often expressed as a False Alarm Rate (FAR). These are related for coherent processing by

$$P_{FA} \approx f_{FA}\left(\frac{\rho_r}{f_p D_r}\right) \tag{52}$$

where

f_{FA} = False Alarm Rate,
ρ_r = range resolution,
D_r = range swath,
f_p = radar PRF. (53)

The FAR metric, though very common, is somewhat problematic, especially when comparing different radar systems. This is discussed in more detail in Appendix F.

In any case, with SNR_{coherent} defined as above for some minimum P_D and maximum P_{FA}, we then require

$$SNR_{\text{image}} \geq SNR_{\text{coherent}} \,. \tag{54}$$

We do note that we have made the tacit assumption here that f_p is constant for the period over which f_{FA} is measured. In GMTI systems that collect CPIs with 'breaks' between the CPIs, this would need to be modified somewhat to account for the CPI 'duty cycle'.

3.2 Optimum Frequency

For this report, the optimum frequency band of operation is that which yields the maximum SNR in the image for the targets of interest.

For constant average transmit power, constant antenna aperture, constant CPI time, constant velocity, and constant system losses, the SNR in the range-Doppler map is proportional to

$$SNR_{image} \propto f^{(n+2)} 10^{\frac{-\alpha R}{10}}. \tag{55}$$

where atmospheric loss rate α also depends on frequency (generally increasing with frequency as previously discussed). Clearly, for any particular range R, some optimum frequency exists to yield a maximum SNR in the image.

Additionally, the optimum frequency will depend somewhat on the RCS characteristic of the target, that is, the frequency dependence n. A pickup truck with a strong trihedral characteristic due to its bed interior may exhibit an $n = 2$ characteristic, whereas a different target with no dominant scatterer will look more distributed in its reflection characteristic, and exhibit perhaps something more like an $n = 1$ characteristic.

Figure 2 through Figure 5 indicate the relative SNR in the GMTI range-Doppler image as a function of slant-range for various frequency bands.

We note that 1 nmi (nautical mile) = 1.852 kilometers, and 1 kft = 304.8 meters. Furthermore, 1 kt = 0.514444 m/s approximately.

In summary, for a constant real antenna aperture size, antenna gain increases with frequency, as does brightness of the target (at least for simple targets). However, as range increases, atmospheric losses increase correspondingly and more so at higher frequencies, eventually overcoming any advantage due to antenna gain and target brightness. Consequently, for any particular atmosphere, radar height and range, there exists an optimum frequency band for GMTI operation. Generally, as range increases and/or weather gets worse, lower frequencies become more attractive. We do note that the target RCS brightness can be a fairly complicated function of frequency, and will depend on the environment within which we wish to detect it, but this is difficult to account for in comparative trade studies, driving us to use simpler models for RCS frequency dependence. Optimal GMTI frequencies for a typical weather specification are illustrated in Figure 6.

It should be noted that other reasons (besides optimal SNR) may exist for choosing a particular radar band for operation (e.g. spectral compatibility, pre-existing hardware, hardware availability, ATR template compatibility, program directive, etc.). We also recall that for some targets, a lower frequency may allow a longer target coherence time.

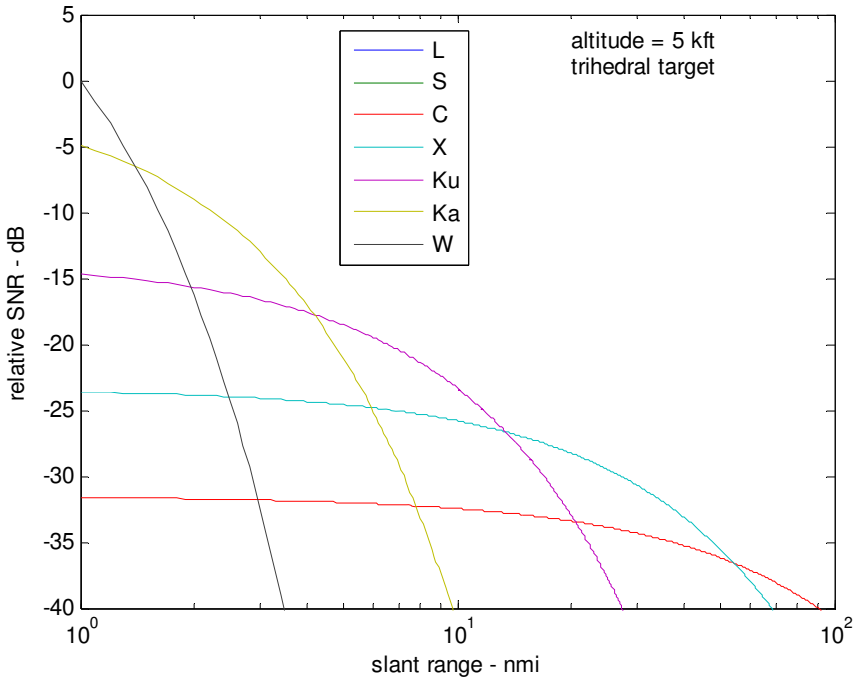

Figure 2. GMTI relative performance of radar bands as a function of range (4 mm/Hr rain, 5 kft altitude, n=2).

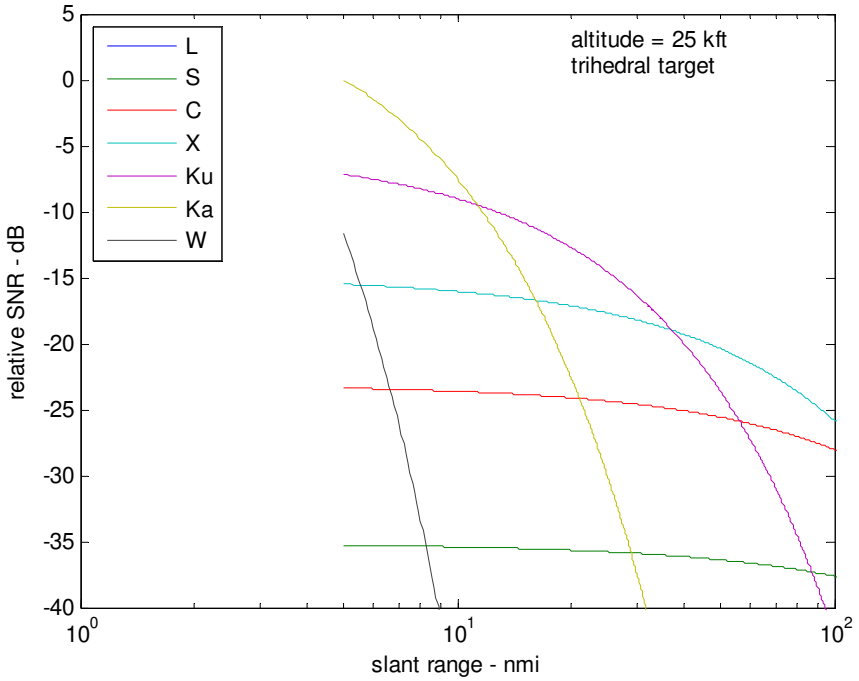

Figure 3. GMTI relative performance of radar bands as a function of range (4 mm/Hr rain, 25 kft altitude, n=2).

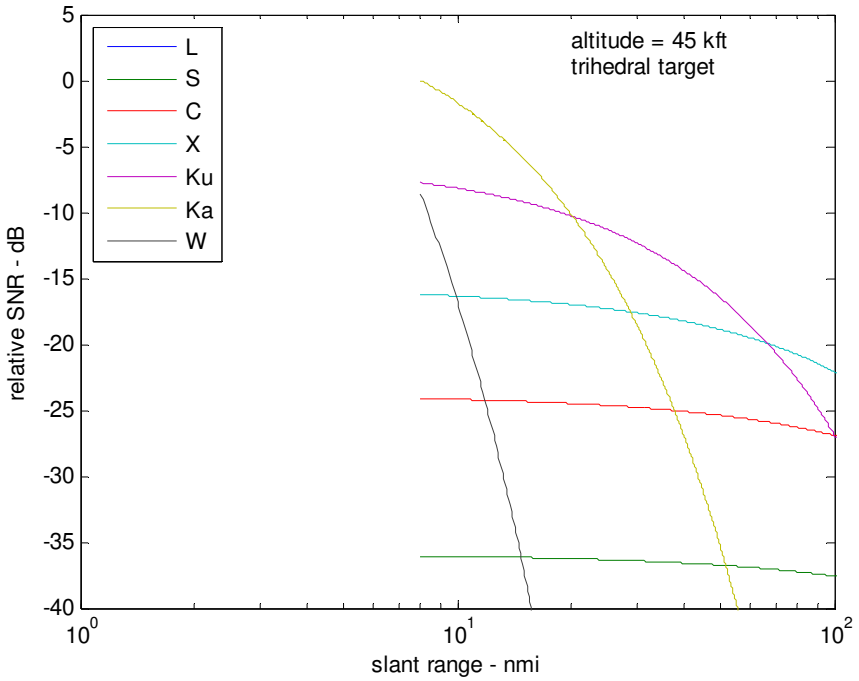

Figure 4. GMTI relative performance of radar bands as a function of range (4 mm/Hr rain, 45 kft altitude, n=2).

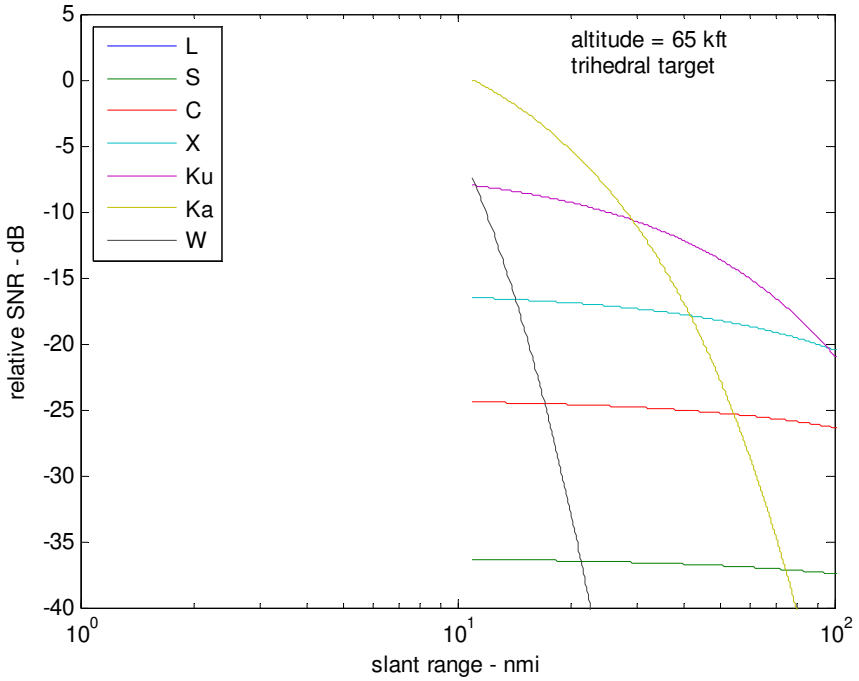

Figure 5. GMTI relative performance of radar bands as a function of range (4 mm/Hr rain, 65 kft altitude, n=2).

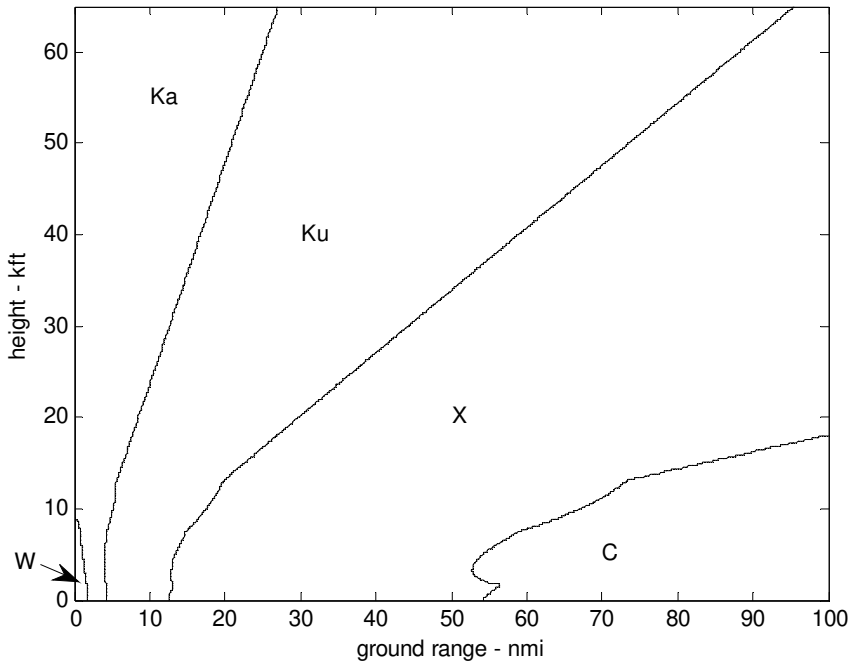

Figure 6. Optimum GMTI radar band as a function of range and altitude (4mm/Hr rain, n=2, constant antenna aperture area).

3.3 Unambiguous Range

Typical operation for terrestrial search radars is to send out a pulse and receive the expected echoes before sending out the subsequent pulse. This places constraints on range vs. velocity measurements for the GMTI radar, otherwise significantly complicating the radar design and operation.

There is a fundamental trade in pulse-Doppler radar systems involving radar PRF. For a given PRF, there is a maximum unambiguous Doppler frequency, hence target closing velocity. For the same PRF there is a maximum unambiguous range. As PRF increases, unambiguous velocity increases, but unambiguous range decreases. Likewise, as PRF decreases, unambiguous velocity decreases, but unambiguous range increases.

We continue with the presumption that the effective pulse width of the SAR is equal to the actual transmitted pulse width. For matched-filter pulse compression this is the case, and for 'stretch' processing (deramping followed by a frequency transform) this is nearly the case and more so for small range swaths compared with the pulse width.

By insisting that the echo return before the subsequent pulse is emitted, we insist that

$$\left(T_{eff} + \frac{2}{c}R\right) \le \frac{1}{f_p} \tag{56}$$

which can be manipulated to

$$R \le \frac{c(1-d)}{2f_p}. \tag{57}$$

The maximum R that satisfies this expression is often referred to as the 'unambiguous range' of the radar. Note the dependence on duty factor, d.

Assuming that positive and negative closing velocities are equally likely, then a constraint on unambiguous line-of-sight velocity can be calculated as

$$|v_{los}| \le \frac{f_p \lambda}{4}. \tag{58}$$

These constraints can be combined to yield the constraint for unambiguous operation (both range and velocity) of

$$|v_{los}| \le \frac{\lambda c(1-d)}{8R}. \tag{59}$$

Figure 7 plots unambiguous range vs. unambiguous velocity for several duty factors and radar bands.

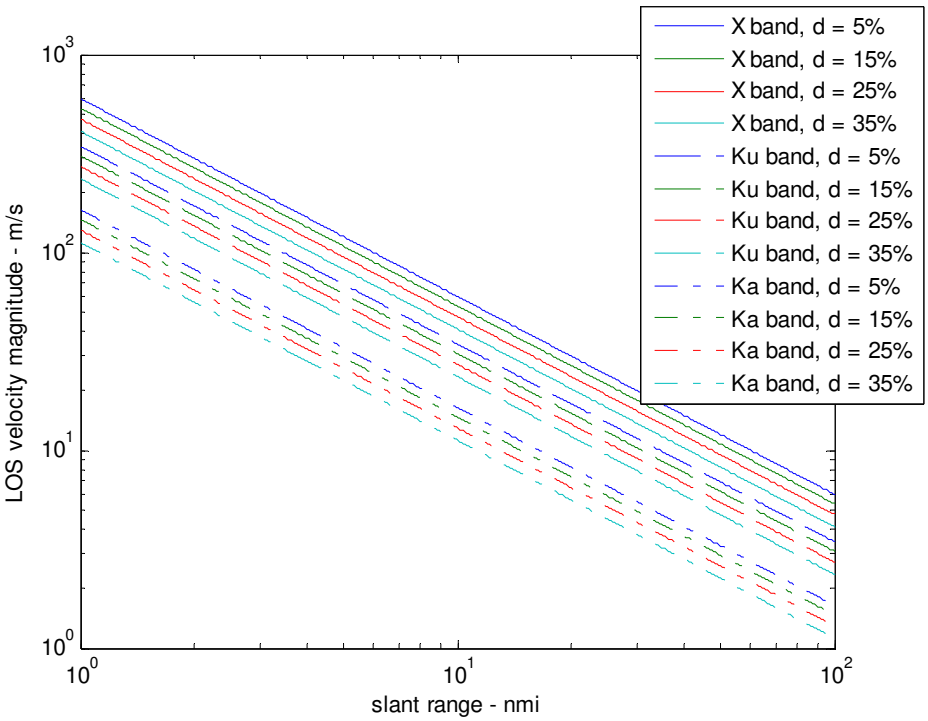

Figure 7. Unambiguous velocity vs. range limits.

Clearly, we can sacrifice unambiguous velocity to enhance range. This is done by selecting the appropriate radar PRF. However, we need to remember that this also moves the inherent 'blind' velocities as well.

If we need to work in the parameter space beyond the unambiguous range vs. unambiguous velocity curves, then we need to either move the curve (by appropriately modifying the radar frequency or duty factor), or we need to operate with pulses 'in the air', that is, transmitting new pulses before the expected arrival of a previous pulse's echo. This is entirely possible and is in fact routine in some radar systems. Ambiguities are resolved by appropriate phase coding or multiple-PRF schemes.

3.4 Extending Range

Extending the range of a GMTI radar is equivalent to

1) ensuring that an adequate SNR is achievable at the new range of interest, and

2) ensuring that the unambiguous range constraint is adequately dealt with.

The unambiguous range issue was addressed in the last section. Here we address methods for increasing SNR at some range of interest.

We begin by writing the expression for SNR in the range-Doppler map as

$$SNR_{image} = \frac{P_{avg} G_A^2 \lambda^2 T_{CPI} \sigma}{(4\pi)^3 (kTF_N) L_{radar} L_r L_a} \left(R^{-4} 10^{\frac{-\alpha R}{10}} \right). \tag{60}$$

Note that SNR falls off as something greater than the 4th power of range.

This can be solved for noise equivalent RCS to yield

$$\sigma_N = \frac{(4\pi)^3 (kTF_N) L_{radar} L_r L_a}{P_{avg} G_A^2 \lambda^2 T_{CPI}} \left(R^4 10^{\frac{\alpha R}{10}} \right). \tag{61}$$

A discussion of increasing range for a particular noise equivalent RCS needs to examine how we can reduce the noise equivalent RCS to offset the effects of increasing range.

3.4.1 Increasing Average TX Power

We recall that the average TX power is the product of the peak TX power and the duty factor of the radar. Obviously we can increase the average power by increasing either one of these constituents, as long as it is not at the expense of the other. For example, a 100-W power amplifier operating at 30% duty factor is still better than a 200-W power amplifier operating at only a 10% duty factor, as far as SNR is concerned.

For a given TX power amplifier operating at full power, all we can do is ensure that we are operating at or near its duty factor limit. Since

$$P_{avg} = P_t d = P_t T_{eff} f_p \tag{62}$$

this is accomplished by increasing either or both the pulse width T_{eff} and the radar PRF f_p. If the radar PRF is constrained by an unambiguous range requirement, then the pulse width must be extended.

For GMTI radars employing stretch processing (generally required for High-Range-Resolution (HRR) modes) we identify

$$T_{eff} = \frac{I}{f_s} \tag{63}$$

where

I = the total number of (fast-time) samples collected from a single pulse, and
f_s = the ADC sampling frequency employed.

We note that to satisfy Nyquist criteria using quadrature sampling,

$$f_s \geq B_{IF} \tag{64}$$

where B_{IF} is the IF bandwidth of the radar.

Consequently, increasing the pulse width requires either collecting more samples I, or decreasing the ADC sampling frequency f_s (and the corresponding IF filter bandwidth B_{IF}).

Two important issues need to be kept in mind, however. The first is that extending the pulse width restricts the nearest range that the radar can image. That is, the TX pulse has to end before the near range echo arrives. The second is that the number of samples I restricts the range swath of the range-Doppler map to $(B_{IF}/f_s)I$ resolution cells. The consequence to this is that relatively wide swaths at near ranges requires lots of samples I at very fast ADC sampling rates with corresponding wide IF filter bandwidths.

At far ranges, where near-range timing is not an issue, for a fixed IF filter bandwidth and ADC sampling frequency, we can always increase pulse width by collecting more samples I. If operating near the unambiguous range, however, prudence dictates that we remain aware that increasing the duty factor does in fact reduce the unambiguous range somewhat.

Operating beyond the unambiguous range limit requires a careful analysis of the radar timing in order to maximize the duty factor, juggling a number of additional constraints. It's enough to make your head spin.

Stretch processing derives no benefit from a duty factor greater than about 50%. A reasonable limit on usable duty factor due to other timing issues is often in the neighborhood of about 35%.

In any case, the easiest retrofit to existing radars for increasing average TX power (and hence range) are first to increase the PRF to the maximum allowed by the timing, and second to increase the pulse width, with a corresponding increase in number of samples collected.

Furthermore, we note that at times it may be advantageous to shorten the pulse and increase the PRF, even if it means operating with pulses in the air (beyond the reduced unambiguous range), just to increase the duty factor. This is particularly true when the hardware is limited in how long a pulse can be transmitted.

In any case, doubling P_{avg} would allow increasing range by less than 19% even in clear weather.

3.4.2 Increasing Antenna Area

A bigger antenna (in either dimension) and/or better efficiency will yield improved SNR.

A larger elevation dimension will, however, reduce the illuminated swath width.

A larger azimuth dimension will also have the positive effect of narrowing the azimuth antenna beam width, thereby facilitating more accurate and precise target bearing determination, that is, target location. We note that although good for GMTI, in a SAR system this will limit stripmap resolutions to coarser azimuth resolutions.

However, for a fixed angular scanning rate, and fixed PRF, a narrower beam will allow lesser number of pulse echoes to be collected, reducing Doppler and velocity resolution.

In any case, doubling the antenna area would allow increasing range by 41% in clear weather, and something less in adverse weather.

3.4.3 Selecting Optimal Frequency

As previously discussed, there is a clear preference for operating frequency depending on range, altitude, and weather conditions. For example, at a 50-nmi range from a 25-kft AGL altitude with 4 mm/Hr rain, X-band offers a 3.2 dB advantage over Ku-band. For perspective, a 1-kW Ku-band amplifier would provide performance equivalent to a 480-W X-band amplifier (for the same real antenna aperture, efficiency, CPI time, yadda, yadda, yadda....).

Choice of operating frequency does need to be tempered, however, by the factors noted earlier in this report.

Interestingly, there may even be significant differences within the same radar band. For example, at 25 kft AGL altitude, we can compare the top and bottom edges of the international Ku-band (15.7 GHz to 17.7 GHz). At 10 nmi, the top edge achieves a 1 dB advantage. Parity is achieved at 20 nmi. Thereafter the bottom edge yields better SNR. The bottom edge advantage is 1.4 dB at 30 nmi, 2.5 dB at 40 nmi, 3.7 dB at 50 nmi, and 9.4 dB at 100 nmi. Clearly, it seems advantageous to operate as near to the optimum frequency as the hardware and frequency authorization allow.

3.4.4 Modifying Operating Geometry

Once above the water-cloud layer, increasing the radar altitude will generally yield reduced average atmospheric attenuation, and hence improved transmission properties for a given range. Consequently, SNR is improved with operation at higher altitudes for any particular typical weather condition.

This translates to increased range at higher altitudes.

3.4.5 Longer CPI Time

Noise equivalent RCS is inversely proportional to the CPI time, T_{CPI}. Larger CPI times allow for larger SNR, and hence longer range.

Figure 8 illustrate a Ku-band example of how range-performance in both clear air and adverse weather depends on CPI times. Acceptable SNR performance is achievable to the left of the contours corresponding to a particular CPI time. Figure 9 corresponds to X-band with noise equivalent RCS adjusted for the difference in frequencies, assuming a square-law relationship.

Although noise equivalent RCS is reduced, the 'goodness' of this presupposes that the SNR for a target is thereby also increased. This in turn presupposes that the target itself remains coherent for the longer CPI time. However, many (if not most) targets have a finite coherence time. Exceeding this time will cause the target to spread in Doppler instead of 'peaking up' with improved SNR. Consequently, an understanding of target characteristics is crucial to proper GMTI performance prediction.

3.4.6 Decreasing Radar Losses, Signal Processing Losses, and System Noise Factor

Any reduction in system losses yields a SNR gain of equal amount. This is also true of reducing the system noise factor. For example, reducing the TX amplifier to antenna loss by 1 dB translates to a 1-dB improvement in SNR. Likewise, a 2-dB reduction in system noise factor translates to a 2-dB improvement in SNR.

We note that high-power devices such as duplexers, switches, and protection devices tend to be lossier than lower power devices. Consequently, doubling the TX power amplifier output power might require lossier components elsewhere in the radar, rendering less than a doubling of SNR in the image. Furthermore, high-power microwave switches tend to be bulkier than their low-power counterparts, requiring perhaps longer switching times which may impact achievable duty factors.

As previously stated, the range processing loss due to window functions for sidelobe control can be eliminated by using appropriate waveforms, such as NLFM chirps.

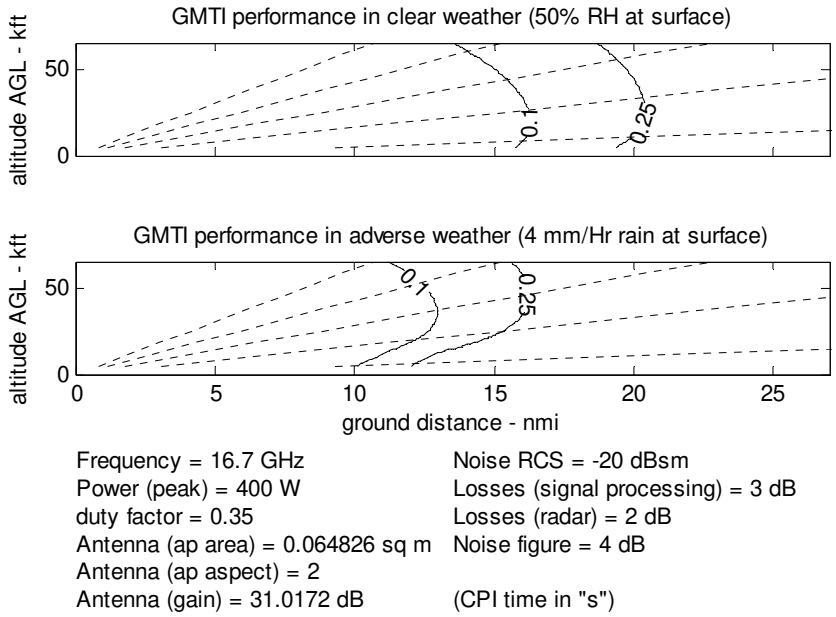

Figure 8. Geometry limits vs. resolution. Contours are CPI times in seconds.

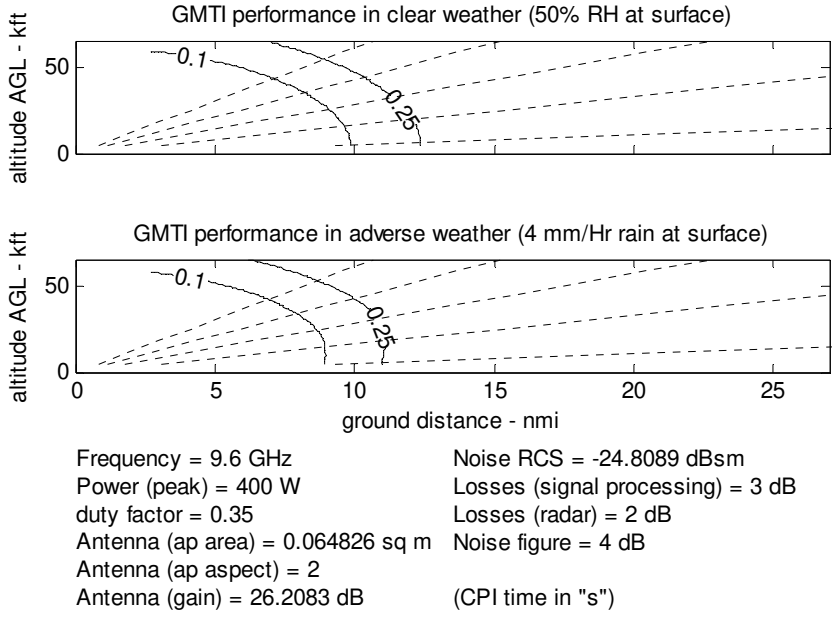

Figure 9. Geometry limits vs. resolution. Contours are CPI times in seconds.

3.4.7 Easing Weather Requirements

Atmospheric losses are less in fair weather than in inclement weather. Consequently SNR is improved (and range increased) for a nicer atmosphere. In real life you get what you get in weather, although a data collection might make use of weather inhomogeneities (like choosing a flight path or time to avoid the worst conditions).

Weather attenuation models are very squishy (of limited accuracy) and prone to widely varying interpretations. Consequently, GMTI performance claims might use this to advantage (and probably often do). The point of this is that while requests for proposals often contain a weather specification/requirement (e.g. 4 mm/Hr rain over a 10 nmi swath), there is no uniform interpretation on what this means insofar as attenuation to radar signals.

3.4.8 Changing Reference Noise Equivalent RCS

This is equivalent to the age-old technique of "If we can't meet the spec, then change the spec."

We note that a radar that meets a requirement for $\sigma_N = -20$ dBsm at some range, will meet a $\sigma_N = -15$ dBsm at some farther range. This is illustrated in Figure 10. SNR performance tends to degrade gracefully with range, consequently a tolerance for poorer GMTI performance will result in longer range operation. Poorer GMTI performance in this regard means lower P_D for small RCS and higher P_{FA} for a given threshold.

Depending on what we might be looking for, data exhibiting a significantly higher noise equivalent RCS can still be quite usable. For example searching for vehicles might allow for a higher noise equivalent RCS than searching for dismounts.

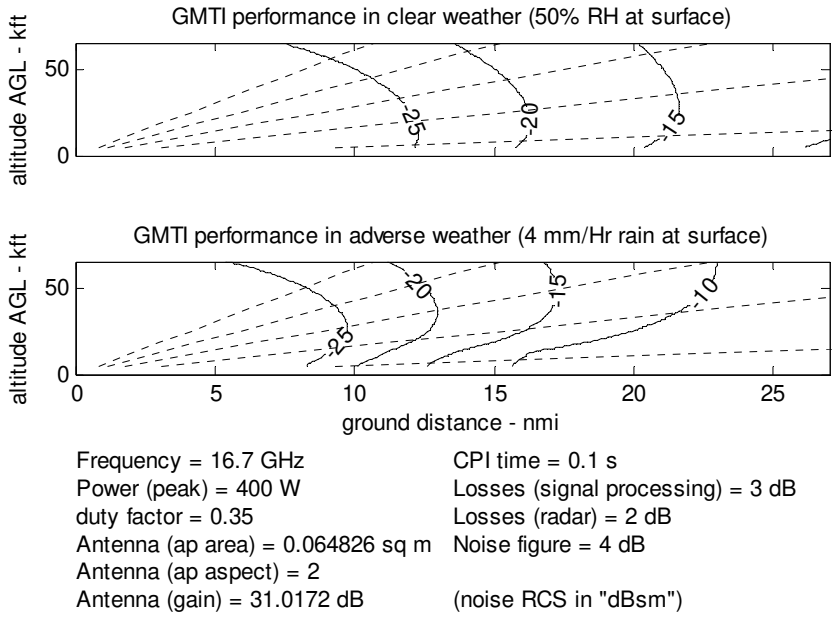

Figure 10. Geometry limits vs. noise equivalent RCS. Contours are noise equivalent RCS in dBsm.

3.5 Other Noise

The analysis in this report assumes that the only 'noise' that obfuscates the signal detection is system 'thermal' noise. This is the black-body radiation received by the antenna and supplemented by similar component noise in the radar itself, accounted for via the Noise Figure.

Other 'noise' signals do exist in the radar, and can often be quite problematic, so much so that radar performance can be seriously degraded. These other noise sources often exhibit characteristics that are decidedly non-Gaussian, and non-white. The typical undesired result is an elevated False Alarm Rate. However, Probability of Detection can also suffer.

Such sources include, but are not limited to

Additive spurious signals (internal EMI)
External EMI
Multiplicative noise
Antenna sidelobe leakage
System RF channel nonlinearities
System I/Q imbalance
ADC Integral and Differential Nonlinearities
ADC Quantization Noise

Of course there are also a myriad of things in the processing that can screw things up, too.

Typically, limits for these noise sources are far more stringent for GMTI modes than for other radar modes like SAR. This is because target detection is competing with the noise floor for exo-clutter GMTI, whereas for SAR the issue is competition with clutter, which may be well above the noise floor, and usually is the case by design. Ideally, for GMTI the problematic noise elements are driven to below the thermal noise floor. Designing a 'good' GMTI system requires great care.

4 Detectable Velocities

This report concerns itself with Exo-clutter GMTI performance. We now discuss the nature of the "exo-clutter" region.

Consider the geometry in Figure 11.

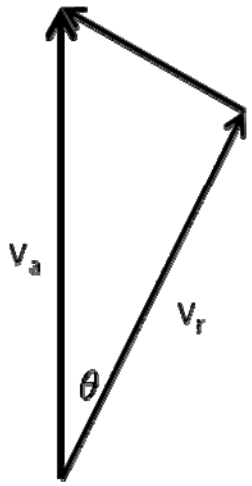

Figure 11. Relationship of aircraft velocity to radial (line of sight) velocity.

We define

$$\begin{aligned} v_a &= \text{aircraft velocity,} \\ v_r &= \text{radial velocity in direction of interest, and} \\ \theta &= \text{angle offset from aircraft velocity vector.} \end{aligned} \tag{65}$$

These are related as

$$v_r = v_a \cos\theta \,. \tag{66}$$

The radar antenna effectively applies a spatial filter that only interrogates a specific solid angle of directions, depending on where it is pointed. Consequently, stationary clutter within that set of directions will manifest as energy over a spread of velocities. This defines the 'clutter ridge' or 'clutter band' in a range-Doppler map.

4.1 Doppler Spectrum of Clutter

Doppler shift (more properly the increase due to a scaling) is calculated as

$$f_d = \frac{2}{\lambda} v_r , \tag{67}$$

where

$$\lambda \text{ = the wavelength of the radar waveform.} \tag{68}$$

The clutter Doppler spectrum is then the spread of the Doppler frequencies that the clutter generates, namely

$$B_{d,clutter} = \left(f_{d,clutter,\max} - f_{d,clutter,\min} \right) = \frac{2}{\lambda} \left(v_{r,clutter,\max} - v_{r,clutter,\min} \right), \tag{69}$$

where

$$\begin{aligned} &f_{d,clutter,\max} \text{ = most positive Doppler shift due to clutter due to } v_{r,clutter,\max}, \\ &f_{d,clutter,\min} \text{ = most negative Doppler shift due to clutter due to } v_{r,clutter,\min}, \\ &v_{r,clutter,\max} \text{ = maximum approaching velocity of observable clutter, and} \\ &v_{r,clutter,\min} \text{ = maximum receding velocity of observable clutter.} \end{aligned} \tag{70}$$

At Ku-band, λ = 0.018 m, so

$$B_{d,clutter,Ku} = 111 \times \left(v_{r,clutter,\max} - v_{r,clutter,\min} \right). \tag{71}$$

The Doppler band containing significant clutter energy is termed the endo-clutter region. The Doppler region containing no significant clutter energy is termed the exo-clutter region.

The key point here is that even stationary clutter will exhibit non-uniform relative motion to a GMTI radar, if the radar itself is in motion. Consequently, stationary clutter will manifest energy over a band of Doppler frequencies. This clutter band is generally unusable for an exo-clutter GMTI radar in detecting targets moving with respect to the clutter.

A final point here is that the clutter Doppler spectrum, indeed the nature of the range-Doppler map, is substantially dependent on the target scene topography. This is discussed in detail in another report.[18]

4.2 Minimum Detectable Velocity (MDV)

A moving target will generate Doppler contributions by two mechanisms. These are

1. The physical location with respect to the radar, and

2. The target's own radial velocity.

For an exo-clutter GMTI system, for the moving target to become distinguishable and detectable, its velocity must be outside the Doppler spectrum of the stationary clutter. For a moving target at the presumed azimuthal center of the antenna beam, the amount of radial velocity that shifts its energy to the exo-clutter region is termed the Minimum Detectable Velocity (MDV). There are some key points to be made about this.

- The MDV for an exo-clutter GMTI system identifies the nominal boundary between the exo-clutter and endo-clutter regions of velocity or Doppler space.

- The nominal antenna beamwidth is often quoted as equal to the one-way –3 dB width. The angular region that is not useable for exo-clutter detection is often greater than the typical nominal –3 dB antenna azimuth beamwidth, to allow for antenna beam roll-off beyond the nominal edge.

- The MDV is not necessarily the lowest velocity that can be detected. Recall that the MDV presumes that the target is at the azimuthal center of the antenna beam. If a closing target is physically located near the positive Doppler edge of the clutter band, then only a slight increase in its closing velocity due to its own motion (less than the MDV) will cause its echo energy to move into the exo-clutter region.

- Targets with radial velocity greater than the MDV are not guaranteed to be detectable. For example, if a receding target is physically located near the positive Doppler edge of the clutter band, then a receding velocity will need to be larger than the MDV to cause its echo energy to move to the exo-clutter region.

- The MDV calculation is for radial velocity in 3D space, which for an airborne radar is always less than a ground target vehicle's horizontal velocity, regardless of bearing.

- For non-broadside squint angles and non-forward squint angles, the clutter region in Doppler is not symmetric with respect to the antenna beam azimuth center line. The MDV for receding targets may be quite different than the MDV for approaching targets.

- The MDV that GMTI processing must assume also relies somewhat on the accuracy with which the antenna can be pointed, or at least the accuracy with which the antenna pointing is known.

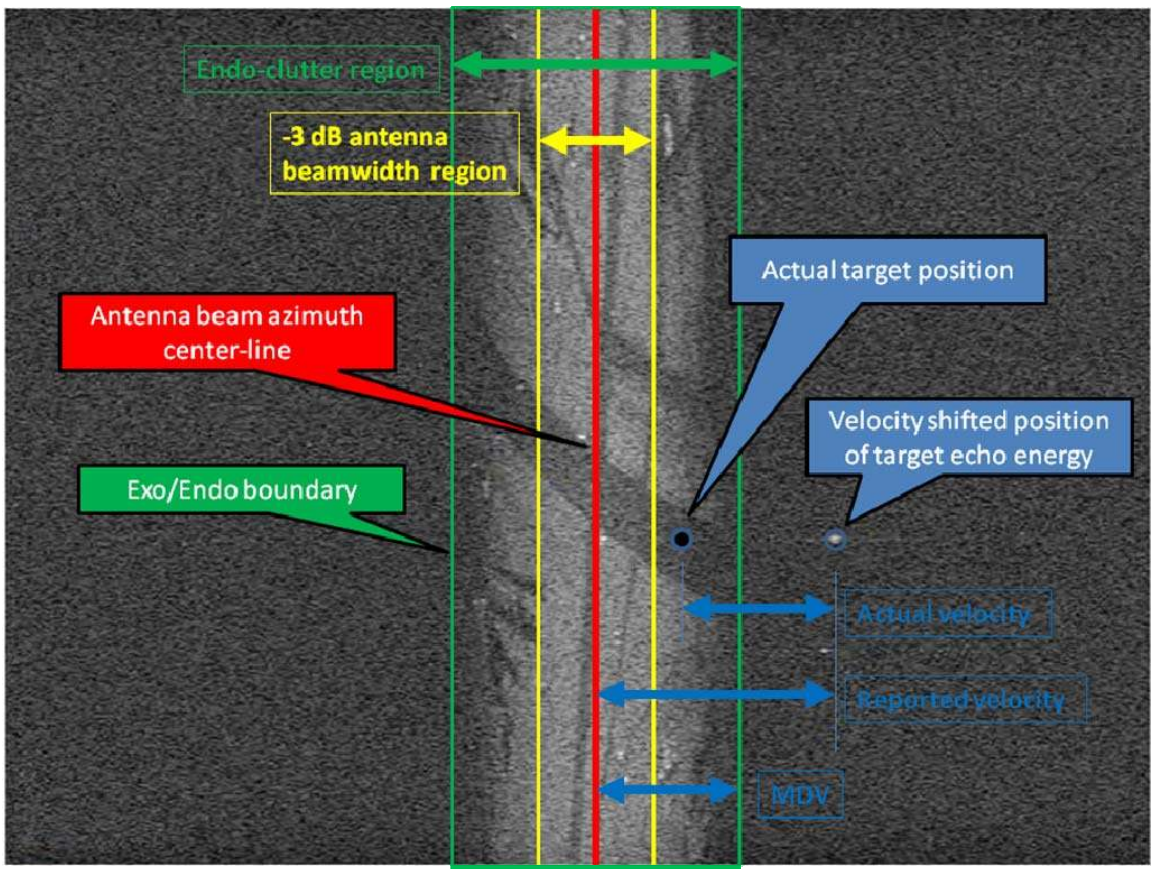

Figure 12. Range-Doppler map showing relationship between various GMTI parameters and measures. Data was collected at broadside geometry.

A number of these concepts are illustrated in Figure 12.

We will proceed to develop expressions for MDV, distinguishing between approaching and receding moving targets. We begin by defining the following

θ_s = squint angle of antenna beam azimuthal center in the horizontal plane,
θ_{pe} = antenna beam maximum pointing error magnitude (always positive), and
$K_{exoclutter}$ = the exo/endo-clutter boundary factor. (72)

We further elaborate that $K_{exoclutter}$ is the ratio of the exo/endo clutter boundary distance from the beam center, to half the nominal (typically the one-way –3 dB) azimuth beamwidth. A typical number is $K_{exoclutter} = 3$.

We begin by defining two angles as namely

$$\varphi_{fore} \approx \max\left(|\theta_s| - K_{exoclutter} \frac{\theta_{bwaz}}{2\cos\psi} - \theta_{pe} \quad , \quad 0 \right), \text{ and}$$

$$\varphi_{aft} \approx \min\left(|\theta_s| + K_{exoclutter} \frac{\theta_{bwaz}}{2\cos\psi} + \theta_{pe} \quad , \quad \pi \right). \tag{73}$$

The forward MDV edge is then calculated as

$$MDV_{approach} \approx v_a \cos\psi \left(\cos\left(\varphi_{fore}\right) - \cos\left(|\theta_s|\right) \right). \tag{74}$$

The aftward MDV edge is then calculated as

$$MDV_{recede} \approx v_a \cos\psi \left(\cos\left(\varphi_{aft}\right) - \cos\left(|\theta_s|\right) \right). \tag{75}$$

We make the following important observations.

- A tacit assumption in this development is a flat target scene. This is embodied in using the same grazing angle ψ for all directions.
- We identify $MDV_{recede} \le 0$, and $MDV_{approach} \ge 0$.
- If we are squinted forward of broadside, then $\left|MDV_{recede}\right| > \left|MDV_{approach}\right|$. If we are squinted aft of broadside, then $\left|MDV_{approach}\right| > \left|MDV_{recede}\right|$.
- If we are squinted straight ahead, with $\theta_s = 0$, then $MDV_{approach} = 0$. Note that this does not depend on antenna beamwidth at all, or radar velocity.
- If we are squinted straight behind, with $|\theta_s| = \pi$, then $MDV_{recede} = 0$. Note that this also does not depend on antenna beamwidth at all, or radar velocity.
- MDV is a function of antenna azimuth beamwidth. As such, for a fixed real antenna aperture size, MDV decreases (in magnitude) with increasing radar center frequency.
- While these equations are useful for design, real-time calculations of explicit parameter values for a particular CPI need to take into consideration other factors, such as the actual velocity vector, terrain variations, etc.

A simplistic approach for an overall MDV is to select the largest magnitude of the two, that is

$$MDV = \max\left(\left|MDV_{approach}\right|, \left|MDV_{recede}\right| \right). \tag{76}$$

We illustrate these observations with a trio of examples.

Example 1

Consider a GMTI radar looking straight ahead and slightly down with the following parameters

$$\begin{aligned}
&\theta_s = 0 \text{ degrees,} \\
&\psi = 20 \text{ degrees,} \\
&v_a = 75 \text{ m/s,} \\
&\theta_{bwaz} = 3.2 \text{ degrees,} \\
&\theta_{pe} = 0.1 \text{ degrees, and} \\
&K_{exoclutter} = 3.
\end{aligned} \tag{77}$$

From these parameters we calculate

$$\begin{aligned}
&MDV_{approach} = 0 \text{ m/s, and} \\
&MDV_{recede} = -0.29 \text{ m/s.}
\end{aligned} \tag{78}$$

Example 2

Consider a GMTI radar looking slightly off the nose and slightly down,

$$\begin{aligned}
&\theta_s = 10 \text{ degrees,} \\
&\psi = 20 \text{ degrees,} \\
&v_a = 75 \text{ m/s,} \\
&\theta_{bwaz} = 3.2 \text{ degrees,} \\
&\theta_{pe} = 0.1 \text{ degrees, and} \\
&K_{exoclutter} = 3.
\end{aligned} \tag{79}$$

From these parameters we calculate

$$\begin{aligned}
&MDV_{approach} = 0.82 \text{ m/s, and} \\
&MDV_{recede} = -1.40 \text{ m/s.}
\end{aligned} \tag{80}$$

Example 3

Consider a GMTI radar looking slightly behind broadside and slightly down,

$$\begin{aligned}
&\theta_s = -100 \text{ degrees,} \\
&\psi = 20 \text{ degrees,} \\
&v_a = 75 \text{ m/s,}
\end{aligned}$$

$$\theta_{bwaz} = 3.2 \text{ degrees},$$
$$\theta_{pe} = 0.1 \text{ degrees, and}$$
$$K_{exoclutter} = 3. \tag{81}$$

From these parameters we calculate

$$MDV_{approach} = 6.35 \text{ m/s, and}$$
$$MDV_{recede} = -6.25 \text{ m/s}. \tag{82}$$

These examples, and calculations for other squint angles are summarized and illustrated in Figure 13. A frequency dependence exists only to the extent that the antenna beamwidth would be a function of frequency.

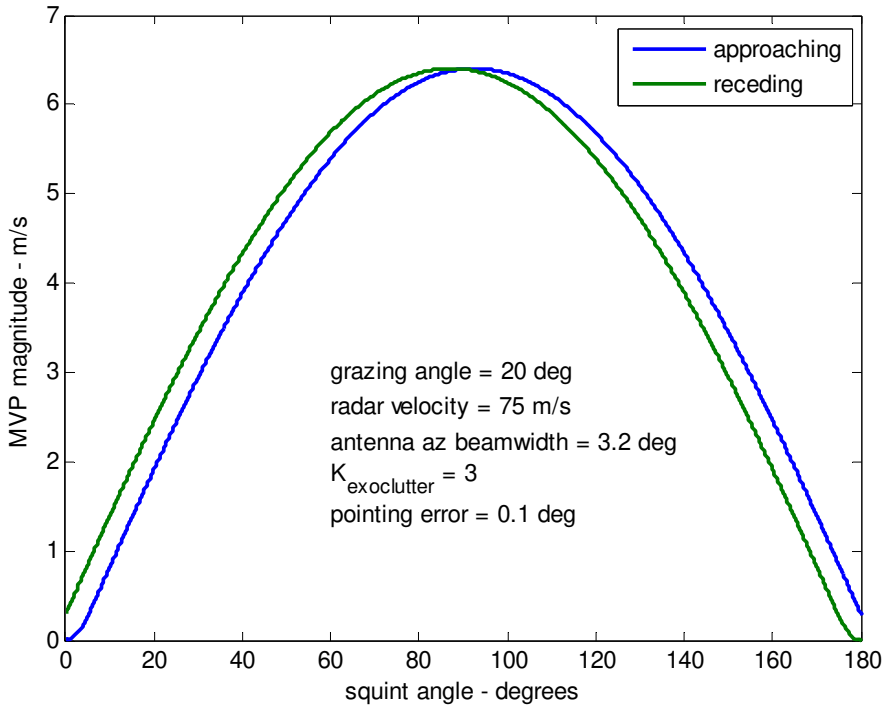

Figure 13. MDV calculations as a function of squint angle.

The significance of these various velocity limits will depend on the kinds of velocities we wish to detect.

A note about dismounts

The foregoing analysis suggests that even a single-channel GMTI offers the possibility of detecting humans walking, albeit with a forward, perhaps nose-on (or nearly so) observation geometry. Rearward observation geometry would also work.

4.3 Blind Velocities

A pulse-Doppler GMTI radar makes velocity measurements on the basis of pulse-to-pulse phase changes observed in the radar echo from a target. As such, each pulse's echo is in fact a 'sample' of the target's Doppler characteristic. The collection of raw phase history data is in fact sampled data, with all the characteristics of sampled data. This includes the concepts of replicated spectrum and aliasing, especially when uniform sampling is employed via a constant PRF.

Figure 14 illustrates a notional Doppler spectrum observed with a constant PRF. Essentially, as predicted by sampling theory, the spectrums of clutter and targets are replicated at Doppler frequency offsets equal to integer multiples of the radar PRF.

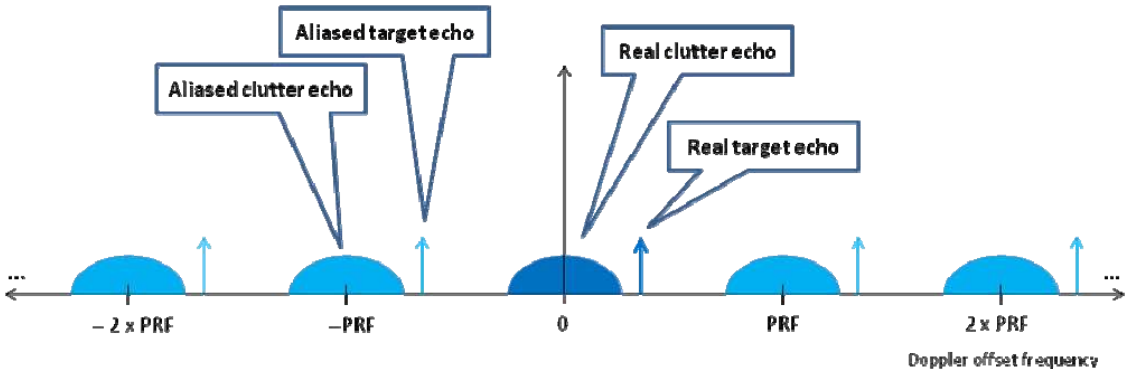

Figure 14. Notional Doppler spectrum illustrating replicated spectrum and aliasing.

We make two critical observations.

- Since Doppler frequency is proportional to target line-of-sight closing velocity, this suggests that any radar echo can be attributed (alias) to multiple possible target velocities as well. There is an inherent velocity ambiguity to the target data.

- The clutter band represents a region where the radar is 'blind' to moving target echoes. Since the clutter region is replicated and aliased to higher velocities in addition to its true spectral location, there exist 'blind' velocity bands well above the MDV limits previously identified.

To continue the analysis, we identify the velocity associated with a Doppler shift equal to the PRF as

$$v_p = \frac{\lambda}{2} f_p . \tag{83}$$

This in fact defines a velocity aliasing factor. We can therefore calculate the velocity intervals (relative to the clutter at the antenna beam azimuth center) to which the radar is blind as all velocities that satisfy

$$\left(n\, v_p + MDV_{recede}\right) \le v_{blind} \le \left(n\, v_p + MDV_{approach}\right), \tag{84}$$

where

$$n \text{ = arbitrary integer.} \tag{85}$$

Recall that MDV_{recede} is negative, and $MDV_{approach}$ is positive.

A common GMTI parameter is the First Blind Velocity (FBV). This depends on the radar PRF and the MDV. Since MDV is different for approaching and receding targets, we separate the FBV on this basis, and calculate

$$\begin{aligned} FBV_{approach} &= v_p + MDV_{recede} \text{ = first blind velocity for approaching target, and} \\ FBV_{recede} &= -v_p + MDV_{approach} \text{ = first blind velocity for receding target.} \end{aligned} \tag{86}$$

These are illustrated in Figure 15.

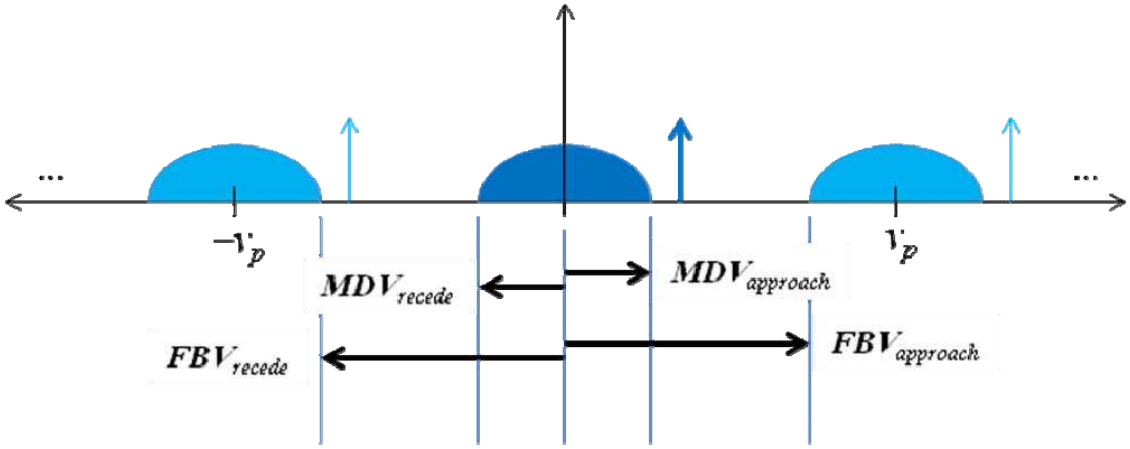

Figure 15. Relationship of MDV and FBV concepts.

We summarize two important observations with respect to Figure 15 as

- For a constant radar wavelength, the MDV depends on geometry and antenna azimuth beamwidth.
- For a constant radar wavelength, the FBV depends on geometry and antenna azimuth beamwidth, and additionally on radar PRF.

Consequently, FBV can be moved by changing radar PRF. Changing, or staggering, radar PRF is a common technique for making blind velocities visible again. This is illustrated in Figure 16.

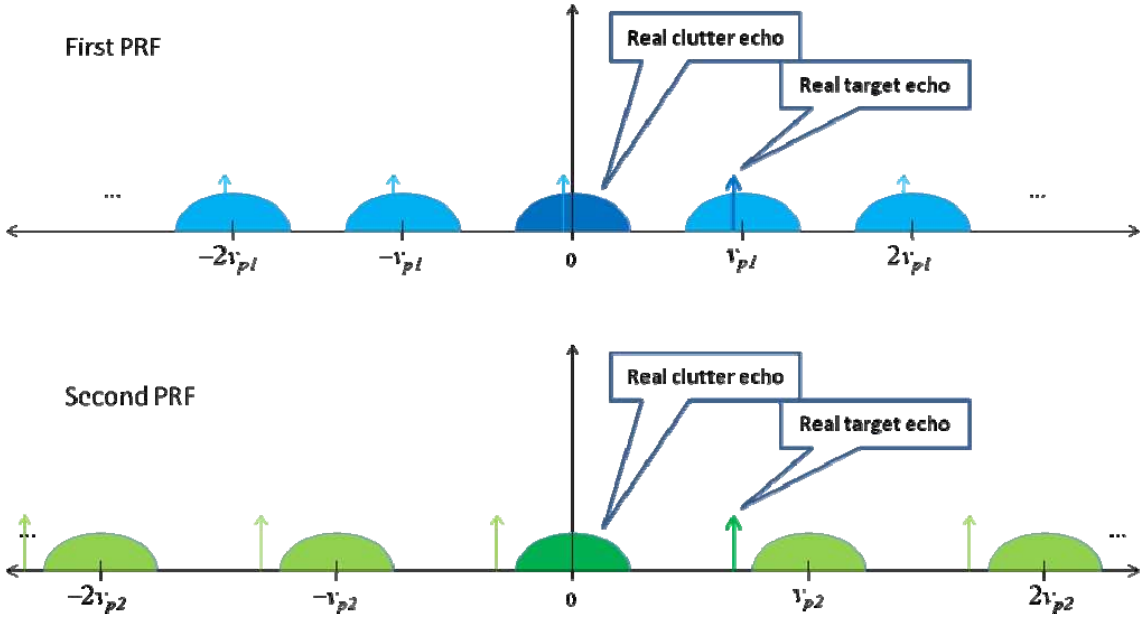

Figure 16. Illustration of blind velocities becoming visible with a change in PRF.

It is not unreasonable, or uncommon, to use more than two PRFs.

We note that changing radar PRF also allows some degree of mitigation of Doppler ambiguity. This is because aliased Doppler returns will scale in Doppler with the changing radar PRF. The true Doppler will not. One technique for resolving the ambiguity is the well-known Chinese Remainder Theorem.

4.4 Effects of Doppler Resolution

While the antenna beam defines the velocity spectrum of the clutter manifested in the data, the spectral characteristics do also depend on data processing techniques. Specifically, the spectral characteristics depend on the Doppler resolution and the sidelobe characteristics of the Doppler matched filter implementation, that is its Doppler Impulse Response (IPR).

Normally, and especially at broadside geometries, the Doppler resolution is small compared to the clutter Doppler bandwidth, so that as long as the sidelobe filters (window functions) used offer low sidelobes, then MDV remains principally a function of the antenna beam. However, especially in forward geometries, where clutter Doppler bandwidth collapses, but Doppler resolution does not, then the effects of Doppler resolution and Doppler IPR need to be revisited.

Doppler frequency resolution (as limited by the CPI) is calculated as

$$\rho_d = \frac{a_{wd}}{\tau}, \tag{87}$$

where

τ = the time span of a Coherent Processing Interval (CPI), and
a_{wd} = the IPR broadening due to sidelobe reduction filters (windows). (88)

We note that the CPI length can be calculated as

$$\tau = \frac{N_a}{f_p}, \tag{89}$$

where

N_a = the number of pulses collected in a CPI, and
f_p = the Pulse Repetition Frequency (PRF). (90)

We also note that a −70 dB Taylor window (nbar = 11) used for sidelobe control, has $a_{wd} \approx 1.6$ and its first null at 1.8 resolution cells away from the peak, for a null-to-null width of 3.6 resolution units. The first null is probably a good position for MDV calculations in appropriate cases.

Of course, Doppler resolution translates to velocity resolution by

$$\rho_v = \frac{\lambda}{2}\rho_d = \frac{\lambda\, a_{wd}}{2\tau}. \tag{91}$$

Example

We will presume processing using the −70 dB Taylor window. Assume a CPI with interval of 0.1 seconds. This suggests a Doppler frequency resolution on the order of 16 Hz. Furthermore, the first null is 28.8 Hz from the peak. This suggests that the Doppler IPR has a null-to-null width of almost 58 Hz. This would be the width of the endo-clutter region if the velocity spread due to the antenna were infinitely narrow, i.e. an impulse, which of course it is not.

At Ku-band, this translates to a velocity IPR with null-to-null width of almost 0.52 m/s.

Of course, doubling the CPI time would halve the resolution, and halve the null-to-null width.

The question becomes "What are the effects of Doppler resolution on MDV?"

The real answer is to convolve the Doppler IPR with the true Doppler spectrum of the clutter, and extract suitable edges from the result, translating them to MDV.

A simplistic solution would be to add half the null-to-null width to $MDV_{approach}$, and subtract half the null-to-null width from MDV_{recede}. This is somewhat overkill, but easy to do.

Example

Continuing with the example above, consider a GMTI geometry with calculated $MDV_{approach} = 0$ and $MDV_{recede} = -0.29$ m/s prior to accounting for any effects of velocity IPR. Now, by including a Ku-band velocity IPR with null-to-null width of almost 0.52 m/s, and the simplistic calculation above, we might expect a worsened MDV situation where

$MDV_{approach} \rightarrow 0.26$ m/s, and
$MDV_{recede} \rightarrow -0.55$ m/s.

Note that this might be a significant impact.

4.5 Frequency Effects

With respect to the observable target velocities, we now examine the effects of changing radar nominal wavelength. Specifically, we examine the MDV and the FBV parameters.

To simplify the discussion somewhat, we limit our attention to squint angles near broadside, and no pointing error.

4.5.1 Minimum Detectable Velocity (MDV)

The MDV for approaching targets at squint angles near broadside is calculated as

$$MDV_{approach} \approx v_a \cos\psi \left(\cos\left(|\theta_s| - K_{exoclutter} \frac{\theta_{bwaz}}{2\cos\psi} \right) - \cos(|\theta_s|) \right). \tag{92}$$

This can be approximated for small antenna beams as

$$MDV_{approach} \approx v_a \cos\psi \sin(|\theta_s|) \sin\left(K_{exoclutter} \frac{\theta_{bwaz}}{2\cos\psi} \right), \tag{93}$$

and further, using small angle approximations as

$$MDV_{approach} \approx \frac{v_a \sin(|\theta_s|) K_{exoclutter} \theta_{bwaz}}{2}. \tag{94}$$

Note that near broadside, $MDV_{recede} \approx -MDV_{approach}$. We include frequency effects by expanding the antenna beamwidth, and arrive at

$$MDV_{approach} \approx \frac{v_a \sin(|\theta_s|) K_{exoclutter} \lambda}{2D_{az}}, \tag{95}$$

where we have ignored beam tapering effects, and

$$D_{az} = \text{azimuth dimension of the antenna aperture.} \tag{96}$$

Consequently, MDV is proportional to wavelength. Higher frequencies will yield a lower MDV, all other factors equal. This is generally good.

4.5.2 First Blind Velocity (FBV)

The FBV near broadside is calculated as

$$FBV_{approach} = v_p + MDV_{recede}. \tag{97}$$

By making the same simplifications as in the previous section, and including frequency effects with the PRF, we arrive at the approximation

$$FBV_{approach} = \lambda \left(\frac{f_p - \frac{v_a \sin(|\theta_s|) K_{exoclutter}}{D_{az}}}{2} \right). \tag{98}$$

The clear result is that FBV is also proportional to wavelength. Higher frequencies will yield a lower FBV, all other factors equal, just like for MDV. Whereas good for MDV, this is generally bad for FBV.

4.5.3 Combined Results

Not surprisingly, all things equal, we expect all observable velocity boundaries to scale with wavelength, and hence inversely with frequency. This is illustrated in Figure 17. Interestingly, the 'percent' of observable velocities remains constant over frequency.

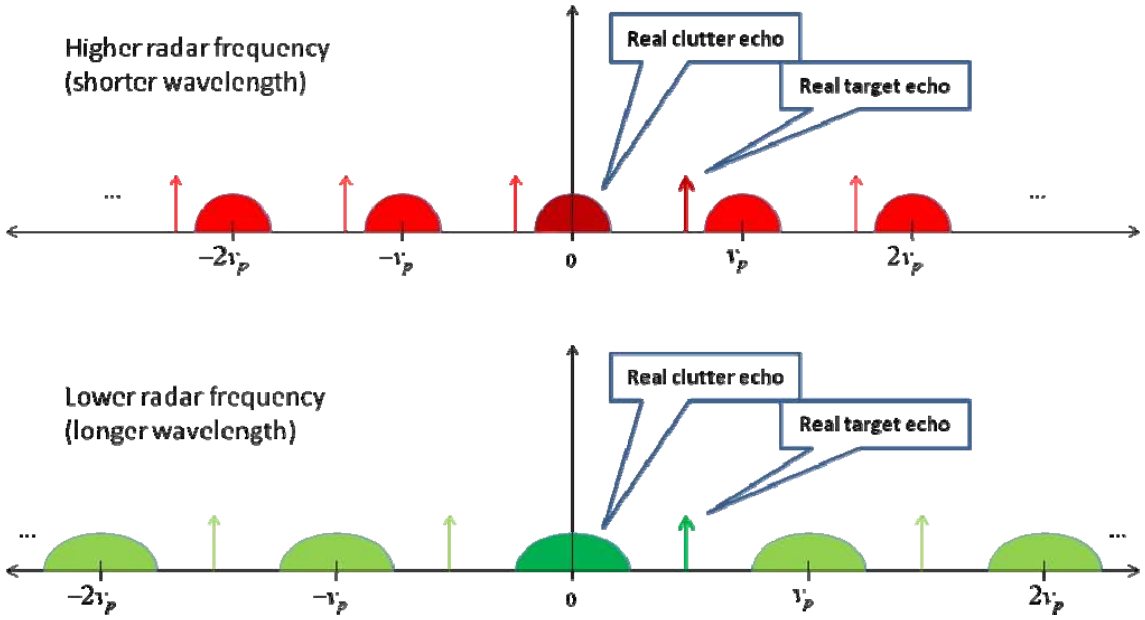

Figure 17. Effect of radar frequency (wavelength) on observable velocities.

5 Some Additional Comments

For a GMTI radar system to work well, it must

1. Provide adequate SNR to yield acceptable Probability of Detection, with acceptable Probability of False Alarm,

2. Provide acceptable observable velocity ranges, embodied in MDV and FBV, and

3. Provide acceptable target location, in both space and time.

Secondary performance factors include the ability to

4. Provide accurate RCS measures, and

5. Provide accurate velocity measures.

This report has heretofore discussed SNR issues and observable velocity ranges. We now offer some comments on space-time target location.

Space/Time Target Location

For a moving target, it is not sufficient to know its location, but we must also know precisely just 'when' it is/was at that location. Unlike SAR, GMTI necessarily deals with spatial dimensions 'and' the time dimension. To facilitate this, we make the following observations.

- The accuracy of a GMTI radar space/time measurement depends on both the accuracy and precision with which the radar knows its own position and orientation in space/time, and the accuracy and precision with which the radar can make a relative range and directional measurement to the target. For a 3-D geospatial solution, we ideally need additionally both azimuth and elevation Direction of Arrival (DOA) measurements. Otherwise, we need topographic information of the target scene along with an azimuth DOA measurement.

- Geospatial and temporal measurement errors can directly impact some methods of calculating Probability of Detection. Consequently such errors need to be well understood with respect to those calculations.

- In the absence of multiple antenna phase centers to provide improved DOA, we can use sequential lobing concepts, or Multiple Observation Signal Processing (MOSP) to improve directional measurements to something finer than the antenna's nominal beamwidth. These techniques generally require high SNR, and are adversely affected by target glint and scintillation. In spite of this, they do in fact typically offer some degree of improvement.

With respect to testing, we observe the following.

- The accuracy and precision with which a GMTI radar's performance can be measured or validated additionally depends on the accuracy and precision with which the target 'truth' position in space/time is known.

- Radar validation accuracy measurements are desired to be reflective of principally the radar's own performance. However, in some circumstances some measurement errors can be dominated by the accuracy and precision of 'truth' data.

- The dimension of time, and the consequence of timestamp errors for position data, adds significant complexity to assessing a radar's performance, and cannot be neglected in such an assessment.

RCS Calibration

We briefly comment here that detection thresholds will often depend on the expected RCS of a target of interest. In addition, target discrimination, classification, and perhaps even identification often requires a measure of the RCS of the target. Consequently, an accurate RCS measure facilitates proper target characterization for these ends.

An accurate RCS measure requires a complete understanding of the gains and losses in a GMTI system, and adequate compensation of them. A GMTI system therefore should be radiometrically calibrated.

Target Velocity Measure

The output detections of a GMTI radar system often feed a target tracker, whose job it is to not only 'connect' past detections, but also to 'predict' in some sense where the target is going. This is true whether the tracker is a machine, or a human observer. In addition, a velocity measure also serves as a discriminant between two or more targets.

As previously identified, for an exo-clutter GMTI radar, target velocity is somewhat inseparable from target location. Consequently, any means to provide a more accurate velocity measure will also have the effect of improving target location accuracy, and vice versa. In fact, more often we will attempt to improve the target's azimuthal bearing thereby allowing for improved velocity calculation.

Accurate velocity measurement also requires an accurate known radar PRF, and fine velocity resolution. In addition, as appropriate, a means of dealing with the Doppler ambiguity is required. Velocity resolution and ambiguity were discussed above.

6 Conclusions

The aim of this report is to allow the reader to understand the nature of relevant physical parameters in how they influence exo-clutter GMTI performance. The radar equation can be (and was) transmogrified to a form that shows these parameters explicitly. Maximizing performance of a GMTI system is then an exercise in modifying the relevant parameters to some optimum combination. This was discussed in detail.

Nevertheless, some observations are worth repeating here.

Increasing Probability of Detection while decreasing False Alarms is accomplished by increasing the SNR of the range-Doppler map.

A fundamental performance parameter is the concept of 'Noise Equivalent' RCS. This is the target RCS required for a 0 dB SNR. It is analogous to the Noise Equivalent Reflectivity for SAR.

Atmospheric losses are typically greater at higher frequency, in heavier rainfall, and at lower altitudes. These conspire to indicate an optimum operating frequency for a constrained antenna area at any particular operating geometry and weather condition.

Extending the range of a GMTI system can be done by incorporating any of the following:

increasing average TX power (peak TX power and/or duty factor)
increasing antenna area and/or efficiency
operating in a more optimal radar band (or portion of a radar band)
increasing CPI length (subject to coherence time limitations)
looking for brighter (higher RCS) targets
decreasing system losses and/or system noise factor
flying at a more optimal altitude (usually higher)
operate with a geometry such that the target has a higher RCS
operating in more benign weather conditions
decreasing Probability of Detection
increasing the False Alarm Rate

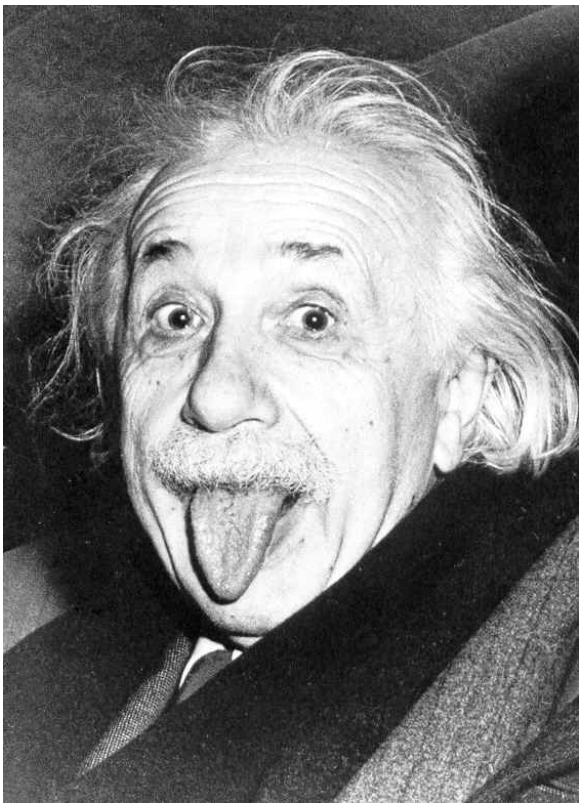

"Any intelligent fool can make things bigger, more complex, and more violent. It takes a touch of genius -- and a lot of courage -- to move in the opposite direction."
-- Albert Einstein

Appendix A – Swerling Target Models

Fluctuating target RCS models are often characterized by Swerling target numbers.[19] These were first proposed by, and hence named after Peter Swerling.[2] These numbers are characterized typically as

> Swerling 1 – many scattering centers without one being dominant, with pulse-to-pulse correlation.
>
> Swerling 2 – many scattering centers without one being dominant, with no pulse-to-pulse correlation.
>
> Swerling 3 – many scattering centers but with one being dominant, with pulse-to-pulse correlation.
>
> Swerling 4 – many scattering centers but with one being dominant, with no pulse-to-pulse correlation.

The non-fluctuating Marcum model is sometimes referred to as Swerling 0, and sometimes as Swerling 5. Other target fluctuation models also can be found in the literature.

The underlying probability distribution for Swerling models is the Chi-square distribution.

Consider a random variable created as the function

$$Y = \sum_{i=1}^{k} X_i^2 , \text{ where } X_i \sim N(0,1). \tag{A1}$$

Then Y is distributed according to a Chi-square distribution with k degrees of freedom. This is written as

$$Y \sim \chi_k^2 . \tag{A2}$$

The Chi-square PDF is then given as

$$f(x,k) = \frac{x^{(k/2)-1} e^{-x/2}}{2^{k/2}\Gamma(k/2)} \quad \text{restricted to } x \geq 0 . \tag{A3}$$

where $\Gamma(z)$ is the Gamma function.

We note that major statistics are calculated as

$$\text{Mean}\left(\chi_k^2\right) = k \tag{A4}$$

and

$$\text{Variance}\left(\chi_k^2\right) = 2k \ . \tag{A5}$$

The Swerling 1 target model presumes the RCS is distributed according to the Chi-square PDF with 2 degrees of freedom, otherwise known as the exponential distribution, or

$$f_{\text{Swerling\_1}}(\sigma) = \frac{1}{\sigma_{\text{avg}}} e^{-\frac{\sigma}{\sigma_{\text{avg}}}} \quad . \tag{A6}$$

where

σ = the actual or instantaneous RCS
σ_{avg} = the average RCS of the target over all fluctuations. (A7)

For Swerling 1, σ is constant during a scan, but varies from scan to scan.

The Swerling 2 target model has the RCS exhibiting the same PDF as for the Swerling 1 PDF, but σ varies from pulse to pulse.

The Swerling 3 target model presumes the RCS is distributed according to the Chi-square PDF with 4 degrees of freedom, or

$$f_{\text{Swerling\_3}}(\sigma) = \frac{4\sigma}{\sigma_{\text{avg}}^2} e^{-\frac{2\sigma}{\sigma_{\text{avg}}}} \quad . \tag{A8}$$

For Swerling 3, σ is constant during a scan, but varies from scan to scan.

The Swerling 4 target model has the RCS exhibiting the same PDF as for the Swerling 3 PDF, but σ varies from pulse to pulse.

Furthermore, the probability of exceeding a minimum relative RCS for each of these is calculated as

$$P_{\text{Swerling\_1,2}}\left\{\frac{\sigma}{\sigma_{\text{avg}}} \geq \beta\right\} = e^{-\beta} \quad \text{, and} \tag{A9}$$

$$P_{\text{Swerling\_3,4}}\left\{\frac{\sigma}{\sigma_{\text{avg}}} \geq \beta\right\} = (1+2\beta)e^{-2\beta} \ . \tag{A10}$$

These probabilities for $\beta \le 1$ are plotted in Figure 18.

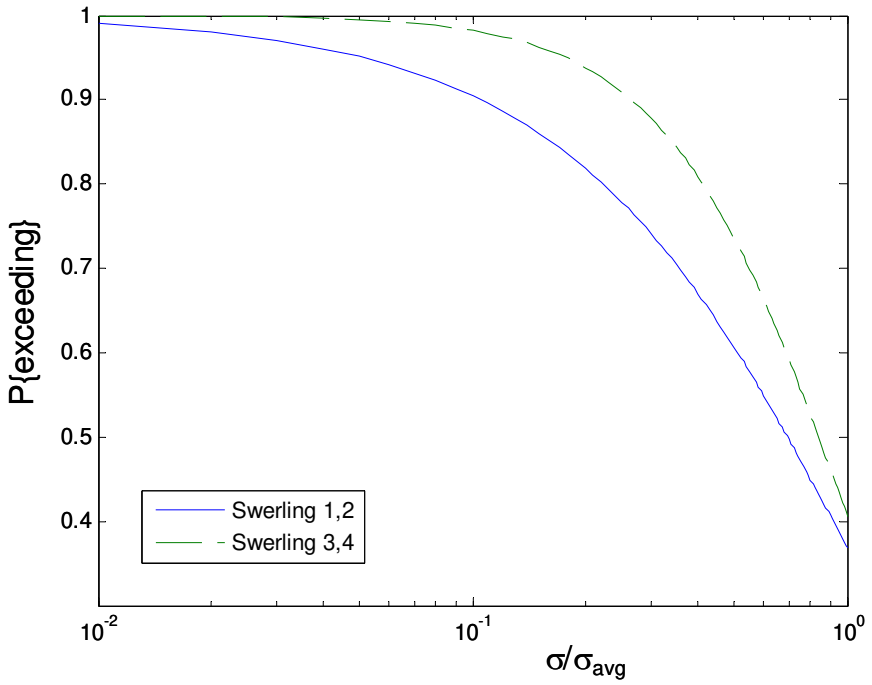

Figure 18. Probability of exceeding a relative RCS.

Note the following specific values

$$P_{\text{Swerling\_1,2}}\left\{\sigma/\sigma_{\text{avg}} \ge 0.1054\right\} = 0.9$$
$$P_{\text{Swerling\_1,2}}\left\{\sigma/\sigma_{\text{avg}} \ge 0.2231\right\} = 0.8$$
$$P_{\text{Swerling\_1,2}}\left\{\sigma/\sigma_{\text{avg}} \ge 0.6931\right\} = 0.5 \qquad \text{(A11)}$$

$$P_{\text{Swerling\_3,4}}\left\{\sigma/\sigma_{\text{avg}} \ge 0.2659\right\} = 0.9$$
$$P_{\text{Swerling\_3,4}}\left\{\sigma/\sigma_{\text{avg}} \ge 0.4122\right\} = 0.8$$
$$P_{\text{Swerling\_3,4}}\left\{\sigma/\sigma_{\text{avg}} \ge 0.8392\right\} = 0.5 \qquad \text{(A12)}$$

This implies that for good detection, we need to set thresholds at a fraction of the average RCS values. For example if we wish to detect a Swerling 1 target 90% of the time, then a threshold will need to be set to less than 1/10 its average value, even with infinite SNR. This corresponds to 10 dB below the average RCS.

For dynamic range considerations, we are often interested in how much 'brighter' a target may appear to the radar. Probabilities for $\beta \ge 1$ are plotted in Figure 19. Note that for a Swerling 1 target, $P_{\text{Swerling\_1,2}}\left\{\sigma/\sigma_{\text{avg}} \ge 2.3026\right\} = 0.1$. This corresponds to a 3.6 dB increase above average RCS.

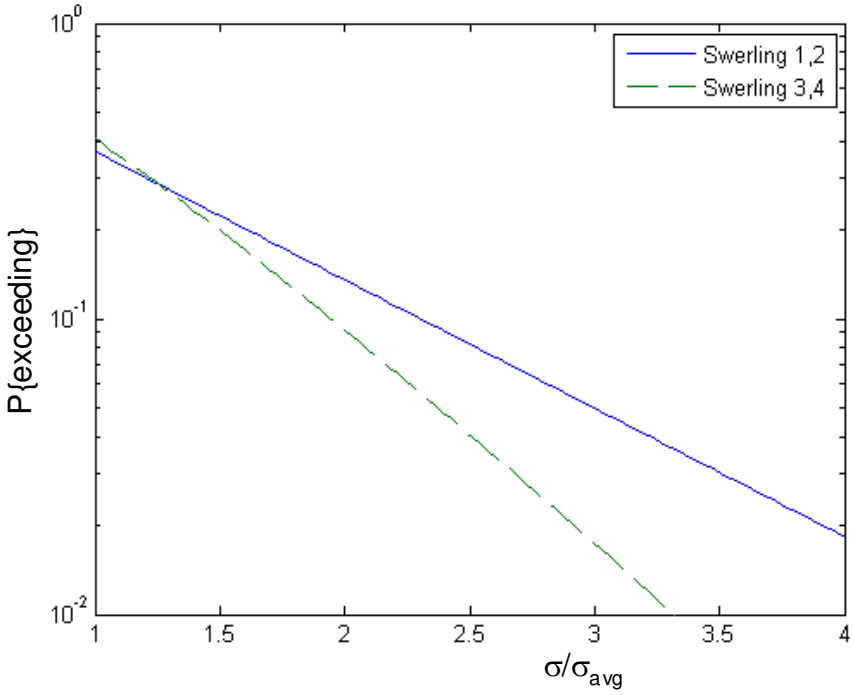

Figure 19. Probability of exceeding a relative RCS.

Appendix B – SNR and Probabilities of Detection and False Alarms

We address in this section the relationship between Probabilities of Detection and of False Alarms to SNR. We define:

> Probability of Detection (P_D) – the likelihood of detecting a target that is present, and
>
> Probability of False Alarm (P_{FA}) – the likelihood of declaring a detection when no target is present.

Detection is an inherently nonlinear process. The probabilities depend strongly on the SNR of the target response. Both noise and clutter characteristics are altered substantially by any non-linear processing, such as envelope detection. Consequently we model the relevant portions of the radar as in Figure 20.

Figure 20. Detector Model.

Note that other detector schemes exist, but for our purposes of assessing nominal performance of the entire GMTI mode of a radar, we will use this relatively common architecture.

Good discussions of target detection issues and techniques are found in Barton[20], and Morris and Harkness[21].

B.1 Input Data

The input coherent data is comprised of both signal and noise, both complex entities. At some time t_0 the Coherent Data input is given by

$$x_{\text{coherent}}(t_0) = s(t_0) + n(t_0), \tag{B1}$$

where

$$\begin{aligned} s(t_0) &= Ae^{j\phi} \text{ = signal, and} \\ n(t_0) &= n_c + j\,n_s \text{ = noise.} \end{aligned} \tag{B2}$$

The signal at time t_0 is nearly a complex constant. Absence of a signal can be analyzed by setting $A = 0$.

We will assume that the noise is such that n_c and n_s are independent zero-mean Normal (Gaussian) random variables, but with equal variances. In the context of this discussion, noise may be thermal noise, as one might expect in the exo-clutter region of a range-Doppler map.

In general, we identify a Normal distribution as

$$N\left(\mu, \sigma^2\right) \tag{B3}$$

where

$$\begin{aligned} &\mu \text{ = the mean value, and} \\ &\sigma^2 \text{ = the variance.} \end{aligned} \tag{B4}$$

Recall that the Probability Density Function (PDF) for a Normal random variable is described by

$$f_N(x) = \frac{1}{\sigma\sqrt{2\pi}} e^{-\frac{(x-\mu)^2}{2\sigma^2}}. \tag{B5}$$

Consequently, we identify the noise components exhibiting the zero-mean Normal characteristic by writing

$$n_c, n_s \sim N\left(0, \sigma^2\right). \tag{B6}$$

Note that the input signal effectively supplies a mean value to the noise. If we define

$$x_{\text{coherent}}(t_0) = x_c + j\, x_s, \tag{B7}$$

then we identify

$$\begin{aligned} &x_c \sim N\left(A\cos\phi, \sigma^2\right), \text{ and} \\ &x_s \sim N\left(A\sin\phi, \sigma^2\right). \end{aligned} \tag{B8}$$

Without loss of generality, we may assume $\phi = 0$. We can then calculate

$$f_{x_c}(x) = \frac{1}{\sigma\sqrt{2\pi}} e^{-\frac{(x-A)^2}{2\sigma^2}}. \tag{B9}$$

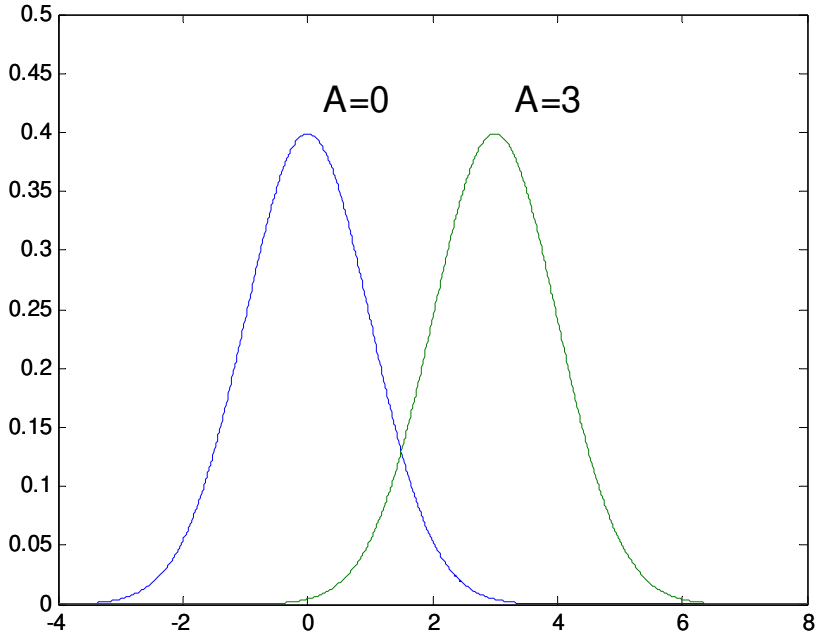

Figure 21. Input signal PDFs with σ=1.

We plot $f_{x_c}(x)$ for two values of A in Figure 21. Recall that $A=0$ is the 'no signal' (just noise) case. Of significance is that negative values of x are allowed as having some probability greater than zero, and noise statistics are independent of signal strength.

In any case, we calculate the SNR at the input to the envelope detector as

$$SNR_{\text{coherent}} = \frac{E\left\{|s(t_0)|^2\right\}}{E\left\{|n(t_0)|^2\right\}} = \frac{A^2}{2\sigma^2}. \tag{B10}$$

B.2 Synchronous Detector Output with Threshold Detection

With malice of forethought, we briefly divert our analysis to employing a synchronous (coherent) detector followed by a threshold detector. Such a detector is considered 'optimum' although not generally practical. This will set a baseline for subsequent analysis. We illustrate the block diagram for this in Figure 22.

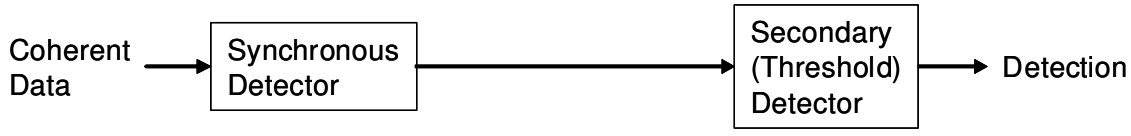

Figure 22. Synchronous detector model.

A synchronous detector has knowledge of the phase of the signal, and sets a threshold accordingly. With the assumption that $\phi = 0$ we are given that the signal is only meaningfully perturbed by n_c and not by n_s. In fact, with this assumption, by taking only the real part of $x_{\text{coherent}}(t_0)$ we can eliminate n_s from having any influence at all. Therefore, the relevant PDF is simply $f_{x_c}(x)$. Since any complex signal with known phase can be rotated to the same axis, this turns the two-dimensional problem into a one-dimensional problem, with same results.

This effectively cuts the noise power in half, thereby raising the SNR of the Synchronous Detector output by a factor of 2. This is sometimes referred to as 'detector gain'. Nevertheless, the SNR at the synchronous detector output is given by

$$SNR_{\text{synchronous}} = \frac{A^2}{\sigma^2} = 2\, SNR_{\text{coherent}} \,. \tag{B11}$$

Given a synchronous detector output, the task at hand is to decide whether a signal was present or not. The presence of a signal clearly moves the PDF to the right. This suggests a decision criteria that whenever the detector output exceeds (is more positive than) some threshold, a target presence is declared, and whenever the detector output does not exceed the threshold, then no target presence is declared. This is illustrated in Figure 23.

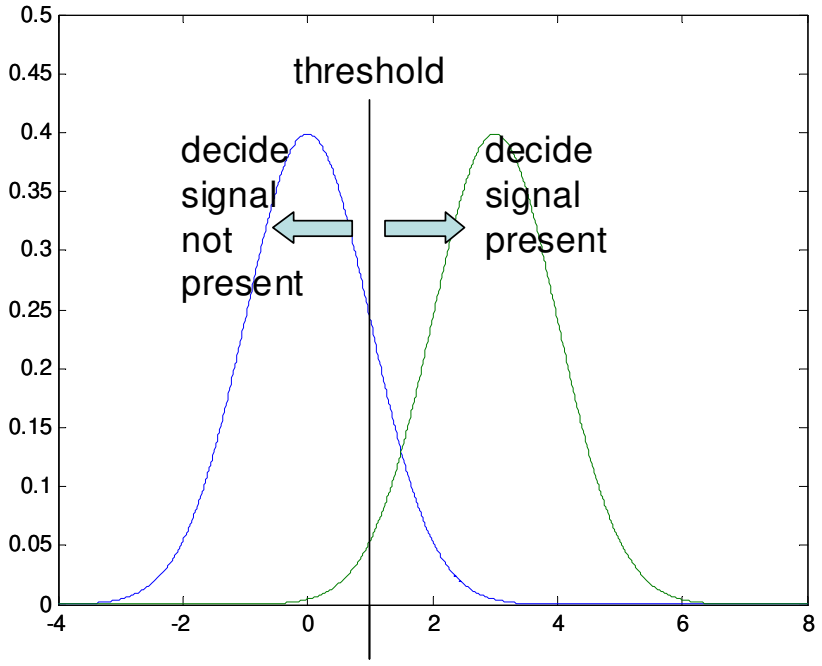

Figure 23. Threshold detector for synchronous detector output.

However, the PDFs of the synchronous detector output are positive for *all* values x. That is, there is some finite non-zero probability of the detector output being within any interval of x regardless of whether a signal is present or not. However, the presence of a signal does alter the mean value of the PDF, and hence the probabilities of being in any particular interval.

Specifically,

> Probability of Detection is the area under the 'signal+noise' PDF to the right of the threshold, illustrated in Figure 24, and
>
> Probability of False Alarm is the area under the 'noise-only' PDF to the right of the threshold, illustrated in Figure 25.

We can calculate these probabilities as follows. We calculate

$$P_D = Q\left(\frac{x_{\text{threshold}} - A}{\sigma}\right) \tag{B12}$$

where

$$Q(z) = \int_z^\infty \frac{1}{\sqrt{2\pi}} e^{-\frac{x^2}{2}}\, dx = \text{Normal Q function.} \tag{B13}$$

$$x_{\text{threshold}} = \text{the decision threshold.} \tag{B14}$$

We calculate for the synchronous detector

$$P_{FA} = Q\left(\frac{x_{\text{threshold}}}{\sigma}\right). \tag{B15}$$

See Appendix C for plots of Normal Q function values. We note that for the expected kinds of values for $x_{\text{threshold}}$, very small relative changes in $x_{\text{threshold}}$ can cause orders of magnitude changes in P_{FA}. Conversely, rather large changes in requirements for P_{FA} may cause only relatively small changes in required $x_{\text{threshold}}$.

Often in operational algorithms a threshold is set for a particular P_{FA}. This is the basic idea for the popular Constant False Alarm Rate (CFAR) detector. Then P_D can be calculated as a function of SNR. Alternately, P_D can be plotted versus P_{FA} for a family of SNR values. These curves are often referred to a Receiver Operating Curves (ROCs). Ziemer and Trantor[22] discuss these in more detail.

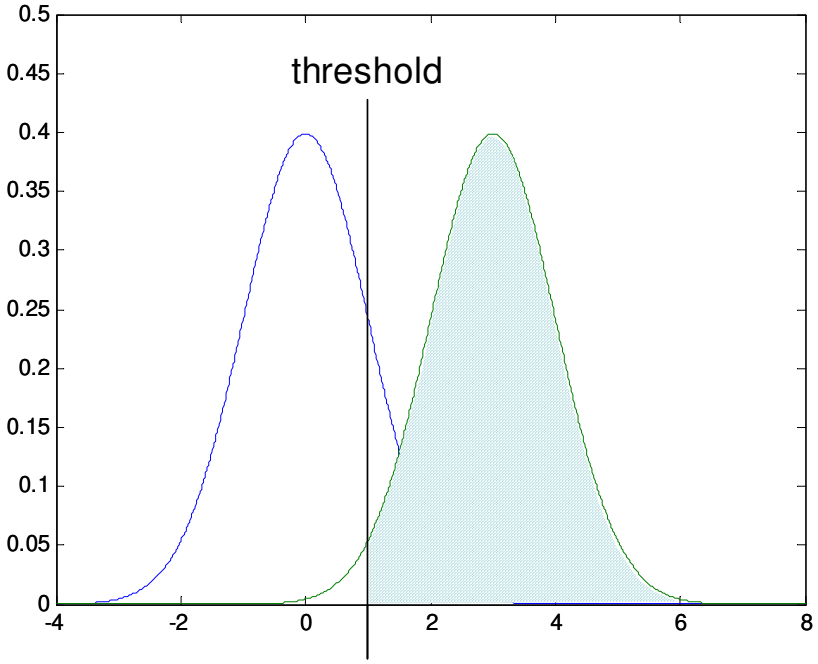

Figure 24. Probability of Detection.

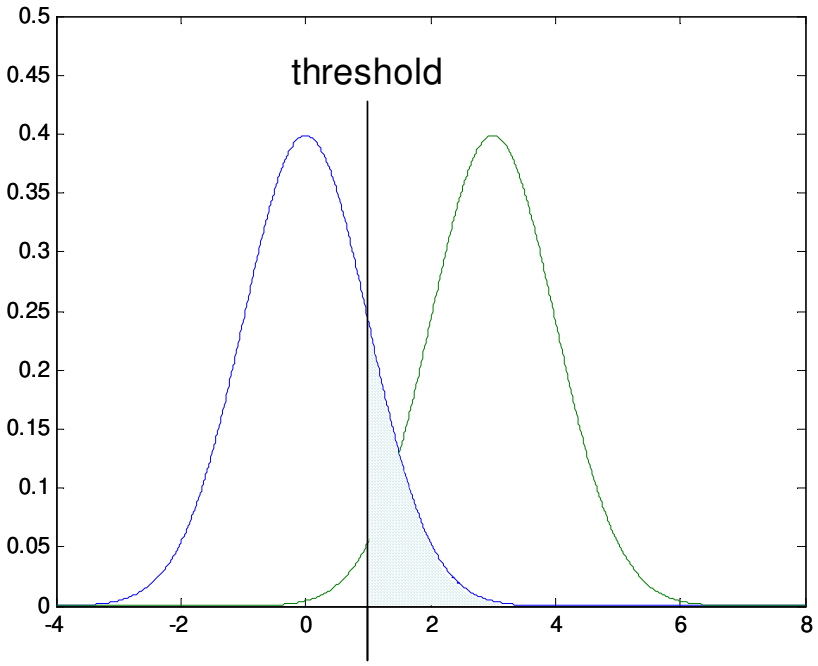

Figure 25. Probability of False Alarm.

Some additional points worth noting include

- P_D depends on SNR_{coherent} when a signal is present, that is, the noise power present when a signal is also present.
- P_{FA} depends on noise power when a signal is absent.

Clearly there is a trade-off. An increase in P_D requires the threshold to move to the left, but necessitates an increase in P_{FA}. A decrease in P_{FA} requires moving the threshold to the right, but necessitates a decrease in P_D. Achieving both a reduction in P_{FA} and an increase in P_D requires decreasing the overlap between the two PDFs. This can only be done by increasing SNR into the threshold detector.

Furthermore, the synchronous detector output is still coherent, consequently averaging (integrating and scaling) *K* samples of like PDF will simply reduce the variance by *K*, that is, increase the SNR by *K*.

$$SNR_{\text{post\_synchronous}} = K\frac{A^2}{\sigma^2} = K\ SNR_{\text{synchronous}} = 2K\ SNR_{\text{coherent}}. \tag{B16}$$

B.3 Envelope Detector Output

At the output of the envelope detector we identify

$$x_{\text{envelope}}(t_0) = \left|x_{\text{coherent}}(t_0)\right| = \left|s(t_0) + n(t_0)\right|. \tag{B17}$$

Consequently $x_{\text{envelope}}(t_0)$ is the magnitude of the sum of two uncorrelated non-zero-mean random variables. That is,

$$x_{\text{envelope}}(t_0) = \left|x_c + j\,x_s\right|. \tag{B18}$$

This yields a probability density function for $x_{\text{envelope}}(t_0)$ described by a Rice distribution. That is

$$x_{\text{envelope}}(t_0) \sim Rice(A,\sigma). \tag{B19}$$

Recall that the PDF for a Rice random variable is described by

$$f_R(x) = \frac{x}{\sigma^2}e^{-\frac{\left(x^2+A^2\right)}{2\sigma^2}}I_0\left(\frac{xA}{\sigma^2}\right), \tag{B20}$$

where

$I_0(z)$ = modified Bessel function of the first kind with order zero. (B21)

The Rice distribution is discussed in some more detail in Appendix D. We plot the envelope PDFs for two values of *A* in Figure 26.

Note that the 'noise only' case ($A = 0$) reduces to a Rayleigh PDF, namely

$$x_{\text{envelope}}(t_0)\Big|_{A=0} \sim Rice(0,\sigma) = Rayleigh(\sigma) \tag{B22}$$

where the PDF is calculated as

$$f_R(x)\Big|_{A=0} = \frac{x}{\sigma^2} e^{-\frac{x^2}{2\sigma^2}}. \tag{B23}$$

Clearly, the 'noise only' case now has a positive mean value at the detector output.

For the large SNR case where $A >> \sigma$, the Rice PDF approaches a Normal PDF, namely

$$x_{\text{envelope}}(t_0)\Big|_{A>>\sigma} \sim Rice(A,\sigma) \rightarrow N\left(A,\sigma^2\right). \tag{B24}$$

A Normal distribution is a reasonably good approximation for the Rice distribution for an envelope detector when SNR_{coherent} exceeds on the order of 10 dB.

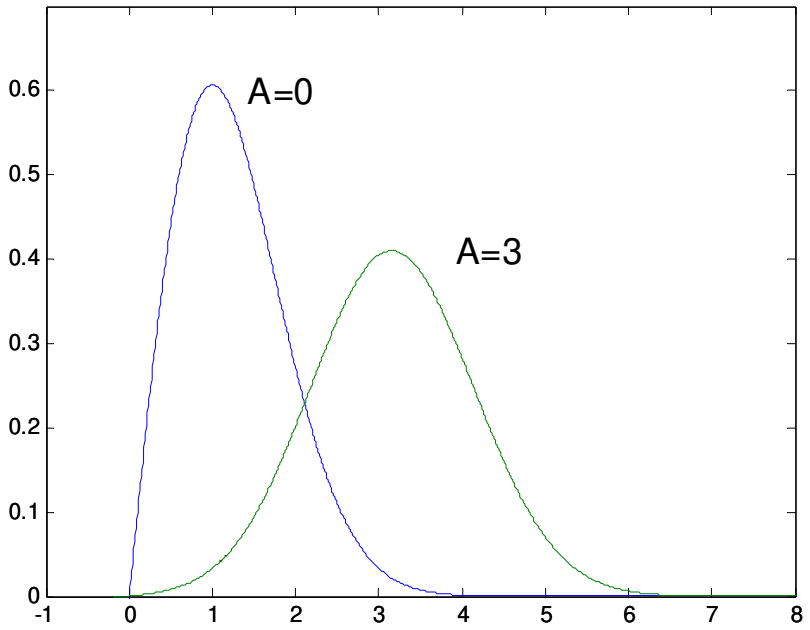

Figure 26. Envelope detector output PDFs for σ=1.

We will typically hereafter presume that SNR_{coherent} is adequate to allow a signal plus noise to be modeled as a Normal distribution.

An interesting note is that the amount of noise power now depends on whether a signal is present, and the signal strength, that is, SNR_{coherent}. This obfuscates the notion of SNR at the envelope detector output. For some data analysis we are interested in the signal levels with respect to noise in the same data cell. For other data analysis we are interested in signal levels in relation to noise levels in adjacent cells where no signal is present. This is the case for most CFAR detectors. These noise levels are different.

B.4 Threshold Detector Output – No Post-Detection Integration

The decision criteria for an envelope detected signal without post-detection integration is illustrated in Figure 27.

However, the PDFs of the envelope detector output are still positive for all values $x > 0$, regardless of the value of A.

We can calculate the relevant probabilities as follows. We calculate

$$P_D = Q_1\left(\frac{A}{\sigma}, \frac{x_{\text{threshold}}}{\sigma}\right) \tag{B25}$$

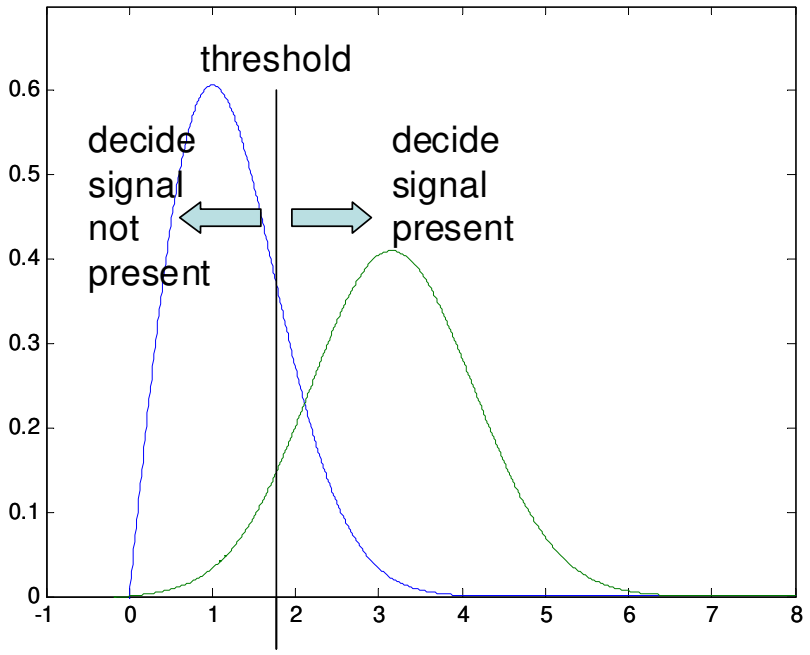

Figure 27. Threshold detector operation for envelope detected signal.

where

$$Q_1(a,z) = \int_z^\infty xe^{-\frac{\left(x^2+a^2\right)}{2}} I_0(xa)dx = \text{Marcum } Q_1 \text{ function}^{23}. \tag{B26}$$

For $A >> \sigma$, this approaches the Normal Q function

$$P_D = Q\left(\frac{x_{\text{threshold}} - A}{\sigma}\right). \tag{B27}$$

The Marcum Q function is elaborated and plotted in Appendix E.

From the Rayleigh PDF, we can calculate the closed form expression

$$P_{FA} = e^{-\frac{x_{\text{threshold}}^2}{2\sigma^2}}. \tag{B28}$$

We can calculate a threshold for a particular P_{FA} as

$$x_{\text{threshold}} = \sigma\sqrt{-2\ln\left(P_{FA}\right)}. \tag{B29}$$

As with the synchronous detector, achieving both a reduction in P_{FA} and an increase in P_D requires decreasing the overlap between the two PDFs. This can be done by increasing SNR_{coherent}. It can also be done by post-detection integration.

B.5 Threshold Detector Output – With Post-Detection Integration

Earlier results can be summarized as follows.

> A constant signal in noise will yield a Rice distribution of values at the envelope detector output. With adequate input SNR, this is reasonably well modeled by a Normal distribution.
>
> Noise alone will yield a Rayleigh distribution of values at the envelope detector output.
>
> Achieving both a reduction in P_{FA} and an increase in P_D requires decreasing the overlap between the two PDFs. One way to do this is with post-detection integration.

Post-detection integration is fundamentally averaging together a number of $x_{\text{envelope}}(t_0)$ that hopefully have correlated signal characteristics, but independent noise characteristics. We identify this by

$$x_{\text{post\_integration}}(t_0) = \frac{1}{K}\sum_{k=1}^{K} x_{\text{envelope}}(t_0, k) \tag{B30}$$

where here k is the index into multiple observations, and $1 \le k \le K$.

We will assume that all observations have identical PDFs, whether signal is present or not. We will also assume that K is large enough that the outputs can be adequately modeled with a Normal distribution in either case via the Central Limit Theorem. As a practical matter, $K \ge 6$ is often adequate for this.

With signal present, the PDF for $x_{\text{post\_integration}}(t_0)$

$$x_{\text{post\_integration}}(t_0) \sim N\left(\mu_{A,\sigma}, \frac{\nu^2_{A,\sigma}}{K}\right) \tag{B31}$$

where

$$\mu_{A,\sigma} = \text{Mean}\left(Rice\left(A,\sigma\right)\right), \text{ and}$$
$$v_{A,\sigma}^2 = \text{Variance}\left(Rice\left(A,\sigma\right)\right) . \tag{B32}$$

Recall that for large input SNR, this approaches

$$\mu_{A,\sigma}\Big|_{A>>\sigma} \to A \text{, and}$$
$$v_{A,\sigma}^2\Big|_{A>>\sigma} \to \sigma^2 \tag{B33}$$

With signal absent, the PDF for $x_{\text{post\_integration}}\left(t_0\right)$ approaches

$$x_{\text{post\_integration}}\left(t_0\right)\Big|_{A=0} \sim N\left(\sigma\sqrt{\frac{\pi}{2}}, \left(\frac{4-\pi}{2}\right)\frac{\sigma^2}{K}\right) \tag{B34}$$

Note that the variance has been reduced in both cases.

Given this, we calculate Probability of Detection as

$$P_D = Q\left(\frac{\left(x_{\text{threshold}} - \mu_{A,\sigma}\right)}{v_{A,\sigma}}\sqrt{K}\right). \tag{B35}$$

We observe that the threshold level also defines the mean signal level for $P_D = 0.5$. This is sometimes a performance specification for some search radars.

We calculate the Probability of False Alarm now as

$$P_{FA} = Q\left(\left(\frac{x_{\text{threshold}}}{\sigma} - \sqrt{\frac{\pi}{2}}\right)\sqrt{\frac{2K}{4-\pi}}\right). \tag{B36}$$

Of interest is "How does this compare to the Synchronous Detector performance?"

In order to make this comparison, we define a new variable

$$y_{\text{post\_integration}}\left(t_0\right) = x_{\text{post\_integration}}\left(t_0\right) - \sigma\sqrt{\frac{\pi}{2}} . \tag{B37}$$

This shifts the noise mean to zero. Consequently, we can approximate

$$y_{\text{post\_integration}}\left(t_0\right) \sim N\left(\mu_{A,\sigma} - \sigma\sqrt{\frac{\pi}{2}}, \frac{v_{A,\sigma}^2}{K}\right). \tag{B38}$$

and

$$y_{\text{post\_integration}}(t_0)\Big|_{A=0} \sim N\left(0, \left(\frac{4-\pi}{2}\right)\frac{\sigma^2}{K}\right). \tag{B39}$$

Given this, we calculate Probability of Detection as

$$P_D = Q\left(\frac{\left(y_{\text{threshold}} - \left(\mu_{A,\sigma} - \sigma\sqrt{\frac{\pi}{2}}\right)\right)}{\nu_{A,\sigma}}\sqrt{K}\right), \tag{B40}$$

and we calculate the Probability of False Alarm now as

$$P_{FA} = Q\left(\frac{y_{\text{threshold}}}{\sigma}\sqrt{\left(\frac{2}{4-\pi}\right)}\sqrt{K}\right). \tag{B41}$$

Since noise power depends on signal power, we face a dilemma regarding defining SNR. The choices for noise power are 1) using the noise power with signal present, and 2) using noise power when signal is absent. Depending on which noise we choose, SNR may vary by a factor of two. Since noise power increases with increasing signal power, we will be conservative and henceforth use the noise power when signal is present for SNR evaluation.

The SNR can be calculated as mean-squared over variance, or

$$SNR_{\text{post\_detection}} = K\left(\frac{\mu_{A,\sigma}}{\nu_{A,\sigma}} - \frac{\sigma}{\nu_{A,\sigma}}\sqrt{\frac{\pi}{2}}\right)^2. \tag{B42}$$

For large input SNR, this approaches

$$SNR_{\text{post\_detection}}\Big|_{A>>\sigma} = K\left(\frac{A}{\sigma} - \sqrt{\frac{\pi}{2}}\right)^2. \tag{B43}$$

This allows ready comparison to the output of a synchronous detector. Recall that

$$(A/\sigma) = \sqrt{2SNR_{\text{coherent}}}. \tag{B44}$$

We define the efficiency factor for non-coherent, or post detection integration as the ratio

$$\kappa_{\text{noncoherent}} = \frac{SNR_{\text{post\_detection}}}{SNR_{\text{post\_synchronous}}} = \frac{\left(\frac{\mu_{A,\sigma}}{\nu_{A,\sigma}} - \frac{\sigma}{\nu_{A,\sigma}}\sqrt{\frac{\pi}{2}}\right)^2}{\left(\frac{A}{\sigma}\right)^2}. \tag{B45}$$

Given this, we identify

$$SNR_{\text{post\_detection}} = \kappa_{\text{noncoherent}} K\left(\frac{A}{\sigma}\right)^2. \tag{B46}$$

This general expression for efficiency factor can be explored under several constraints.

Case 1: High input SNR

For high input SNR ($A >> \sigma$), this can be simplified to

$$\kappa_{\text{noncoherent}} \approx \left(1 - \frac{\sqrt{\pi/2}}{(A/\sigma)}\right)^2 = \left(1 - \frac{\sqrt{\pi/4}}{\sqrt{SNR_{\text{coherent}}}}\right)^2. \tag{B47}$$

It is reasonably accurate for input SNR greater than 10 or so.

Case 2: Medium input SNR

For the input SNR over the range $1 \le SNR_{\text{coherent}} \le 100$, the model may be simplified to

$$\kappa_{\text{noncoherent}} \approx 0.2 + 0.35\log_{10}\left(SNR_{\text{coherent}}\right). \tag{B48}$$

Case 3: Low input SNR

By fitting the general expression to a sigmoid function, we can generate an approximation of the form

$$\kappa_{\text{noncoherent}} \approx \frac{1}{1 + 5\left(SNR_{\text{coherent}}\right)^{-0.85}} = \frac{SNR_{\text{coherent}}^{\;0.85}}{SNR_{\text{coherent}}^{\;0.85} + 5}. \tag{B49}$$

This works reasonably well over the range $0.01 \le SNR_{\text{coherent}} \le 100$.

Case 4: Low input SNR - Barton

The sigmoid can be fit over a range of lesser SNR_{coherent} to yield slightly different parameters. For example, Barton arrives at the approximation

$$\kappa_{\text{noncoherent}} \approx \frac{SNR_{\text{coherent}}}{SNR_{\text{coherent}} + 2.3} \tag{B50}$$

which fits well for $SNR_{\text{coherent}} < 1$.

These various cases are plotted in Figure 28. Clearly, in any case, noncoherent integration efficiency takes quite a hit for $SNR_{\text{coherent}} < 1$.

B.6 Cumulative Detection Probability

It is not uncommon for some radars (especially search radars) to specify a rather low Probability of Detection for a single sweep (on the order of 0.5), and then rely on multiple sweeps or scans to detect the target at least once. This is referred to by Nathanson[24], among others, as "Cumulative Detection of a Radar Target".

The Cumulative Detection Probability of detecting the target at least once in N_{scan} scans is calculated as

$$P_{D,\text{cum}} = 1 - \left(1 - P_D\right)^{N_{\text{scan}}} \tag{B51}$$

where in this case P_D is the detection probability of a single scan. Note that with $P_D = 0.5$ and $N_{\text{scan}} = 3$, then $P_{D,\text{cum}} = 0.875$.

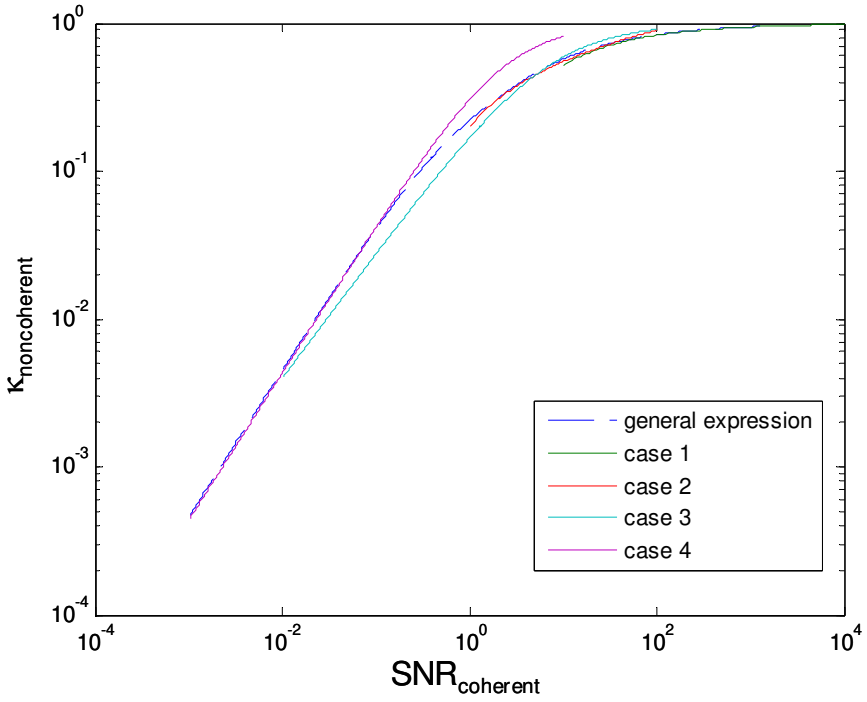

Figure 28. Noncoherent integration efficiency for various approximations.

Of course the Probability of False Alarm over multiple sweeps has also increased to

$$P_{FA,\text{cum}} = 1 - (1 - P_{FA})^{N_{\text{scan}}} \approx N_{\text{scan}} P_{FA} \,. \tag{B52}$$

Various other detection logic schemes may also be utilized. For example, one might declare a final detection if the target response exceeds threshold some number '*m*' out of '*n*' opportunities. Barton[20] refers to these as "Binary Integration", and indicates these as less optimal than noncoherent integration. He identifies Cumulative Detection as a special case of Binary Integration.

These algorithms are more generally described as "track before detect" algorithms. The reader is referred to Nathanson[24] for elaboration.

B.7 False Alarm Rate

Rather than Probability of False Alarm, tolerance for erroneous detections is frequently specified in terms of a False Alarm Rate (FAR).

The FAR is the expected number of false alarms per unit time interval. Some issues regarding this measure are discussed in Appendix F. Nevertheless, we calculate FAR as

the Probability of False Alarm multiplied by the number of independent opportunities for a false alarm in some time period.

Cumulative detections notwithstanding, the time period we choose is the processing interval. A processing interval is defined as the duration of the collection of N_{total} pulses, and is calculated as

$$T_{PI} = T_p N_{\text{total}} . \tag{B53}$$

where

$$T_p = 1/f_p \text{ = the Pulse Repetition Interval (PRI).} \tag{B54}$$

In general, for each processing interval, a range-Doppler map exists, allowing for independent range samples and independent Doppler samples.

We begin with the definition of the range swath of interest. This defines the parameters

$$\begin{aligned} R_{\text{near}} &= \text{the slant range to the near edge of the range swath, and} \\ R_{\text{far}} &= \text{the slant range to the far edge of the range swath of interest.} \end{aligned} \tag{B55}$$

We identify

$$\text{Number of independent range samples} = \frac{R_{\text{far}} - R_{\text{near}}}{\rho_r} . \tag{B56}$$

This is not the same as the number of range pixels, as pixel spacing may be (and often is) less than the resolution of the radar, thereby causing adjacent pixels to be correlated, i.e. not independent.

The number of independent Doppler samples available is equal to the number of pulses coherently integrated, N_{coherent}. However, the radar detection algorithm may choose to ignore some subset of these as having negligible likelihood for containing target returns, for example, if some Doppler frequencies correspond to excessive velocities unlikely to be associated with vehicle traffic of interest. Otherwise, if the system disallows the clutter region, this also effectively reduces the number of opportunities for a false alarm.

Nevertheless, the FAR will be bounded by assuming that the full Doppler spectrum offers opportunity for false alarms. Consequently, we will assume

$$\text{Number of independent Doppler samples} = N_{\text{coherent}} . \tag{B57}$$

This allows calculating the FAR conservatively as

$$f_{FA} = P_{FA}\left(\frac{N_{\text{coherent}}\left(R_{\text{far}} - R_{\text{near}}\right)/\rho_r}{T_{PI}}\right). \tag{B58}$$

Sometimes radar specifications are in terms of a "False Alarm Time" or "False Alarm Interval". We define this as

$$T_{FA} = 1/f_{FA}\,. \tag{B59}$$

B.8 A Second Look at What is a False Alarm

Heretofore, we have presumed that a false alarm is just the occasion of front-end thermal noise breaching the threshold for declaration of a legitimate signal. In fact, to a radar operator, a false alarm is the apparent detection of 'anything' that he isn't specifically looking for, which for a GMTI radar, is anything that isn't a target of interest to him.

The list of possible sources of false alarms might include any of the following

Thermal Noise
Multiplicative Noise from clutter or targets
Artifacts from spurs, EMI, etc.
Strong targets in the antenna sidelobes
Animals such as flocks of birds, other wildlife, etc.
Foliage in the wind
Rotating structures such as turbines, windmills, fans, propellers, etc.
Other radar antennas
Vibrating objects such as vent pipes, engine cowlings, etc.
Weather effects
Chaff

In maritime environments, the water itself will move, and move anything in it or on it, including any of the following

Buoys, Mooring balls
Floating trash, debris, flotsam, jetsam
Icebergs, Ice flows
Breaking waves

False alarms due to unknown or non-apparent sources are often referred to as 'artifacts', 'ghosts', or 'angels'.

Note that some of these are due simply to uncertainty in the echo energy, some are due to non-ideal radar performance, and some are legitimate targets – but simply not the kind of target of interest to the radar operator.

B.9 Calculating a SNR Requirement

The aim here is to identify an SNR requirement for the radar.

We begin with a basic FAR requirement, and a Probability of Detection requirement, and use the previously developed results.

From the FAR requirement we calculate the Probability of False Alarm as

$$P_{FA} = f_{FA}\left(\frac{N_{\text{total}}/f_p}{N_{\text{coherent}}\left(R_{\text{far}} - R_{\text{near}}\right)/\rho_r}\right). \tag{B60}$$

To facilitate the following discussion we define the Inverse Q function as

$$Q^{-1}(w) = z \tag{B61}$$

such that $w = Q(z)$,

We examine 2 cases of interest.

Case 1. No Non-Coherent Integration (K=1)

We begin with the equation for P_D

$$P_D = Q\left(\frac{x_{\text{threshold}} - A}{\sigma}\right) = Q\left(\frac{x_{\text{threshold}}}{\sigma} - \frac{A}{\sigma}\right). \tag{B62}$$

Assuming large coherent SNR, we can make appropriate substitutions to yield

$$P_D = Q\left(\sqrt{-2\ln(P_{FA})} - \sqrt{2SNR_{\text{coherent}}}\right). \tag{B63}$$

Solving this for the SNR yields

$$SNR_{\text{coherent}} = \left(\sqrt{-\ln(P_{FA})} - \frac{Q^{-1}(P_D)}{\sqrt{2}}\right)^2. \tag{B64}$$

Note that in this case $SNR_{\text{post\_detection}} = SNR_{\text{coherent}}$.

Case 2. Coherent Integration Gain (K>>1)

With sufficient non-coherent integration we may assume

$$\frac{x_{\text{threshold}}}{\sigma} = \left(\sqrt{\frac{4-\pi}{2K}}\right) Q^{-1}\left(P_{FA}\right) + \sqrt{\frac{\pi}{2}}$$
$$\approx \frac{0.6551}{\sqrt{K}} Q^{-1}\left(P_{FA}\right) + 1.2533 . \qquad \text{(B65)}$$

Recall that the threshold level also defines the mean signal level for $P_D = 0.5$. For more general Probability of Detection, we identify

$$\frac{\mu_{A,\sigma}}{\nu_{A,\sigma}} = \frac{\sigma}{\nu_{A,\sigma}} \left(\frac{x_{\text{threshold}}}{\sigma}\right) - \frac{1}{\sqrt{K}} Q^{-1}\left(P_D\right) \qquad \text{(B66)}$$

where the Rice mean and variance are related to A and σ. This is a rather involved computation. Formulas are given in Appendix D. The ratio $\sigma/\nu_{A,\sigma}$ is plotted in Figure 29.

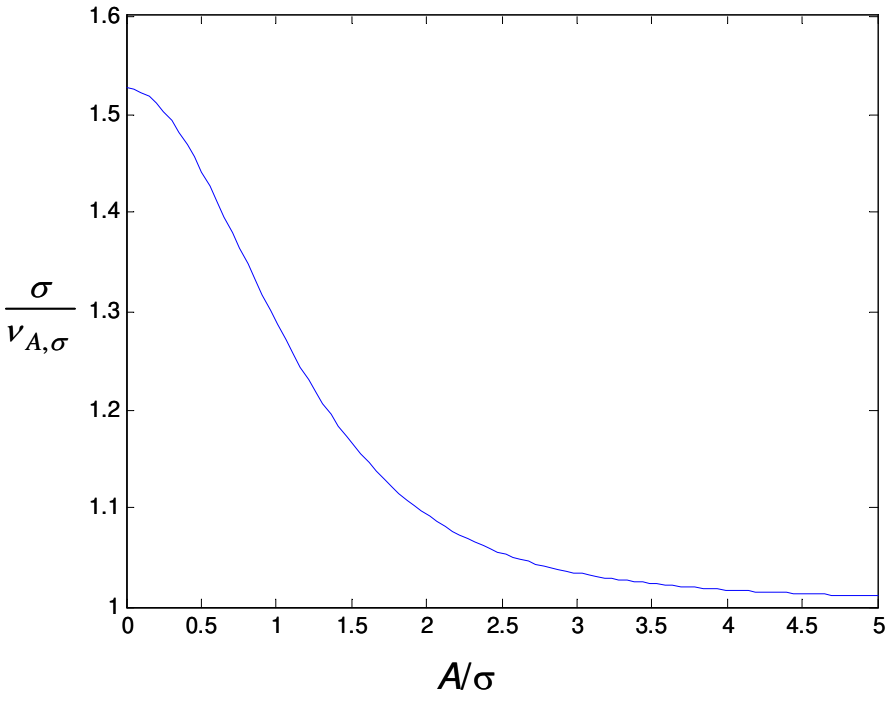

Figure 29. Ratio of standard deviations for Rice distribution.

Recall that

$$SNR_{\text{post\_detection}} = K\left(\frac{\mu_{A,\sigma}}{\nu_{A,\sigma}} - \frac{\sigma}{\nu_{A,\sigma}}\sqrt{\frac{\pi}{2}}\right)^2 = \kappa_{\text{noncoherent}} K\left(\frac{A}{\sigma}\right)^2. \tag{B67}$$

Combining results yields

$$SNR_{\text{post\_detection}} = K\left(\frac{\sigma}{\nu_{A,\sigma}}\left(\frac{x_{\text{threshold}}}{\sigma} - \sqrt{\frac{\pi}{2}}\right) - \frac{1}{\sqrt{K}}Q^{-1}(P_D)\right)^2. \tag{B68}$$

Combining further for $K >> 1$ yields

$$SNR_{\text{post\_detection}} = \left(\frac{\sigma}{\nu_{A,\sigma}}\left(\sqrt{\frac{4-\pi}{2}}\right)Q^{-1}(P_{FA}) - Q^{-1}(P_D)\right)^2. \tag{B69}$$

This is bounded by

$$SNR_{\text{post\_detection}} = \left(Q^{-1}(P_{FA}) - Q^{-1}(P_D)\right)^2. \tag{B70}$$

For large input SNR to the envelope detector, ($A >> \sigma$), we can approximate

$$SNR_{\text{post\_detection}} = \left(0.6551\,Q^{-1}(P_{FA}) - Q^{-1}(P_D)\right)^2. \tag{B71}$$

Typical conditions that allow this will require $SNR_{\text{post\_detection}}$ in the mid to upper teens of dB.

In terms from the development of the radar equations, we require the output SNR of the signal processing chain to minimally be

$$SNR_{\text{out}} \geq SNR_{\text{post\_detection}}. \tag{B72}$$

What this means is that for any targets to meet P_D and P_{FA} requirements, we need them to exhibit SNR greater than or equal to the minimum calculated.

Example 1

Consider a radar with the following requirements

False Alarm Time = 10 sec
Range swath = 1000 range resolution cells
PRF = 4000 Hz
No non-coherent Integration
$P_D = 0.9$

We calculate $P_{FA} = 2.5 \times 10^{-8}$, and via equation (B64) calculate the required $SNR_{\text{coherent}} \approx 14.2$ dB.

Example 2

Consider a radar with the following requirements

False Alarm Time = 3600 sec = 1 hour
Range swath = 1000 range resolution cells
PRF = 4000 Hz
No non-coherent Integration
$P_D = 0.99$

We calculate $P_{FA} \approx 6.9 \times 10^{-11}$, and via equation (B64) calculate the bound $SNR_{\text{coherent}} \approx 16.2$ dB. Note that a substantially increased P_D with a substantially reduced FAR requires only an additional 2 dB of SNR from the previous example.

Example 3

Consider a radar with the following requirements

False Alarm Time = 3600 sec = 1 hour
Range swath = 1000 range resolution cells
PRF = 4000 Hz
Noncoherent Integration factor = 10
$P_D = 0.99$

We calculate $P_{FA} \approx 6.9 \times 10^{-11}$, and via equation (B71) calculate the bound $SNR_{\text{post\_detection}} \approx 16.3$ dB. Note that although we are relying on non-coherent integration to achieve the minimal required SNR, we are in a situation with large input SNR to the envelope detector. The bottom line is that we need adequate SNR, regardless of how we get there.

B.10 Human Observer Detection

Heretofore we have been concerned with automatic detection algorithms. A human observer of radar 'blips' on a screen has his own unique detection characteristics.

A human observer of, say, a Plan-Position-Indicator (PPI) display naturally provides scan-to-scan integration or cumulative detection, as well as hysteresis, pattern analysis, feature enhancement, and contextual interpretation. Consequently, many texts refer to a typical 10 dB to 13 dB as a minimal useful SNR for a single scan.[25]

Note, however, that an operator's performance will depend heavily on the operator's training, motivation, alertness, and the design of the actual interface that the operator is operating.

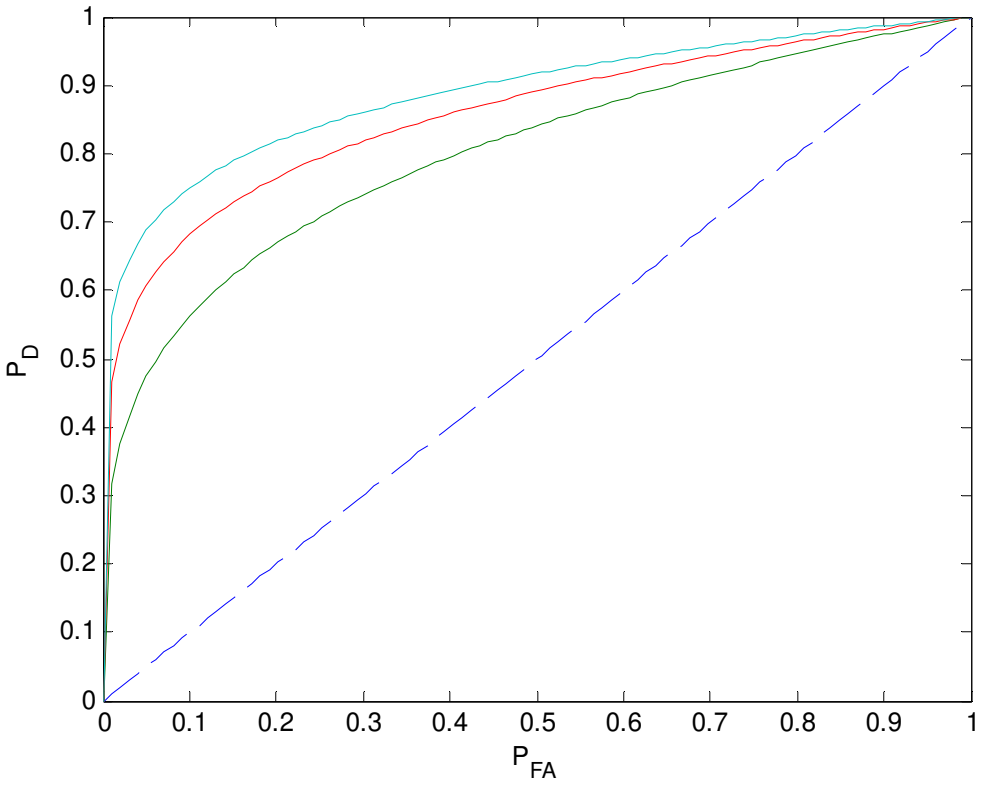

Figure 30. Notional Receiver Operating Curves (ROCs). Curves farther above and to the left represent 'better' performance, as is typically achievable with better SNR.

Appendix C – The Normal Q Function

The Normal Q function (or simply 'Q function') is defined as

$$Q(z) = \int_{z}^{\infty} \frac{1}{\sqrt{2\pi}} e^{-\frac{x^2}{2}} dx \tag{C1}$$

Figure 31 shows Q function values typical for Probability of Detection calculations. Several relationships of typical interest include

$$\begin{aligned} Q(-0.843) &\approx 0.8 \\ Q(-1.283) &\approx 0.9 \\ Q(-1.645) &\approx 0.95 \\ Q(-2.327) &\approx 0.99 \end{aligned} \tag{C2}$$

Figure 32 shows Q function values typical for Probability of False Alarm calculations.

The Q function is bounded by

$$\frac{1}{z\sqrt{2\pi}}\left(1-\frac{1}{z^2}\right)e^{-\frac{z^2}{2}} < Q(z) < \frac{1}{z\sqrt{2\pi}} e^{-\frac{z^2}{2}} \quad \text{for } z > 0\,. \tag{C3}$$

The upper bound is often used as an approximation for large arguments ($z > 3$).[22]

Finally, in terms of the "error function" defined as

$$\operatorname{erf}(z) = \frac{2}{\sqrt{\pi}} \int_{0}^{z} e^{-x^2} dx \tag{C4}$$

we calculate

$$Q(z) = \frac{1}{2} - \frac{1}{2}\operatorname{erf}\left(\frac{z}{\sqrt{2}}\right). \tag{C5}$$

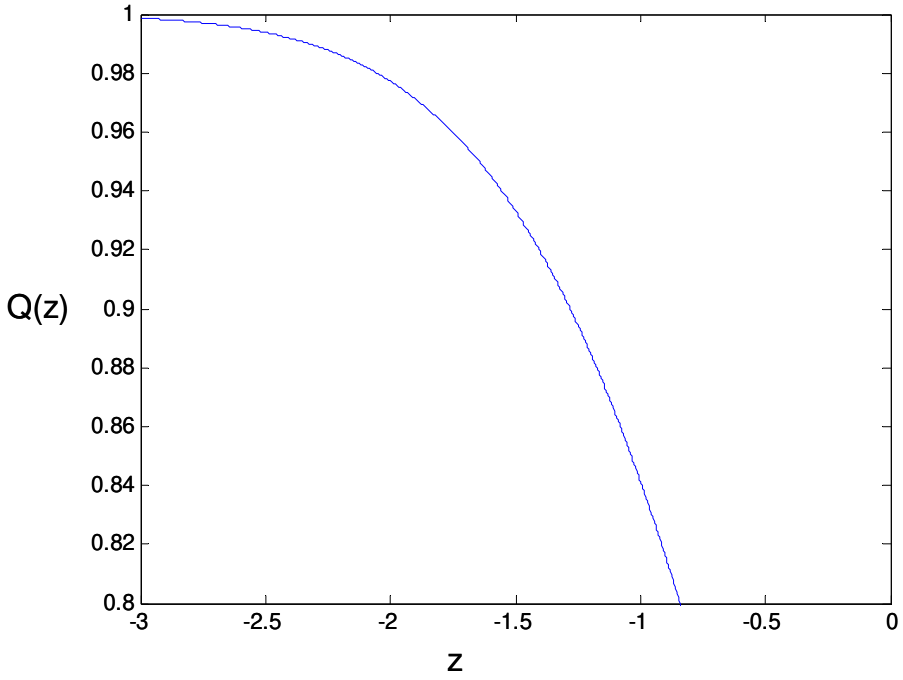

Figure 31. Q function for typical Probability of Detection calculations.

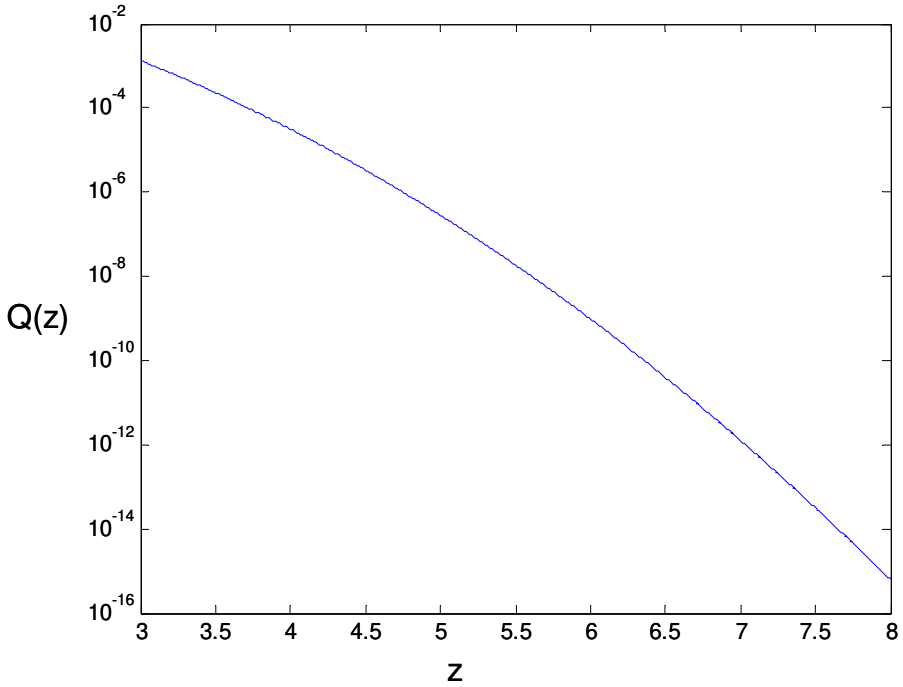

Figure 32. Q function for typical Probability of False Alarm calculations.

Appendix D – The Rice Distribution

The Rice PDF is defined as

$$f_R(x) = \frac{x}{\sigma^2} e^{-\frac{\left(x^2+A^2\right)}{2\sigma^2}} I_0\left(\frac{xA}{\sigma^2}\right), \tag{D1}$$

where

$$I_n(z) = \text{modified Bessel function of the first kind with order } n. \tag{D2}$$

We plot the envelope PDFs for two values of A in Figure 33.

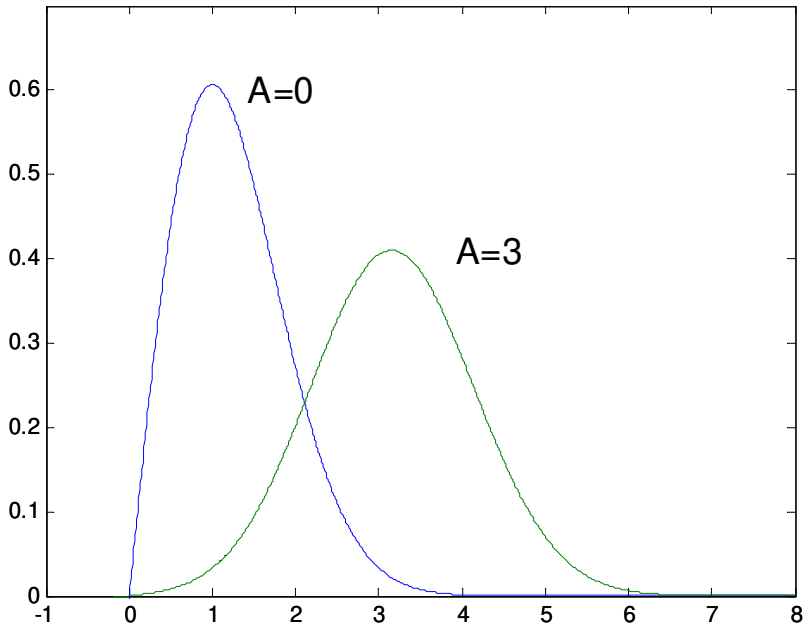

Figure 33. Envelope detector output PDFs for σ=1.

For the Rice distribution

$$\text{Mean}\left(Rice(A,\sigma)\right) = \sigma\sqrt{\frac{\pi}{2}} L_{1/2}\left(\frac{-A^2}{2\sigma^2}\right) \tag{D3}$$

and

$$\text{Variance}\left(Rice\left(A,\sigma\right)\right)=2\sigma^2+A^2-\frac{\pi\sigma^2}{2}L_{1/2}^2\left(\frac{-A^2}{2\sigma^2}\right). \tag{D4}$$

where

$$L_v\left(z\right) = \text{denotes a Laguerre polynomial.} \tag{D5}$$

For $v=1/2$, we can calculate

$$L_{1/2}\left(z\right)=e^{z/2}\left[\left(1-z\right)I_0\left(\frac{-z}{2}\right)-z\,I_1\left(\frac{-z}{2}\right)\right]. \tag{D6}$$

A plot of the characteristics of the mean is shown in Figure 34, and a plot of the characteristics of the variance is shown in Figure 35. These show that as *A* increases, the mean of the Rice distribution remains greater than *A* but approaches *A*, and the variance of the Rice distribution remains less than σ^2, but approaches σ^2.

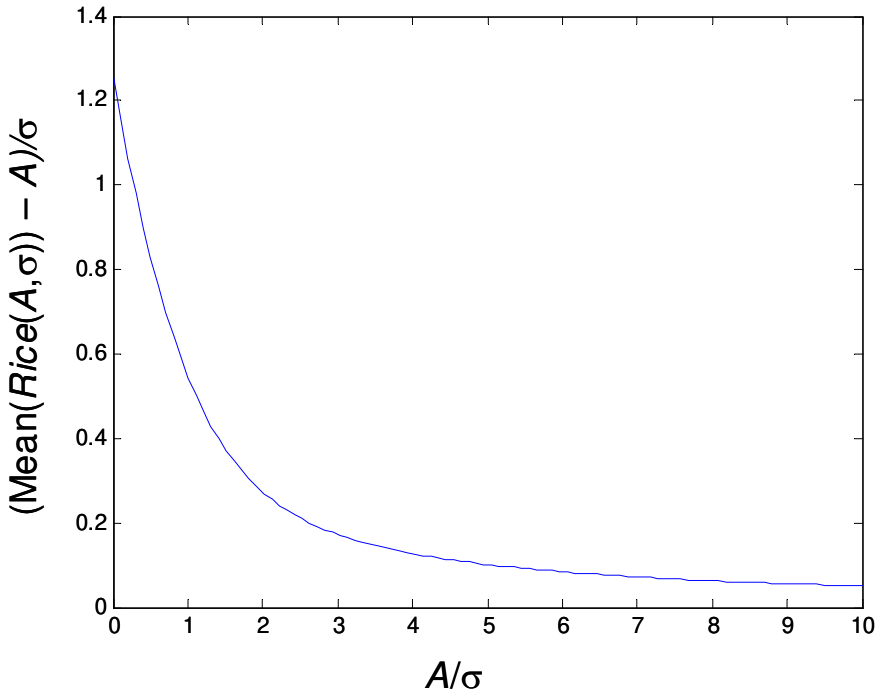

Figure 34. Behavior of the mean of the Rice distribution.

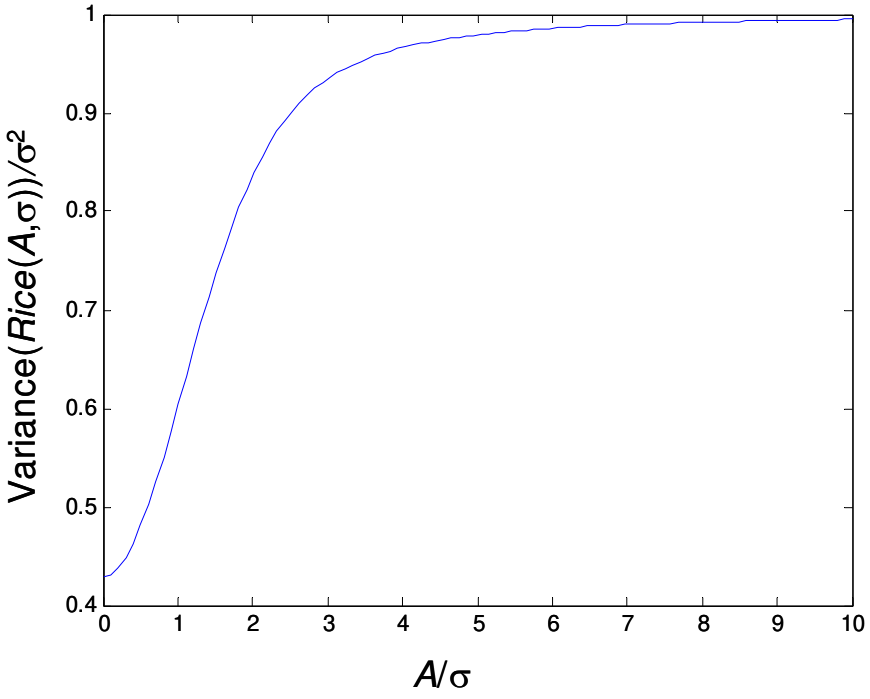

Figure 35. Behavior of the variance of a Rice distribution.

The area under regions of a Rice distribution is calculated via a Marcum Q function. Plots for the relevant Marcum Q function are given in Appendix E.

Note that for the case $A = 0$, the Rice PDF reduces to a Rayleigh PDF, namely

$$Rice(0,\sigma) = Rayleigh(\sigma) \tag{D7}$$

where the Rayleigh PDF is calculated as

$$f_R(x)\big|_{A=0} = \frac{x}{\sigma^2} e^{-\frac{x^2}{2\sigma^2}} \quad \text{restricted to } x \geq 0. \tag{D8}$$

Statistics for the Rayleigh PDF include

$$\text{Mean}(Rayleigh(\sigma)) = \sigma\sqrt{\pi/2}, \text{ and} \tag{D9}$$

$$\text{Variance}(Rayleigh(\sigma)) = \frac{4-\pi}{2}\sigma^2. \tag{D10}$$

For the large SNR case where $A >> \sigma$, the Rice PDF approaches a Normal PDF, namely

$$Rice(A,\sigma)\big|_{A>>\sigma} \rightarrow N\left(A,\sigma^2\right). \tag{D11}$$

Rice PDFs and a Normal PDF are compared for several values of A in Figure 36. Recall that for A = 3, 6, and 9, then SNR_{coherent} = 6.5 dB, 12.5 dB, and 16 dB respectively.

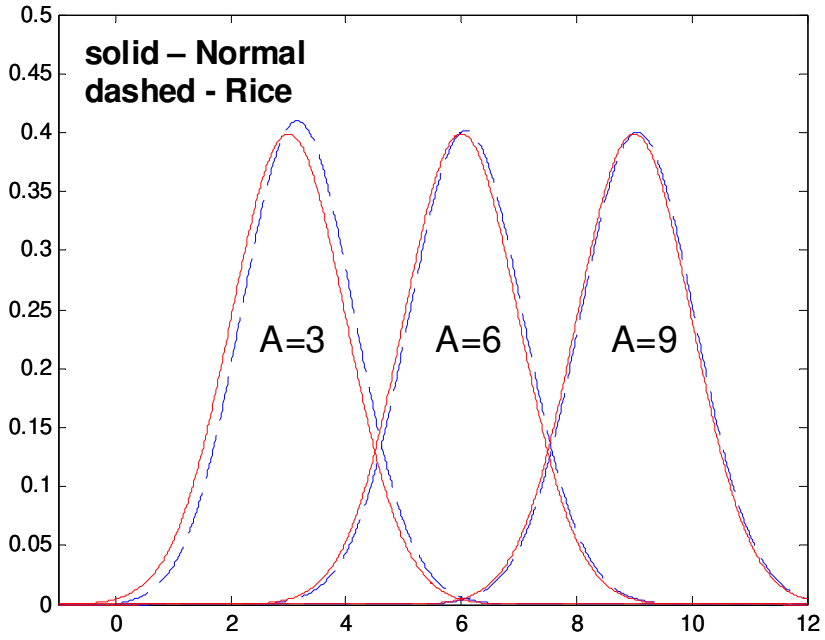

Figure 36. Comparison of Rice and Normal distributions for σ=1.

Also indicated by the figure is that the Normal distribution has more area to the left of the Rice distribution. This indicates that approximating with a Normal distribution will yield a lower P_D for any given specified detection threshold. That is, assuming a Normal distribution is somewhat pessimistic. Note that at the $P_D = 0.9$ level this might be about 5% for A = 3, and perhaps 2% for A = 6.

Another perspective is that assuming a Normal distribution is tantamount to assuming a slightly worse SNR_{coherent} for the signal. At the $P_D = 0.9$ level, this amounts to about 0.6 dB for A = 3, and 0.1 dB for A = 6. In the larger scheme of radar design, these fractional dB numbers are 'in the noise' as it were.

In any case, a Normal distribution is a reasonably good approximation for the Rice distribution for an envelope detector when SNR_{coherent} exceeds on the order of 10 dB, and is usable even down to 6 dB or so.

Appendix E – The Marcum Q Function

The generalized Marcum Q function is calculated as

$$Q_M(a,z) = \int_z^\infty \frac{x^M}{a^{M-1}} e^{-\frac{\left(x^2+a^2\right)}{2}} I_{M-1}(ax)dx . \tag{E1}$$

We are interested in the case $M = 1$. This corresponds to finding the area of a region under the Rice probability density function curve. Figure 37 shows Marcum Q_1 function values typical for Probability of Detection calculations.

Figure 38 shows Marcum Q_1 function values typical for Probability of False Alarm calculations.

Recalling the Rice distribution of Appendix D, this formulation of the Marcum Q_1 function presumes $\sigma = 1$.

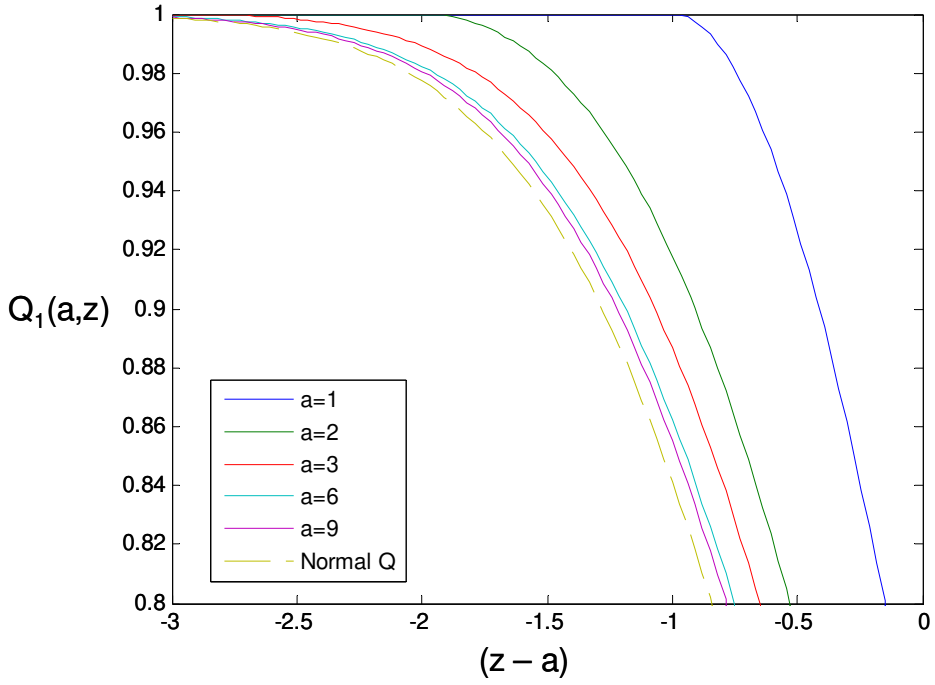

Figure 37. Marcum Q_1 function.

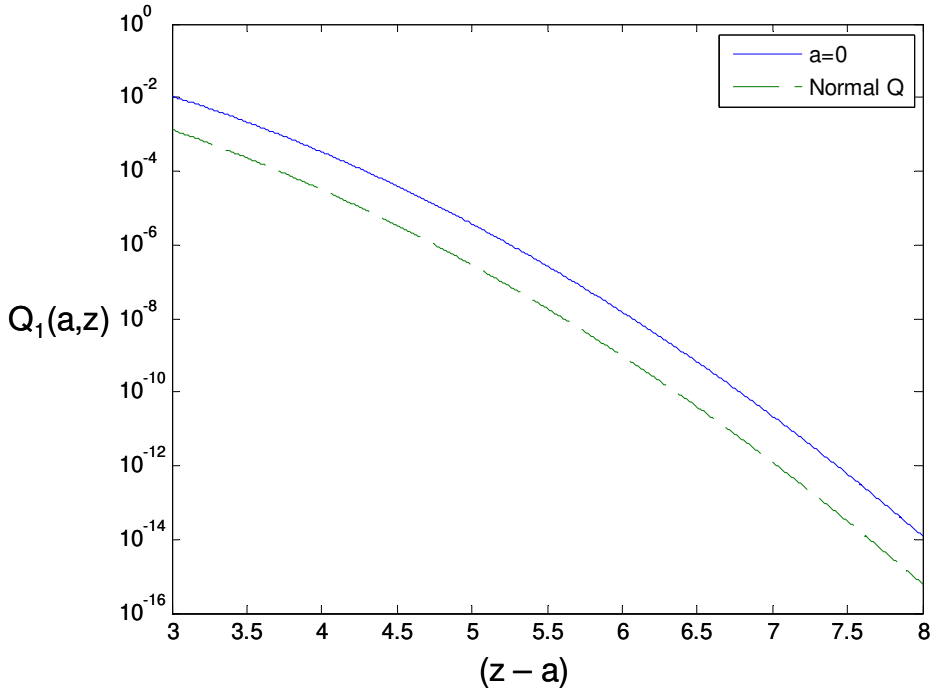

Figure 38. Marcum Q_1 function.

Appendix F – Measuring False Alarm Rate (FAR)

A typical Ground Moving Target Indicator (GMTI) specification includes the following parameters

Probability of Detection (P_D) – typically on the order of 0.85
False Alarm Rate (FAR) – typically on the order of 0.1 Hz

There are others, but for the discussion below we focus on the False Alarm Rate. The P_D is normally associated with a particular target 'size', such as Radar Cross Section (RCS) with perhaps some statistical description (e.g. Swerling number).

Indeed, the concept of FAR is embodied at a fundamental level in the detection process, which traditionally employs a Constant-FAR (CFAR) detector to set thresholds for initial decisions on whether a target is present or not.

While useful, such a metric for radar specification and system comparison is not without some serious shortcomings. We address some of these below.

F.1 False Alarm Rate and Probability of False Alarm

A fundamental measure of 'goodness' is the likelihood that a single detection calculation makes a mistake to indicate a target is present when in fact it is not, that is, indicates a False Alarm (FA). This is embodied in a measure called the Probability of False Alarm (P_{FA}) for that single detection calculation.

As a probability, the P_{FA} can be expressed as the number of independent occurrences of a FA for an independent opportunity. That is,

$$P_{FA} = \frac{\#\, False\ Alarms}{Independent\, Opportunity} \tag{F1}$$

An independent opportunity is often a range-Doppler resolution cell in a non-overlapping Coherent Processing Interval (CPI).

The P_{FA} depends on the relative noise level of the processed data at the stage on which detection occurs. Consequently, it depends on processing gains in Signal to Noise Ratio (SNR). It may also depend on 'spatial noise', that is clutter, or clutter residue.

However, P_{FA} is too far removed from the experience base of most radar operators, and the people that buy radars. They are interested in False Alarms, to be sure, but in a framework to which they can relate. Convention has caused the GMTI community to converge on the metric "False Alarm Rate" (FAR).

The FAR is thus calculated as

$$FAR = \frac{\#\,False\ Alarms}{\sec} = P_{FA} \times \frac{Independent\ Opportunities}{\sec}. \tag{F2}$$

Of course, a low FAR is good, and a high FAR is bad.

What becomes immediately obvious is that for a given P_{FA}, we can influence the FAR by adjusting the rate of Independent Opportunities. Consequently, we can influence the FAR just by adjusting the number of independent range-Doppler resolution cells (their size remaining equal). The number of independent range-Doppler resolution cells is directly proportional to the range swath being interrogated.

One formulation for FAR is as follows.

$$FAR = P_{FA} \times \frac{Independent\ Opportunities}{\sec} = P_{FA} \times \left(\frac{D_r}{\rho_r} \right) \times PRF\,, \tag{F3}$$

where

$$\begin{aligned} &D_r \text{ = range swath,} \\ &\rho_r \text{ = range resolution in the same plane as the range swath,} \\ &PRF \text{ = Pulse Repetition Frequency.} \end{aligned} \tag{F4}$$

This assumes that all pulses are used from a constant PRF, and that the entire Doppler spectrum is used for detection. If only the exo-clutter region is used, then the endo-clutter spectrum represents discarded opportunities. Consequently the FAR becomes

$$FAR = P_{FA} \times \left(\frac{D_r}{\rho_r} \right) \times \left(PRF - B_{clutter} \right), \tag{F5}$$

where

$$B_{clutter} = clutter\ bandwidth\,. \tag{F6}$$

For exo-clutter operation, we often desire the PRF to be large compared to the clutter bandwidth.

In any case, other things being equal, two radars with different range swaths will indicate different FAR metrics. The radar with the larger range swath will be penalized.

Example:

> Radar A scans a 1 km swath with a FAR of 0.1 per second. Radar B scans a 10 km swath with a FAR of 0.4 per second. Other things equal, which is better performance?
>
> Since radar B can always reduce its swath to 1 km by throwing away data, if false alarms are uniformly distributed across the swath, then by throwing away 9 km of swath it will reduce its FAR to 0.04 per second, making it the clear 'winner'.
>
> The question becomes "Would a radar operator eagerly trade the swath to enhance FAR?" It seems doubtful.

This suggests that when comparing FAR statistics, the swath must be considered. This also suggests that a better metric than FAR is a 'swath normalized' FAR, with perhaps units "false alarms per second per km swath".

We note that other parameters can also be 'adjusted' to influence FAR, although these also have important secondary effects. For example coarsening resolution may reduce FAR but makes clutter brighter. Reducing PRF reduces FAR but also adversely affects velocity ambiguity, and may reduce observable velocity ranges. Reducing PRF may also reduce SNR for targets, reducing P_D as well.

F.2 False Alarm Rate and Area

In the previous discussion we associated FAR with P_{FA}, and noted that FAR depends on the swath of interest. We extend this concept now from the other direction.

We now pose the question "What would we expect for a FAR in a limited subregion of the overall scan?"

We construct the relationship

$$FAR = \frac{\#\,False\ Alarms}{\sec} = \frac{\#\,False\ Alarms\ in\ total\ scan\ area}{total\ scan\ area} \times \frac{total\ scan\ area}{total\ scan\ time}. \quad \text{(F7)}$$

We note that for a single scan or sweep

$$\frac{total\ scan\ area}{total\ scan\ time} = area\ scan\ rate \approx \dot{\theta}\, R\, D_r, \quad \text{(F8)}$$

where

$\dot{\theta}$ = angular scan rate,
R = nominal range to center of range swath. (F9)

However, if we believe that false alarms are uniformly distributed in the scanned area, then we can equate

$$\frac{\#\,False\ Alarms\ in\ total\ scan\ area}{total\ scan\ area} = \frac{\#\,False\ Alarms\ in\ subregion}{subregion\ area} = FAAR\,, \qquad \text{(F10)}$$

where we define

$FAAR$ = False Alarm Area Rate, with units of False Alarms per reference area. (F11)

We identify a subregion as having some area within the scanned region of the GMTI radar. A subregion might be, for example, a particular 1 km^2 area. Putting these observations together yields

$$FAR = FAAR \times \dot{\theta}\, R\, D_r\,. \qquad \text{(F12)}$$

F.3 FAR Testing

The foregoing analysis suggests a reasonable testing strategy as follows.

1. Define a 'test region' where movers are controlled. It need not be the entire scanned area. Ascertain the area of the test region. This becomes the subregion area in the equation.

2. Scan over the test region, counting all detections that are not controlled movers, but limited to those detections assigned to the subregion. The False Alarm count for the subregion is another element of the equation.

3. Calculate FAAR using the above equation.

4. Calculate FAR using the above equation.

This also suggests that perhaps FAAR might be an important metric all by itself, perhaps with units False Alarms per square km. We note that this figure of merit would generally depend on range and scan rate.

Recall also that this is for a single scan.

F.4 Which Probability of Detection?

GMTI processing functionality can be roughly divided into the following major blocks.

1. Single CPI processing
2. Inter-CPI processing (across multiple CPIs) within a single scan
3. Inter-scan processing (across multiple scans)

Although we use the nomenclature CPI, we allow that this might also be some degree of noncoherent processing.

We note that depending on the processing architecture, that is the degree to which inter-CPI and inter-scan processing is used, different P_D and FAR performance is achieved. A reasonable question is "To which output do we want to measure and specify P_D and FAR performance?"

Recall that the previous development measured FAR after a single scan, therefore allowing measurement of inter-CPI processing. To incorporate inter-scan processing, we need to account for the fact that the same area is scanned multiple times. The FAR equation then becomes

$$FAR = FAAR \times \frac{\dot{\theta} R D_r}{N_{scan}}, \tag{F13}$$

where

N_{scan} = the number of scans over which data was collected. (F14)

In addition, FAAR now is a count of the cumulative false alarm detections over all scans for the test region. To be fair, any 'start-up' scans for which GMTI reports were not valid need to be omitted from the count.

F.5 Summary

We reiterate the following points.

- False Alarm Rate comparison between different GMTI systems can be misleading. An improved measure normalizes FAR for swath width.
- FAR can be calculated from False Alarms counted just over a test area. This allows controlling movers over only the test area, and not the entire swath or scanned area.

"Trust only movement. Life happens at the level of events, not of words. Trust movement." -- Alfred Adler.

References

[1] Armin W. Doerry, "Performance Limits for Synthetic Aperture Radar – second edition", Sandia Report SAND2006-0821, Unlimited Release, February 2006.

[2] Peter Swerling, "Probability of detection for fluctuating targets", *IRE Transactions on Information Theory*, Vol. 6, Issue 2, pp. 269-308, 1960.

[3] Gintautas Palubinskas, Hartmut Runge, "Radar Signatures of a Passenger Car", *IEEE Geoscience and Remote Sensing Letters*, Vol. 4, No. 4, October 2007.

[4] William E. Nixon, H. J. Neilson, G. N. Szatkowski, Robert H. Giles, William T. Kersey, L. C. Perkins, Jerry Waldman, "A Variability Study of Ka-band HRR Polarimetric Signatures on Eleven T-72 Tanks", Proceedings of the SPIE Conference on Algorithms for Synthetic Aperture Radar Imagery V, Vol. 3370, pp. 369-382, Orlando, FL, 14 April 1998.

[5] R.H. Giles, W.T. Kersey, M.S. McFar1in, R. Fin1ey, H.J. Neilson, W.E. Nixon, "A Study of Target Variability and Exact Signature Reproduction Requirements for Ka-Band Radar Data", Proceedings of the SPIE Conference on Signal Processing, Sensor Fusion, and Target Recognition X, Vol. 4380, pp. 117-126, Orlando, FL, 16 April 2001.

[6] Thomas M. Goyette, Jason C. Dickinson, Christopher Beaudoin, Andrew J. Gatesman, Robert Giles, Jerry Waldman, and William E. Nixon, "Acquisition of UHF and X-Band ISAR imagery using 1/35th Scale-models", Proceedings of the SPIE Conference on Algorithms for Synthetic Aperture Radar Imagery XII, Vol. 5808, pp. 440-449, Orlando, FL, 28 March 2005.

[7] G. Palubinskas, H. Runge, P. Reinartz, "Radar signatures of road vehicles", Proceedings of the 2004 IEEE International Geoscience and Remote Sensing Symposium, IGARSS '04., Vol. 2, pp. 1498-1501, Anchorage, Alaska, 20-24 September 2004.

[8] Calvin Le, Traian Dogaru, ""Numerical Modeling of the Airborne Radar Signature of Dismount Personnel in the UHF-, L-, Ku-, and Ka-Bands", Army Research Laboratory (ARL) report ARL-TR-4336, December 2007.

[9] Michael Otero, "Application of a continuous wave radar for human gait recognition", Proceedings of the SPIE 2005 Defense and Security Symposium, Conference on Signal Processing, Sensor Fusion, and Target Recognition XIV, Vol. 5809, pp. 538-548, Orlando, FL, USA, 28 March 2005.

[10] Armin W. Doerry, "Reflectors for SAR Performance Testing", Sandia Report SAND2008-0396, Unlimited Release, January 2008.

[11] S. M. Soliday, "Lane Position Maintenance by Automobile Drivers on Two Types of Highways", Ergonomics, Vol. 18, No. 2, pp. 175-183, 1975.

[12] Ronan Boulic, Nadia Magnenat Thalmann, Daniel Thalmann, "A global human walking model with real-time kinematic personification", The Visual Computer, Springer-Verlag, Vol. 6, pp. 344-358, 1990.

[13] Thomas L. Lewis, Brian Rigling, "Analysis of Focused Dismount Signatures", Proceedings of the SPIE Conference on Algorithms for Synthetic Aperture Radar Imagery XVII, Vol. 7699, Orlando, FL, 8-9 April 2010.

[14] Armin W. Doerry, "Generating Nonlinear FM Chirp Waveforms for Radar", Sandia Report SAND2006-5856, Unlimited Release, September 2006.

[15] A. W. Doerry, "SAR Processing with Non-Linear FM Chirp Waveforms", Sandia Report SAND2006-7729, Unlimited Release, December 2006.

[16] A. W. Doerry, "Atmospheric loss considerations for synthetic aperture radar design and operation", Proceedings of the SPIE 2004 Defense & Security Symposium, Radar Sensor Technology IX, Vol. 5410A, pp. 17-27, Orlando FL, 12-16 April 2004.

[17] A. W. Doerry, "Atmospheric attenuation and SAR operating frequency selection", Workshop on Synthetic Aperture Radar Technology", Redstone Arsenal, AL, October 22 & 23, 2003.

[18] A. W. Doerry, "Clutter in the GMTI Range-Velocity Map", Sandia Report SAND2009-1797, Unlimited Release, April 2009.

[19] M. I. Skolnik, *Introduction to Radar Systems, second edition*, ISBN 0-07-057909-1, McGraw-Hill, Inc., 1980.

[20] David K. Barton, *Modern Radar System Analysis*, ISBN 0-89006-170-X, Artech House, Inc., 1988.

[21] Guy Morris, Linda Harkness, *Airborne Pulsed Doppler Radar*, second edition, ISBN 0-89006-867-4, Artech House, Inc., 1996.

[22] R. E. Ziemer, W.H. Tranter, *Principles of Communications – Systems, Modulation, and Noise, Fourth Edition*, ISBN 0-471-12496-6, John Wiley & Sons, Inc., 1995.

[23] Robert N. McDonough, Anthony D. Whalen, *Detection of Signals in Noise - 2nd edition*, ISBN 0-12-744852-7, Academic Press, 1995.

[24] F. E. Nathanson, *Radar Design Principles*, second edition, ISBN 0-07-046052-3, McGraw-Hill, Inc., 1990.

[25] Lamont V. Blake, “Chapter 2 - Prediction of Radar Range”, Merril I. Skolnik, editor, *Radar Handbook*, McGraw Hill, Inc., 1970.

Distribution

Unlimited Release

1	MS 0532	J. J. Hudgens	5240	
1	MS 0532	B. L. Burns	5340	
1	MS 0519	T. J. Mirabal	5341	
1	MS 0533	S. Gardner	5342	
1	MS 0533	S. D. Bensonhaver	5342	
1	MS 0533	T. P. Bielek	5342	
1	MS 0533	J. D. Bradley	5342	
1	MS 0533	D. W. Harmony	5342	
1	MS 0533	J. A. Hollowell	5342	
1	MS 0533	M. S. Murray	5342	
1	MS 0533	C. Musgrove	5342	
1	MS 0533	R. Riley	5342	
1	MS 0533	J. A. Rohwer	5342	
1	MS 0533	B. G. Rush	5342	
1	MS 0533	G. J. Sander	5342	
1	MS 0533	D. G. Thompson	5342	
1	MS 0532	W. H. Hensley	5344	
1	MS 0532	S. Nance	5344	
1	MS 0533	K. W. Sorensen	5345	
1	MS 0533	B. C. Brock	5345	
1	MS 0533	D. F. Dubbert	5345	
1	MS 0533	G. K. Froehlich	5345	
1	MS 0533	F. E. Heard	5345	
1	MS 0533	G. R. Sloan	5345	
1	MS 0532	S. M. Becker	5348	
1	MS 0532	D. M. Small	5348	
1	MS 0532	B. L. Tise	5348	
1	MS 0519	D. M. Brouhard	5349	
1	MS 0519	A. W. Doerry	5349	
1	MS 0519	J. Luck	5349	
1	MS 0519	C. Smithpeter	5354	
1	MS 0519	D. L. Bickel	5354	
1	MS 0519	A. Martinez	5354	
1	MS 0519	A. M. Raynal	5354	
1	MS 0899	Technical Library	9536	(electronic copy)
1	John Fanelle	General Atomics ASI, RSG		(electronic copy)

;-)